UNIVERSITY OF OKLAHOMA

GRADUATE COLLEGE

UNDERSTANDING ECOSYSTEM CARBON DYNAMICS BY MODELING APPROACHES

A DISSERTATION

SUBMITTED TO THE GRADUATE FACULTY

in partial fulfillment of the requirements for the

Degree of

DOCTOR OF PHILOSOPHY

By

ENSHENG WENG
Norman, Oklahoma
2011

UNDERSTANDING ECOSYSTEM CARBON DYNAMICS BY MODELING APPROACHES

A DISSERTATION APPROVED FOR THE
DEPARTMENT OF COMMUNICATION

BY

Dr. Yiqi Luo, Chair

Dr. Xiangming Xiao

Dr. Rebecca A. Sherry

Dr. Ming Xue

Dr. Nikola P. Petrov

To Hui and Ethan

ACKNOWLEDGEMENTS

I owe a tremendous debt of gratitude to my advisor, Dr. Yiqi Luo, for his excellent advice and guidance on my study and research in the past five years. I have been fortunate to benefit from such a good mentor with profound knowledge, patience, and vision. He helped me learn to know the importance of focusing on the big picture of science without stumbling on trivial details. He spent so much time with me on the writing of my manuscripts. It would be impossible for me to finish this dissertation without his guidance.

I would like to thank Dr. Nikola P. Petrov for his help in solving the mathematical problems of theoretical disturbance framework and the discussions with him in his classes. Without his advices and input, this dissertation would be totally different. I would like to extend my appreciation to Drs. Linda L. Wallace, Rebecca A. Sherry, Xiangming Xiao, and Ming Xue for their advice, support, and willingness to serve as members of my advisory committee. I thank Dr. A. David McGuire of University of Alaska, Fairbanks, and Dr. Daniel J. Hayes of Oak Ridge National Laboratory for providing their TEM simulated results.

Thanks to the members and former members of Dr. Luo's research group: Dr. Xuhui Zhou, Jianzhong Lu, Xiaowen Wu, Dr. Jesse E. Bell, Oleksandra Hararuk, Chao Gao, Shenfeng Fei, Zhongda Zhang, Xia Xu, Dr. Christina Schadel, for their help and

providing an enjoyable working atmosphere. Special thanks go to Jianzhong and Xiaowen for their friendship, encouragement, and helps in using data assimilation approaches.

I would also like to express my gratitude to my former advisor, Prof. Hong Hu of Kunming institute of botany, Chinese Academy of Sciences, Dr. Bo Li and Prof. Jiakuan Chen of Fudan University for their support for my pursuit of PhD degree. I'd also like to thank Drs Weile Wang, David Schimel, Han Wang, Alan Hastings for their help in the manuscript of disturbance.

Finally and most importantly, I would like to thank my wife, Huimin Zhao. Her support, encouragement, and unwavering love were the bedrock of this dissertation. I also would like to than my son, Ethan, who is only 21 months now and might not remember anything he experienced here. But he brought me so much joy and happiness, and enthusiasm.

TABLE OF CONTENTS

LIST OF TABLES

Chapter 1

Chapter 2

Chapter 3

Chapter 4

LIST OF FIGURES

Chapter 1

Chapter 2

Chapter 3

Chapter 4

ABSTRACT

Ecosystem models are a useful tool to explore ecological processes and their responses to climate change. The basic structures of current ecosystem C cycle models are similar and robust, but their uncertainties are high, especially when coupled with water and nutrient cycles and disturbance effects. In this dissertation, I studied three issues in ecosystem C cycle modeling: interactions between water and C processes, information contribution of theoretical basis (model structure) vs. observations (data), and ecosystem C storage capacity at disequilibrium state due to effects of disturbances. These three issues represent the basic theoretical problems in the development and application of ecosystem models: 1) how the representations of interactions among ecological processes affect the simulation of ecosystem C cycle? 2) Once a model is built up, how much information can be brought in by model calibration? 3) For large spatial C cycle modeling, how will the paradigm of ecosystem states affect our C cycle modeling?

In the first study, we evaluated the effects of soil hydrological properties on the interactions of water and carbon dynamics of a grassland ecosystem in response to altered precipitation amount and frequency, increased temperature, elevated atmospheric CO_2 with changes in soil available water capacity (AWC). A process-based terrestrial ecosystem (TECO) model was used to simulate responses of soil moisture, evaporation, transpiration, runoff, net primary production (NPP), ecosystem respiration (R_h), and net

ecosystem production (NEP) to changes in precipitation amounts and intensity, temperature, and CO_2 concentration along a soil texture gradient. Simulation results showed that soil AWC altered partitioning of precipitation among runoff, evaporation, and transpiration, and consequently regulated ecosystem responses to global environmental changes. Fractions of precipitation that were used for evaporation and transpiration increased with soil AWC but decreased for runoff. High AWC could greatly buffer water stress during long drought periods, particularly after a large rainfall event. NPP, R_h, and NEP usually increased with AWC under ambient and 50% increased precipitation scenarios but increased from 7% to 7.5% of AWC followed by declines under the halved precipitation amount. Warming and CO_2 effects on soil moisture, evapotranspiration, and runoff were magnified by soil AWC. CO_2 effect on NPP, R_h, and NEP increased with soil AWC. Our results indicate that variations in soil texture may be one of the major causes underlying variable responses of ecosystems to global changes observed from different experiments. These results also imply that the interactions between C and water processes can be some soil texture.

In the second study, I evaluated the information contribution of model and observations to model predictions by a data assimilation approach. Eight sets of ten-year data (foliage, woody, and fine root biomass, litter fall, forest floor carbon (C), microbial C, soil C, and soil respiration) collected from Duke Forest were assimilated into a Terrestrial ECOsystem model (TECO) using a Monte Carlo Markov Chain approach. The relative information contribution was measured by the Shannon information index

calculated from probability density functions (PDF) of carbon pool sizes. Our results showed that the information contribution of the model to constrain carbon dynamics increased with time whereas the data contribution declined. The eight data sets contributed more than the model to constrain C dynamics in foliage and fine root pools over the 100-year forecasts. The model, however, contributed more than the data sets to constrain the litter, fast soil organic matter (SOM), and passive SOM pools. For the two major C pools, woody biomass and slow SOM, the model contributed less information in the first few decades and then more in the following decades than the data. The knowledge on relative information contributions of model vs. data is useful for model development, uncertainty analysis, future data collection, and evaluation of ecological forecasting.

In the third study, I integrated the temporal patterns of C storage and spatial patterns of ecosystem states to develope a model to analytically describe relationships between ecosystem carbon storage and NPP, C residence time, and disturbance intervals and severity. The model represents a disequilibrium perspective for examining C storage dynamics in light of the impacts of disturbances and improves our predictive understanding of regional C dynamics. The carbon cycle at the scale of the ecosystem is almost always in dynamic disequilibrium with most ecosystems accumulating carbon at various stages of recovery with intermittent disturbances that release large amounts of carbon. This disequilibrium perspective is critical for scaling of site-level observations to

estimate regional and global carbon sinks, for modeling studies on carbon-climate feedbacks, and for design of field experiments and observation networks.

These studies showed that current ecosystem C modeling protocols, i.e., a Farquhar model based canopy model simulating C input to the system and a compartmentalized C pool model simulating C allocation, transfer, and decomposition, work well in simulating the short-term patterns of ecosystem C dynamics, but have high uncertainties in simulating the interactions of multiple processes and are very sensitive to some parameters and boundary conditions. Data assimilation is an effective method to combine information from models and data and improve model parameterization and accuracy of predictions and reduce model uncertainties. However, once a model structure is given, optimizing parameters by data assimilation approaches can only find out the best agreement with observations within the space defined by the given model. The theoretical understanding of ecosystem dynamics is central to ecosystem modeling studies. As illustrated by our disturbance model (the third study), new theories and paradigms can fundamentally change the way in which ecosystems are represented in models.

Keywords: global change, terrestrial ecosystems, carbon cycle, TECO model, available water capacity, soil moisture, data assimilation, information theory, disturbance, dynamic disequilibrium, Duke Forest FACE

CHAPTER 1 Ecosystem carbon cycle modeling: introduction

1.1 Introduction

Terrestrial ecosystems are key the components of the Earth system. Terrestrial plants, as the fundamental component of terrestrial ecosystems, started to move to land 385 million years ago (Stein et al. 2007), and gradually dominated the landscape. During the long history of evolution, they evolved trunks to better compete for light with their neighbors and huge root systems to absorb nutrients and water from the soil. In doing so, they stored a large amount of carbon (C) in their bodies. After plants die, this carbon was partly decomposed by microbes and partly turned into soil organic C, forming the largest organic C pool on land. In doing so, they lowered the CO_2 concentration of the atmosphere and stored the C in terrestrial ecosystems.

Terrestrial ecosystems have around 550 Pg C in vegetation, and two to three times this amount (1500-2300 Pg C) in soil, while the atmosphere stores around 800 Pg C with an increase rate of 3.2 Pg C yr-1. Photosynthesis assimilates 120 Pg C yr^{-1} from atmosphere while autotrophic and heterotrophic respirations release 117 Pg C yr^{-1} (Houghton 2007). Thus, terrestrial ecosystems are a sink of atmospheric CO_2. By changing their physiological and physical activities, ecosystems can regulate the atmospheric CO_2 concentration by their biological processes, such as photosynthesis and decomposition, therefore affecting greenhouse gas concentration and land surface temperature (Fig. 1). Terrestrial ecosystems also control the interaction between the land surface and the atmosphere with their reflectance of solar radiation (albedo), and

properties of evapotranspiration (e.g. Bowen ratio) (Bonan et al. 2008). Environmental factors, such as temperature, precipitation, solar radiation, and soil properties can affect terrestrial ecosystems, leading to complicated positive and negative feedbacks in the Earth system (Field et al. 2007).

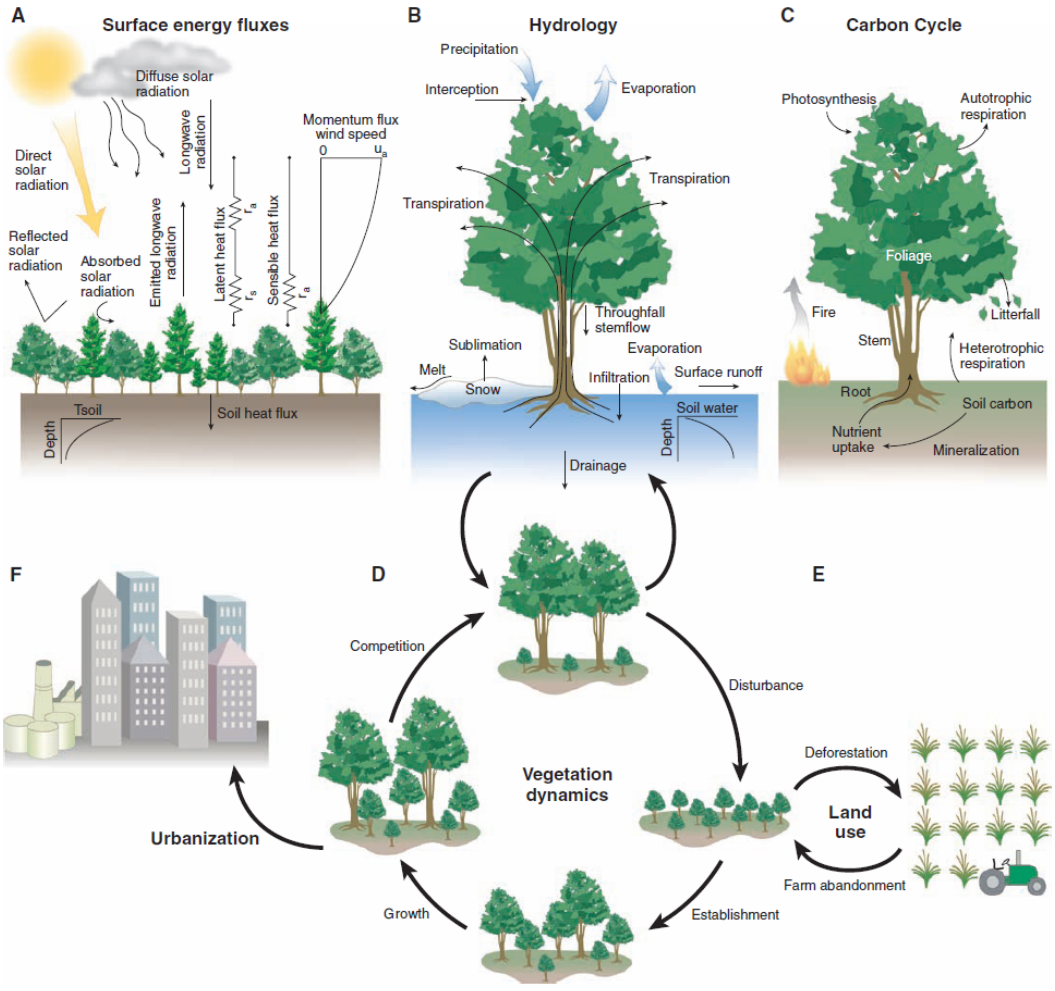

Figure 1.1 The roles of terrestrial ecosystem (*from* Bonan et al. 2008)

A: Energy budget; B: water balance; C: Carbon cycle; D: vegetation dynamics; E: land use change; F: Urbanization

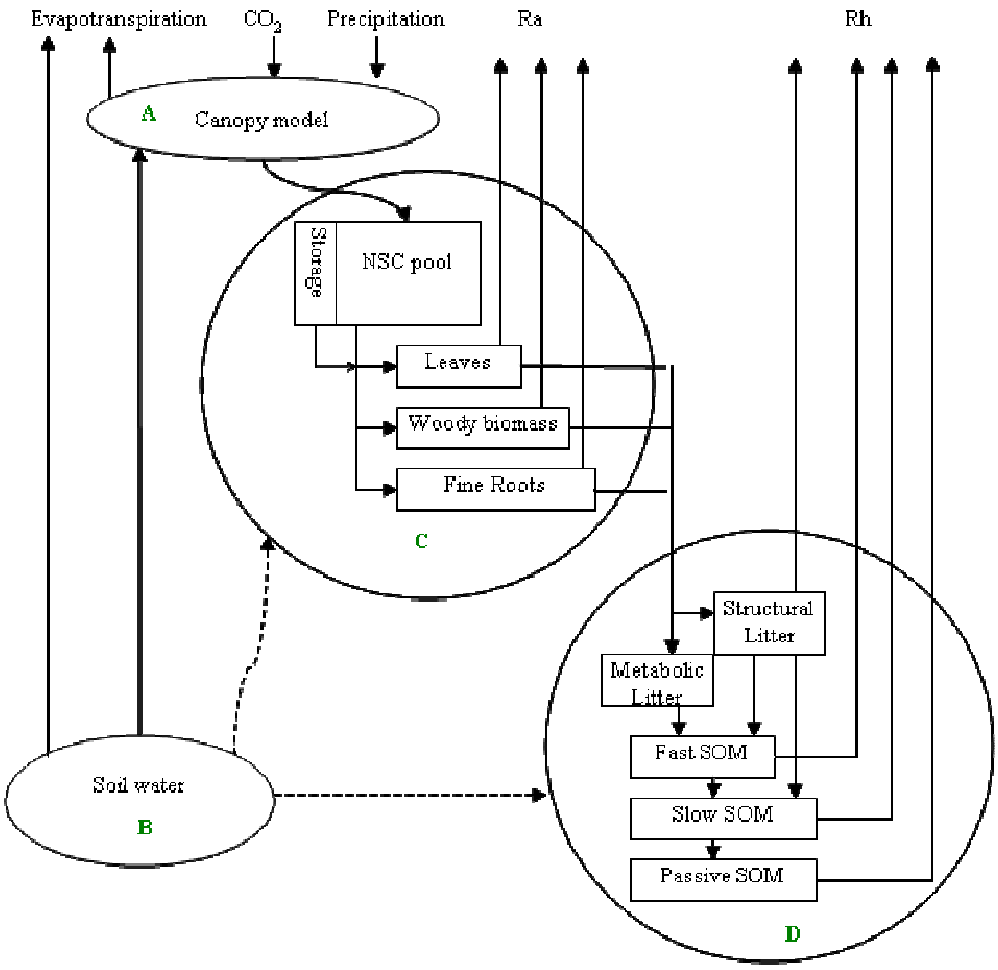

Figure 1.2 Basic structure of an ecosystem model. A: photosynthesis model; B: soil water dynamics; C: plant growth model: D: soil C model

Human activities have profoundly changed the Earth system by altering land cover types, atmospheric chemical components, and hydrological cycles (Vitousek et al. 1997). In the past century, the concentration of atmospheric CO_2 has increased from 270 ppm to 380 ppm. 50% of land cover was changed from natural vegetations to human use (Foley et al. 2005). Dams and irrigation changed the patterns of river runoff and evapotranspiration (Vitousek et al. 1997). As a result of the increases in atmospheric

[CO_2], global surface temperature increased 0.74 ± 0.18 °C during the 20th century, which consequently induced changes in hydrologic cycles, leading to more extreme precipitation events (IPCC, 2007). These changes feedback to terrestrial ecosystems, and then result in more complicated negative and positive feedbacks between terrestrial ecosystems and climate, which may lead to environmental problems affecting human welfare.

Ecosystem models play a fundamental role in synthesizing these feedbacks and explore the possibilities of ecosystems' responses and feedbacks to those changes. Ecosystem models put the pieces of knowledge together and provide people predictive understanding on ecosystems or explore the possibilities of ecosystem changes in responses to climate change. An ecosystem model is a highly simplified representation of the complex real world, and usually designed for specific questions. Many models for exploring C cycle have been developed in past twenty years, e.g., CENTURY (Parton et al. 1987), TEM (McGuire et al. 1992), IBIS (Foley et al. 1996), LPJ (Sitch et al. 2003). And most of them share similar model structure. Photosynthetically fixed carbon, for example, is allocated to multiple plant and soil pools (VEMAP 1995, Kucharik et al. 2000, Sitch et al. 2003). Photosynthesis is usually simulated using the Farquhar model (Farquhar et al. 1980) as regulated by light, CO_2 concentration, temperature, and nutrients (e.g., nitrogen). Allocation of carbohydrates from photosynthesis to plant organs (i.e., leaves, stems, and roots) is often determined by fixed fractions or regulated by functional balance among multiple resources (Luo et al. 1994, Friedlingstein et al. 1999). Soil C is

usually compartmented into a couple of C pools, such as litter pools, soil fast and slow C pools (Fig. 2). Carbon transfers among pools are generally governed by pool size and specific transfer coefficients as affected by environmental variables (Luo et al. 2001).

Model intercomparison and data-model comparison studies show tremendous variation among models for either short-term forecasts or long-term projections even if models are calibrated against historical and/or contemporary conditions (e.g., Friedlingstein et al. 2006, Sitch et al. 2008), although most biogeochemical models share a similar structure. High uncertainties of model projections generally result from differences in less understood processes, initial values, model parameterizations, and response functions that link those key carbon processes to environmental and biological variables. For example, using the observed soil carbon content as model initial values could lead to a higher carbon accumulation rate than the assumption of equilibrium state over 100-year simulations in a beech forest (Wutzler and Reichstein 2007). Knorr and Heimann (2001) illustrated that the uncertainties of key parameters were too large for reliable predictions of global net primary production (NPP). Burke et al. (2003) found the response functions that represent the sensitivities of litter decomposition to temperature differed dramatically after comparing eight widely used biogeochemical models. Water limitations to C processes, the coupling of nitrogen and C cycles, and effects of disturbances on ecosystems are represented in recently published models. But, our understanding of these processes is not well developed and incorporation of these processes based on arbitrary algorithms can lead high uncertainties in models.

In this chapter, I review the basic structure and processes of current ecosystem models of the C cycle, and how they deal with the interactions of C processes with water and nutrient cycles. I also discuss model parameterization, validation, and new approaches of data assimilation that currently are being used to improve models and evaluating uncertainties of parameters and model structure.

1.2 Major processes of C cycle in ecosystem models

An ecosystem is usually compartmentalized into a couple of plant, litter, and soil C pools in C cycle modeling (Fig. 2). C cycle is initiated at the assimilation of atmospheric CO_2 by plant leaves by photosynthesis. The assimilated C is then allocated to plant C pools, such as leaves, steps, and roots, with around 50% of C respired by plants. Dead leaves, stems, and roots enter into litter pools. With decomposition of litter, part of the C in litter pools is respired by microbes, the rest becomes soil organic matter and compose soil C pools, which has long residence times and contain most C of terrestrial ecosystems. Soil organic matter is decomposed slowly, releasing CO_2 to atmosphere as heterotrophic respiration. These processes can be represented by a first-order differential equation (Luo et al. 2003):

$$\begin{cases} \dfrac{d}{dt}X(t) = \xi ACX(t) + BU(t) \\ X(t=0) = X_0 \end{cases} \qquad (1.1)$$

where $U(t)$ is the photosynthetically fixed carbon and usually estimated by canopy photosynthetic models, B is a vector of partitioning coefficients of the photosynthetically

fixed carbon to non-woody biomass and woody biomass, $X(t)$ is a vector of carbon pool sizes, X_0 is a vector of initial values of the carbon pools, A and C are carbon transfer coefficients between plant, litter, and soil pools. ξ is an environmental scalar representing effects of temperature and moisture on the carbon transfer among pools.

For a carbon cycle model as depicted in Fig. 1.2, the vector of allocation coefficients can be expanded to $B = (b_1 \quad b_2 \quad b_3 \quad 0 \quad 0 \quad 0 \quad 0 \quad 0)^T$, where b_1, b_2, and b_3 are partitioning coefficients of photosynthetically fixed C into foliage, woody, and fine root pools, respectively. $X(t) = \left(x_1(t), \quad x_2(t), \quad .... \quad x_8(t)\right)^T$ is a 8×1 vector describing C pool sizes, A and C are 8×8 matrices describing transfer coefficients and given by:

$$A = \begin{pmatrix} -1 & 0 & 0 & 0 & 0 & 0 & 0 & 0 \\ 0 & -1 & 0 & 0 & 0 & 0 & 0 & 0 \\ 0 & 0 & -1 & 0 & 0 & 0 & 0 & 0 \\ f_{41} & f_{42} & f_{43} & -1 & 0 & 0 & 0 & 0 \\ f_{51} & f_{52} & f_{53} & 0 & -1 & 0 & 0 & 0 \\ 0 & 0 & 0 & f_{64} & f_{65} & -1 & f_{67} & f_{68} \\ 0 & 0 & 0 & 0 & f_{75} & f_{76} & -1 & 0 \\ 0 & 0 & 0 & 0 & 0 & f_{86} & f_{87} & -1 \end{pmatrix}$$

$$C = diag(c)$$

where f_{ij} is the transfer coefficients from pool j to pool i, $diag(c)$ denotes the diagonal matrix with diagonal components given by elements of vector $c = (c_1, c_2, ..., c_8)^T$, and $c_j, (j = 1,2,...8)$ represents transfer coefficients (i.e., exit rates of carbon) from the eight carbon pools $X_j, (j = 1,2,...8)$. The initial value vector can be expanded to $X_0 = \left(x_1(0), \quad x_2(0), \quad .... \quad x_8(0)\right)^T$.

1.2.1 Photosynthesis models

Photosynthesis at leaf level for C_3 plants is usually simulated using Farquar model (Farquar 1980). The major processes of photosynthesis include the light reaction, carboxylation, and photosynthetic carbon reduction (Calvin cycle). Stomata aperture controls the rates of CO_2 and water exchange between leaf and bulk air, and therefore photosynthesis rate. The complexity of a photosynthesis model depends on the aims of the study and available data. At regional or global scales, light use efficiency (LUE) is used to simulate photosynthesis (GPP), such as in CASA model, when remote sensing data is available. Photosynthesis is controlled by photosynthetically active radiation, temperature, water availability, VPD, and nitrogen in leaves.

The Farquhar model calculates gross leaf CO_2 assimilation rate (A, μmol CO_2 m^{-2} s^{-1}) as:

$$A = \min(J_c, J_e) - R_d \tag{1.2}$$

where J_c is the rate of carboxylation with CO_2 limitation, J_e is the rate of light electron transport, and R_d is dark respiration. The leaf-level photosynthesis is determined by the one with the lowee rate of the two processes. The rate of carboxylation is calculated by the following equation.

$$J_c = V_m \frac{C_i - \Gamma_*}{C_i + K_C\left(1 + {O_x}/{K_o}\right)} \tag{1.3}$$

And, the light electron transport process (J_e) is:

$$J_e = \frac{\alpha_q \cdot I \cdot J_m}{\sqrt{J_m^2 + \alpha_q^2 \cdot I^2}} \cdot \frac{C_i - \Gamma_*}{4 \cdot (C_i + 2\Gamma_*)} \tag{1.4}$$

where C_i is the leaf internal CO_2 concentration (μmol CO_2 mol^{-1}), O_x is oxygen concentration in the air (0.21 mol O_2 mol^{-1}), V_m is the maximum carboxylation rate (μmol CO_2 m^{-2} s^{-1}), Γ_* is CO_2 compensation point (μmol CO_2 mol^{-1}), K_c and K_o are Michaelis-Menten constants for carboxylation and oxygenation, respectively, (μmol CO_2 mol^{-1}), I is absorbed photosynthetically active radiation (PAR, μmol m^{-2} s^{-1}), α_q is quantum efficiency of photon capture (mol mol^{-1} photon), J_m is the maximum electron transport rate (μmol CO_2 m^{-2} s^{-1}). The leaf internal CO_2 concentration, C_i, is regulated by stomatal conductance (G_s) and related to leaf photosynthesis by:

$$A_n = G_s \cdot (C_a - C_i) \tag{1.5}$$

and

$$G_s = g_l \cdot \frac{A}{(C_i - \Gamma_*) \cdot \left(1 + \frac{D}{D_0}\right)} \tag{1.6}$$

where C_a is ambient CO_2 concentration, g_l and D_0 (kPa) are empirical coefficients and D is vapor pressure deficit (kPa). The parameters, V_m, Γ_*, K_c, K_o, J_m, and R_d, are sensitive to temperature. The temperature sensitivities of these parameters can be expressed by Arrhenius equation (Farquhar et al. 1980) (Eqn 1.7).

$$P = P_{25} \cdot \exp\left(\frac{E_p \cdot (T_k - 298)}{R \cdot T_k \cdot 298}\right) \tag{1.7}$$

where P is any one of the temperature sensitive parameters, E_P is the activation energy (J mol^{-1}), R is universal gas constant (8.314 J K^{-1} mol^{-1}), T_k is canopy temperature in Kelvin (K), P_{25} is the rate at 25 °C.

When leaf photosynthesis is scaled up to the canopy level, the gradients of solar radiation, water vapor pressure, and nitrogen distribution within a canopy are considered. The penetration of solar radiation through canopies can be described by Beer's law (Monsi and Saeki 1953) as:

$$I = I_0 \exp(-kL) \tag{1.8}$$

where I is the radiation at leaf area index L, I_0 is the solar radiation at the top of canopy, k is light extinction coefficient. Water vapor pressure is different for the leaves within a canopy. Canopies can slow down wind speed and decrease boundary layer conductance, leading to changes in the microclimate of leaves in canopies. The photosynthetic capability as related to nitrogen concentration of leaves differs with their positions in a canopy. Usually, nitrogen is distributed in proportion to the distribution of absorbed irradiance in canopy when there are no other limitations (Ryan et al. 2006).

Many models have been developed to scale up photosynthesis from the leaf to the canopy level based on canopy structure and gradients of environmental factors. These models can be categorized into big-leaf (single layer) models, two-leaf models, and multi-layer models according to how canopy structure is represented and the environmental gradients are treated. The single-layer models take the whole canopy as one "big leaf", by assuming all the leaves in a canopy are the same and have the same water conditions (i.e., the humidity of air in the canopy are the same). The integration of leaf photosynthesis only considers the gradient of solar radiation (Sellers et al. 1992). The photosynthesis rate (carbon assimilation rate) at canopy level is thus calculated by

$$A_c = A_n \frac{1-\exp(-kL)}{k} \quad (1.9)$$

where A_c is canopy photosynthesis rate, A_n is net photosynthesis rate at leaf level.

Multi-layer models consider the different properties of leaves and the gradients of solar radiation and microclimatic conditions in canopies by separating a canopy into many layers and calculating water and carbon fluxes at each layer according to its physiological properties and climatic conditions (Leuning et al. 1995). The distribution of nitrogen in canopies is optimized for maximizing photosynthesis according to the gradient of solar radiation. The "two-leaf" models simplify the multi-layer models by separating leaves into two classes, sunlit and shaded, thereby integrating photosynthesis in these two classes of leaves individually (De Pury and Farquhar 1997). For the leaves in a canopy, the shaded leaves have a linear response to radiation, while the sunlit leaves are often light saturated, and independent of irradiance, which allows averaging of solar radiation in sunlit and shaded leaves separately and therefore many numerical integrations can be solved analytically. The separation of sunlit and shade leaves is based on the structure of canopy and the angles of solar radiation (de Pury and Farquhar 1997).

The single-layer models overestimate photosynthesis rate and transpiration. These biases are usually corrected by adding curvature factors or tuning parameters. Single-layer models are appropriate when the details of canopy structure and its microclimate can be ignored, such as when vegetation is taken as a lower boundary of the atmosphere in GCMs or when the system has a much larger scale than the vegetation itself. Multi-layer models have the flexibility to incorporate the details of canopy

environmental physiological variables, but their complexity and demands of calculations limit their application at large scales. “Two-leaf” models can be as accurate as multi-layer models, are are much simpler. They are widely used in current ecosystem and earth system models.

1.2.2 Allocation of photosynthate to plant C pools

The carbon assimilated through photosynthesis is allocated into leaves, wood, and roots. Allocation coefficients are usually fixed as vector B in Eqn (1.1) because there are not enough data for modeling the factors controlling allocation in biogeochemical models (Hirsch et al., 2004). The relative C ratios are calibrated to be reasonable by tuning the parameters of allocation ratios and turnover rates of the plant C pools.

In dynamic global vegetation models (DGVMs), a couple of rules are employed to define the physiognomy of plant functional types (PFTs) and constrain C allocation among the three plant C pools. As in LPJ-DGVM (Sitch et al. 2003), four rules are used. The pipe model (Shinozaki et al. 1964) is used to determine the relative areas of plant leaves to sapwood cross sectional area.

$$LA = k_{la:sa} SA \qquad (1.10)$$

The C investment to leaves and fine roots is regulated by the availability of soil water and nutrients. Water or nutrient- limited environments require more C to be allocated to fine root. This relationship is controlled by the following equation.

$$C_{leaf} = lr_{\max} f(\omega, N) C_{root} \qquad (1.11)$$

The height of a tree and its stem diameter is represented by

$$H = k_1 D^{k_2} \quad (1.12)$$

The relationship between crown area and stem diameter is represented by the inversion of Reinecke's rule (Zeide, 1993).

$$CA = k_3 D^{k_4} \quad (1.13)$$

where LA is the average individual leaf area (m^2), SA (m^2) is the sapwood cross area, and $k_{la:sa}$ is a constant. C_{leaf} and C_{root} are C content of leaves and fine roots, respectively. lr_{max} is the maximum leaf/root ratio. $f(\omega,N)$ is a scalar, which is a function of soil moisture (ω), and nitrogen availability (N). k_1, k_2, k_3, and k_4 are experimental parameters.

1.2.3 Litter and soil carbon decomposition

Litter pools contain withered leaves, dead woods and roots. Litter production is a process transferring carbon from plant tissues to soil carbon. It is simulated by intrinsic turnover rate of live plant carbon pools (e.g., foliage, woody, and fine roots), and regulated by environmental variables, such as temperature and soil moisture. Litter is accumulated and decomposed, and then transferred to soil as organic matter.

The decomposition of litter and soil C releases C back to atmosphere as CO_2 and transfers C among litter and soil C pools. A first order differential equation is used to model litter and soil C decomposition (Reichstein et al. 2000; Knorr et al. 2005; Giardina and Ryan 2000).

$$dc(t)/dt = -k(T) \cdot c(t) \quad (1.14)$$

where $c(t)$ is the carbon content at time t. $k(T)$ is the turnover rate at temperature T.

The temperature sensitivity of soil organic matter (SOM) is important because it determine the feedbacks between terrestrial C cycling and climate change. There is no consensus whether the temperature sensitivity differs between labile and recalcitrant C (e.g. Giardina and Ryan 2000; Davidson et al. 2000; Knorr et al. 2005; Fang et al. 2005). Soil incubation is a usual way to examine the dynamics of soil carbon decompositions at different temperatures. The temperature sensitivity of decomposition (k(T)) can be estimated in many ways. Usually it is represented by Q_{10}, which is the factor by which the decomposition rate increases with a 10 °K warming. The Q_{10} equation is as following (Reichstein et al. 2000, Fang et al. 2005, Fierer et al. 2005, Holland et al. 2000)

$$k(T) = k_{ref} Q_{10}^{\frac{T-T_{ref}}{10}} \qquad (1.15)$$

where, T is temperature.

The temperature sensitivity (Q_{10}) is usually calculated by the following equation (Reichstein et al. 2000; Fissore et al. 2009):

$$Q_{10} = (R_w / R_c)^{\left(\frac{10}{T_w - T_c}\right)} \qquad (1.16)$$

where, R_w and R_c are respiration rates at a warmer temperature (T_w) and colder one (T_c), respectively. In this equation, it is assumed that carbon content and quality of the incubated samples at the two temperature levels are the same over time.

The respiration rates measured from the incubated samples at different temperature levels are also fitted to an exponential model (Fang et al. 2005; Fierer et al. 2005):

$$R(T) = R_{ref} \cdot e^{kT} \quad (1.17)$$

Then, Q_{10} is calculated as:

$$Q_{10} = e^{10k} \quad (1.18)$$

The kinetic equation (Palmer et al. 1996; Knorr et al. 2005; Fissore et al. 2009) is more realistic in representing the temperature sensitivity of decomposition.

$$k(T) = A \cdot \exp(\frac{-E}{RT}) \quad (1.19)$$

where, E is the activation energy, R the universal gas constant, T is temperature, and A is the theoretical decay rate at E=0. According to this equation, Q_{10} is

$$Q_{10} = \exp\left(\frac{E}{R} \cdot (\frac{1}{T} - \frac{1}{T+10})\right) \quad (1.20)$$

Thus, the value of Q_{10} in the kinetic equation is dependent on the quality of soil organic matter (SOM) (represented by its activation energy E) and temperature (T). SOM with low quality has a high Q_{10} because of its high E and the value of Q_{10} is also inversely related to the temperature at which it is measured.

Soil carbon is classified according to its turnover time: fast, slow , and passive C pools. Three or four carbon pools are usually classified depending on data and the questions addressed. The CENTRURY model has three soil C pools (Parton et al., 1986), while the Roth-C model has four (Jenkinson, 1990). It is well established that SOM should be classified into at least two pools, labile and recalcitrant carbon pools (Kätterer et al. 1998; Davidson and Janssens 2006). Using multiple carbon pools can avoid the

assumption that the soil carbon content and quality at different temperature levels are the same at measurement time *t*.

Table 1.1 Governing functions in ecosystem models

Name	Equation	Ecosystem processes
Resource limited rates	$J = Min(J_1, J_2, J_3,...)$	Resource limited ecological processes, e.g., photosynthesis, plant growth, evapotranspiration, etc.
First-order differential equation	$dc(t)/dt = -k(T) \cdot c(t)$	Decomposition of soil C pools
Piecewise function	$J = \min(1, 0.33W)$	Responses to limited resources
Michaelis-Menten kinetics	$V_c = V_{c\max} \frac{C_i}{C_i + K_m}$	Photosynthesis
Arrhenius equation	$k(T) = A \cdot \exp(\frac{-E}{RT})$	Temperature sensitivity of enzymatic responses
Richards equation	$W = A(1 - be^{-t/\tau_1})^k$	Plant growth or ecosystem recovery
Power equation	$F = aM^b$	Metabolic rates, functional rates and biomass

Overall, current ecosystem models have quite similar model structures because they are simulating the same system. A handful of equations are repeatedly used in simulating ecosystem processes (Table 1.1). For example, $J = Min(J_1, J_2, J_3,...)$ is used to simulate multi-resource limited processes such as photosynthesis, rates of multi-element biogeochemical cycles. The Michaelis-Menten kinetics equation is used to represent enzymatic reactions, which can be saturated by substrates. The Arrhenius

equation is used to simulate biological responses to temperature. Richards and logistic equations are used to represent temporal development of C storage and fluxes. These equations represent the basic principles of ecological and biological responses to environmental factors.

1.3 Key issues in ecosystem C cycle modeling

Though the basic principles have been well established and accepted in ecosystem C cycle modeling, there are still many problems in modeling ecosystem C processes when considering the coupling with other element cycles, model calibration and validation, and disturbance effects modeling. We chose one problem from each one of these three issues to explore how they happen and the possible solutions.

1.3.1 Interactions between carbon and water dynamics at different soil conditions

Water conditions have profound effects on ecosystem C cycle by affecting photosynthesis, allocation of assimilated C, plant mortality, and plant community structure. Most models use vapor pressure deficit (VPD) or soil moisture index to limit the rate of photosynthesis and thus indirectly affect C processes following photosynthesis. Plant-water interactions are not well represented in current ecosystem models since ecosystem responses to water are diverse and there are no general equations to describe those relationships (Katul et al. 2007).

Soil stores precipitation water for plant use over time and regulates partitioning of precipitation between alternative outflows such as runoff, evaporation, and transpiration (Rodriguez-Iturbe and Porporato, 2004). The capability of soil to store water is mainly determined by soil texture and quantified by a soil moisture release curve. Two points of the soil moisture release curve are particularly important: field capacity and permanent wilting point. The difference between field capacity and wilting point defines available water capacity (AWC), the amount of water that is available for plants.

Soil hydrological properties likely regulate ecosystem responses to global change. General circulation models forecast a higher frequency of extreme rainfall events, a lower frequency of rainfall days, and longer intervening dry periods (Easterling et al., 2000). Global warming and elevation of atmospheric [CO_2] also alter ecosystem water availability. Warming usually induces drought by increasing evapotranspiration (Wan et al., 2002), leading to higher possibility of drought stress to ecosystems (Harte et al., 1995). Elevated CO_2 reduces leaf stomatal conductance, increases soil moisture, and decreases water stress for plant growth (Knapp et al., 1993; Owensby et al., 1999; Morgan et al., 2004; Moore and Field, 2006). However, the role of soil hydrological properties in regulating ecosystem responses to climate warming and elevated CO_2 via soil water dynamics has not been carefully examined.

1.3.2 Data assimilation approach to verify information contribution of ecosystem models

To improve models for accurate projections and representations of ecosystem processes, data assimilation approaches have recently been developed in ecology to inform initial conditions, constrain parameters, evaluate alternative response functions, and assess model uncertainties (Raupach et al. 2005, Williams et al. 2009). Most data assimilation studies focused on estimation of fast-response parameters, i.e., photosynthesis, respiration and evapotranspiration with short-term data sets (e.g., Knorr and Kattge 2005, Wang et al. 2007, Wu et al. 2009, and Braswell et al. 2005) A few data assimilation studies have been conducted to constrain long-term processes and parameters with simplified carbon cycle models (e.g., Luo et al. 2003, Xu et al. 2006, Williams et al. 2005, and Fox et al. 2009). However, since biogeochemical models are often used to evaluate ecosystem responses to climate changes at decadal and century time scales (e.g., Fung et al. 2005, Friedlingstein et al. 2006, Jones et al. 2006), one key question that has not been addressed is how much improvement data assimilation can make for short- vs. long-term forecasts of ecosystem carbon sequestration.

1.3.3 Disturbance effects on C cycles

Human activities have exerted strong influences on ecosystems by starting or suppressing natural fire, changing land use, or harvesting. These activities have changed the land surface deeply, altered ecosystem states and brought many environmental

problems, which affected human welfare and living conditions. For evaluating the effects of human activities on ecosystems, and developing better management approaches, many studies have been conducted to reveal the processes and mechanisms of ecosystem responses to anthropogenic disturbances and management. Models provide a platform to synthesize known ecological mechanisms and available data and models also work well in extrapolating our understanding of ecosystems and disturbances at longer time scales and broader spatial extents. Simulation models also enable us to evaluate complicated interactions among the processes of ecosystems (Burke et al. 2003).

Modeling approaches have been widely used to analyze mechanisms of ecological responses to disturbances, evaluate effects of management on disturbances, and estimate current ecosystem states by multiple datasets. Wutzler and Reichstein (2007) simulated soil carbon dynamics and carbon accumulation when soil is apart from equilibrium by Yasso model (Liski et al., 2005). They showed that carbon storage capacity of disturbed forest soils was potentially much higher if current soil carbon was not assumed to be in equilibrium state. This study showed the importance of informing terrestrial ecosystem initial states in evaluating the capacity of ecosystem carbon storage. Balshi et al. (2007) used the TEM model to explore the roles of historical fire in carbon dynamics in the pan-boreal region. Their analysis indicated that fire played an important role in interannual and decadal scale variation of source/sink relationships of northern terrestrial ecosystems and also suggested that it was important to consider changes in climate and fire disturbance in studying effects of atmospheric CO_2. They pointed out that there are

substantial uncertainties in the effects of fire on carbon storage in simulations. The Biome-BGC model was used to produce a carbon budget for the forested region of Oregon, and to determine the relative influence of differences in climate and disturbance among the ecoregions on carbon stocks and fluxes (Law et al., 2004). An ecosystem demography model was used to quantify the contributions of disturbance history, CO_2 fertilization and climate variability to the past, current, and future terrestrial carbon fluxes in the Eastern United States (Albani, et al., 2006). It was found that tropical and temperate forests are carbon sink. However, it is not clear that if it is due to increases in atmospheric CO_2 concentration or the recovery from historic disturbances.

These modeling efforts to link specific disturbance events with ecosystem processes to characterize and project ecosystem C dynamics have been conducted to reveal the mechanisms by which disturbances affect C processes and possible changes in C dynamics in the future. Models are used to count these effects and/or extrapolate them to a large spatial or temporal scale. Prescribed fire events and effects on ecosystems are needed. We still lack a macroscopic equation to describe effects of disturbances on ecosystem C processes.

1.4 Studies conducted in this dissertation

Three studies were conducted in this dissertation to explore the problems of representation of ecological processes, how information of observed data and model reasoning were synthesized in a data assimilation approach, and how disturbance affect

ecosystem C storage at large spatial scales. In the first study (Chapter 2), I used a comprehensive ecosystem model of C and water processes to explore the roles of soil water dynamics in ecosystem response to warming and elevated CO_2 with different soil conditions. In the second study (Chapter 3), I used a highly simplified C-pool model (eight C pools) to quantify model uncertainty and information contribution to model predictions by model and data with a data assimilation approach. In the third study (Chapter 4), I developed a stochastic method to represent disturbance effects on ecosystems and their C storage, which can improve our predictive understanding of C dynamics with changes in disturbance regime. These studies improve our insights on the interactions of ecosystem processes and model validation, and highlight the importance of new theories in ecosystem modeling.

CHAPTER 2 Soil hydrological properties regulate grassland ecosystem responses to multifactor global change: a modeling analysis[1]

[1]This part has been published in Journal of Geophysical Research – Biogeosciences doi:10.1029/2007JG000539

Abstract:

We conducted a modeling study to evaluate how soil hydrological properties regulate grassland ecosystem water and carbon dynamics in response to altered precipitation amount and frequency, increased temperature, elevated atmospheric [CO_2] with changes in soil available water capacity (AWC). In this study, we used a process-based terrestrial ecosystem (TECO) model, which was calibrated against data from two experiments with warming and clipping or doubled precipitation in Great Plains. The model was used to simulate responses of soil moisture, evaporation, transpiration, runoff, net primary production (NPP), ecosystem respiration (R_h), and net ecosystem production (NEP) to changes in precipitation amounts and intensity, temperature, and CO_2 concentration along a soil texture gradient (sand, sandy loam, loam, silt loam, and clay loam). Simulation results showed that soil AWC altered partitioning of precipitation among runoff, evaporation, and transpiration, and consequently regulated ecosystem responses to global environmental changes. Fractions of precipitation that were used for evaporation and transpiration increased with soil AWC but decreased for runoff. High AWC could greatly buffer water stress during long drought periods, particularly after a large rainfall event. NPP, R_h, and NEP usually increased with AWC under ambient and 50% increased precipitation scenarios but increased from 7% to 7.5% of AWC followed by declines under the halved precipitation amount. Warming and CO_2 effects on soil moisture, evapotranspiration, and runoff were

magnified by soil AWC. Regulatory patterns of AWC on responses of NPP, R_h, and NEP to warming were complex. In general, CO_2 effect on NPP, R_h, and NEP increased with soil AWC. Our results indicate that variations in soil texture may be one of the major causes underlying variable responses of ecosystems to global changes observed from different experiments.

Keywords: global change, grassland ecosystems, available water capacity, soil moisture, TECO model

2.1 Introduction:

Increased atmospheric concentration of carbon dioxide ($[CO_2]$) has resulted in increase in global surface temperature and altered precipitation regimes (IPCC, 2001). Many experimental and modeling studies have shown that terrestrial ecosystems have diverse responses to climate change. Experimental warming in a range of 0.3~6.0°C, for example, significantly increased soil respiration rates by 20% and plant productivity by 19% with considerable variation among individual sites (Rustad et al., 2001). Meta-analyses of data published in the literature about ecosystems responses to elevated $[CO_2]$ reveals a wide range of responses to increases in atmospheric $[CO_2]$ (Jastrow et al., 2005; Luo et al. 2006), from no biomass responses in alpine grasslands (Körner et al., 1997) and in the sub-humid tall grass prairie for wet years (Owensby et al., 1999), to

consistent and substantial production responses in semi-arid shortgrass steppe (Morgan et al., 2004). How to explain the variations in observed terrestrial ecosystem responses to climate change has been a great challenge in the research community.

Various ecosystem responses to global change may be partially caused by soil hydrological properties for at least two reasons. First, soil water availability strongly regulates plant growth and primary productivity for most terrestrial ecosystems, particularly in arid and semi-arid regions (Schulze et al., 1987). Second, all global change factors, such as climate warming, rising atmospheric CO_2 concentration, and altered precipitation intensity and frequency, induce changes in soil water availability (Niklaus et al., 1998; Wan et al., 2002) and, therefore, indirectly affect plant and ecosystem processes (Saleska et al., 1999; Shaver et al., 2000; Morgan et al., 2004; Luo, 2007). However, how soil hydrological properties regulate ecosystem responses to global change factors, to the best of our knowledge, has not been well examined.

Soil stores precipitation water for plant use over time and regulates partitioning of precipitation between alternative outflows such as runoff, evaporation, and transpiration (Rodriguez-Iturbe and Porporato, 2004). The capability of soil to store water is mainly determined by soil texture and quantified by soil moisture release curve. Two points of the soil moisture release curve are particularly important: field capacity and permanent wilting point. The difference between field capacity and wilting point defines available water capacity (AWC), the amount of water that is available for plants. Soil texture varies greatly over spatial scales (Miller and White, 1998). In the Northern Territory, Australia,

for example, along the precipitation gradient from north to south, predominant soils in the wetter end of a precipitation gradient are loams and sands, and clay soils are more extensive in the drier sectors of the gradient (Williams et al., 1996). At a local scale, soil texture varies dramatically with landform (Rosenbloom et al., 2001). Variation in soil texture creates diverse soil moisture environments in an area even with the same amount of precipitation. In dry regions, for example, soil evaporation is lower in sandy soils than that in loamy soils (Buckman and Brady, 1960).

This diversity in soil hydrologic properties and water environments results in considerably diverse plant production and ecosystem function (McAuliffe, 2003). Among the most noticeable hypotheses is the inverse-texture hypothesis (ITH) by Noy-Meir (1973) that production is greater on coarse-texture soils than that on fine-texture soils in dry regions because the water availability will be high at coarse soil in dry regions. The hypothesis has been supported by many studies (e.g. Sala, 1988; Lane et al., 1998; Epstein et al., 1997). In the central grassland region of the United States, sandy soil with low AWC is more productive than loamy soil with high AWC when annual precipitation is less than 370 mm. However, sandy soil is less productive than loamy soil when precipitation is more than 370 mm according to the observations of central grassland region of the United States (Sala et al., 1988).

Soil hydrological properties also likely regulate ecosystem responses to global change. General circulation models forecast a higher frequency of extreme rainfall events, a lower frequency of rainfall days, and longer intervening dry periods (Easterling

et al., 2000). It is well known that changes in precipitation directly alter soil water content and dynamics. An experimental study has demonstrated that increased temporal variability in precipitation and soil moisture increased plant water stress and reduced plant productivity (Knapp et al., 2002). It is not clear whether this experimental conclusion from the Konza prairie reserve is general, regardless of variations in soil hydrological properties and climate scenarios.

Global warming and elevation of atmospheric [CO_2] also alter ecosystem water availability. Warming usually induces drought by increasing evapotranspiration (Wan et al., 2002), leading to higher possibility of drought stress to ecosystems (Harte et al., 1995). Elevated CO_2 reduces leaf stomatal conductance, increases soil moisture, and decreases water stress for plant growth (Knapp et al., 1993; Owensby et al., 1999; Morgan et al., 2004; Moore and Field, 2006). However, the role of soil hydrological properties in regulating ecosystem responses to climate warming and elevated [CO_2] has not been carefully examined. To understand how soil hydrological properties regulate ecosystem responses to climate change, we have to examine inputs, storages and losses of water (Lauenroth and Bradford, 2006).

Grassland ecosystems are one of the most widespread vegetation types worldwide, covering nearly 1/5 of the world's land surface where soil and climatic conditions are diverse (Parton et al., 1995). Many experiments have shown rapid and diverse responses of grasslands to changes in temperature, water, and atmospheric [CO_2] (Zavaleta et al., 2003; Luo, 2007). It is necessary to use wide soil textures and multiple combinations of

climatic scenarios to explore the possible the possible mechanisms of ecosystem responses. In this paper, we conducted a modeling study to evaluate how soil texture regulates ecosystem water and carbon dynamics in response to altered precipitation amount and frequency, climate warming, elevated atmospheric [CO_2] with its hydrological properties. We used a process-based ecosystem model to explore soil water dynamics and carbon processes in five soil texture types. Our modeling study mainly addressed the following two questions. First, how does soil texture regulate partitioning of precipitation among runoff, evaporation, and transpiration? Second, how does soil texture regulate ecosystem responses to changes in precipitation frequency and amount, warming, and elevated atmospheric [CO_2]?

2.2 Material and method:

2.2.1 The Terrestrial ECOsystem (TECO) model

The **TECO** model has evolved from its precursor model TCS (Luo and Reynolds, 1999). It is a process-based ecosystem model and designed to examine critical processes in regulating interactive responses of plants and ecosystems to elevated CO_2, warming, altered precipitation. The detailed description of the TECO model was provided in the appendix. Here is its brief description.

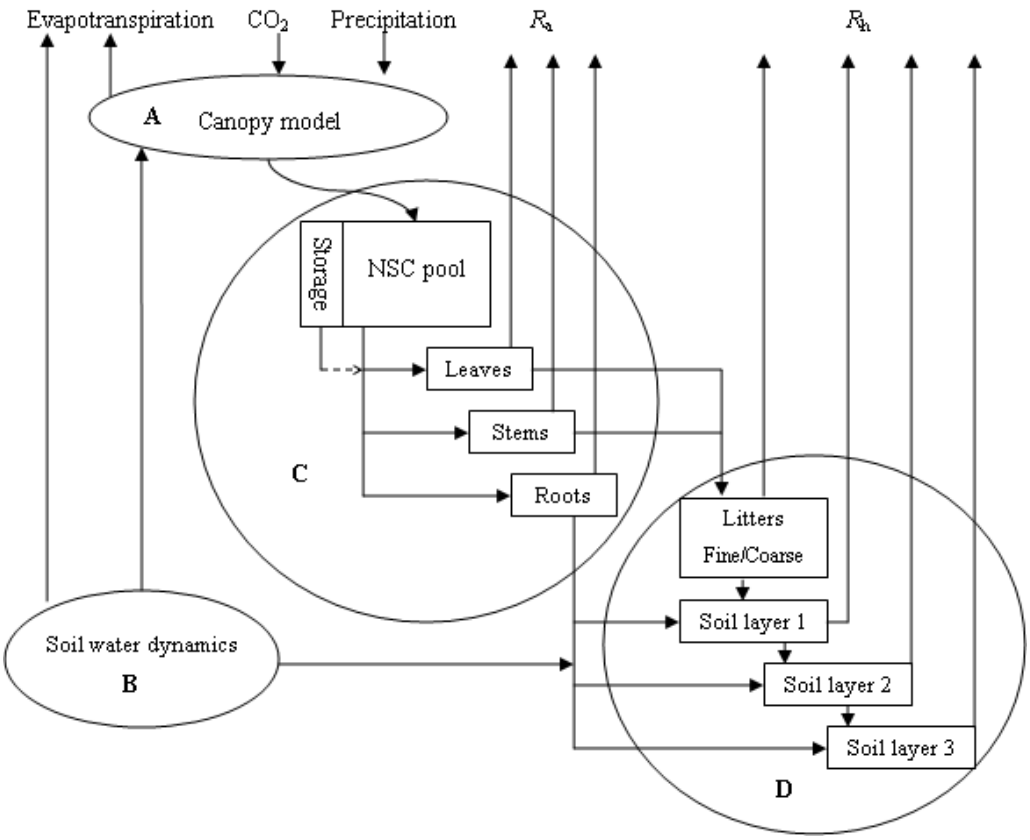

Figure 2.1 Schematic presentation of TECO model. A. Canopy model; B. Soil water dynamics model; C. Plant growth model; D. Carbon transfer model. Rectangles represent the carbon pools. Soil is stratified into three layers. R_a: autotrophic respiration. R_h: heterotrophic respiration, NSC: non-structure carbohydrate.

TECO has four major components: canopy photosynthesis sub-model, soil water dynamic sub-model, plant growth (allocation and phenology) sub-model, soil carbon transfer sub-model (Fig. 2.1). Canopy photosynthesis sub-model and soil water dynamic sub-model run at the hourly step. The plant growth model and soil carbon model run at daily step.

The canopy sub-model is a multi-layer process-based model which mainly evolved from the model developed by Wang and Leuning (1998). It simulates radiation transmission in the canopy based on Beer's law. For each layer, foliage is divided into sunlit and shaded leaves. Leaf photosynthesis is estimated based on the Farquhar photosynthesis model (Farquhar et al., 1980) and a conductance model proposed by Ball et al. (1987). The soil water dynamic sub-model stratifies soil into ten layers. The thickness of the first layer is 10 cm. And, the other 9 layers are 20 cm. Soil water content of these layers is determined by mass balance between water influx and efflux. The water influx is precipitation for the surface layer and percolation for deeper layers. The water efflux includes evaporation, transpiration, and runoff. Evaporation rate is mainly controlled by the water content of the first soil layer and evaporative demand of atmosphere. Transpiration changes the water content of the layers where roots reach.

Plant growth sub-model simulates carbon allocation and phenology following ALPHAPHA model (Luo et al., 1995; Denison and Loomis, 1989) and CTEM (Arora and Boer, 2005), respectively. Allocation of assimilated carbon among the leaves, stems, and roots depends on their growth rates, and varies with phenology. Phenology is represented by annual variation of leaf area index (LAI). Leaf onset is initiated by growing degree days (GDD). Leaf fall is induced by low temperature and soil drought. When LAI is below a certain level (LAI<0.1), the end of growing season comes. Rooting depth and root vertical distribution define the soil volume from which plants could potentially extract water. Most of the grass roots distribute in the soil layers less than 70 cm depth

and the distribution of roots vary little with soil texture and soil moisture profiles (Jackson et al., 1996; Nippert and Knapp, 2007; Singh et al., 1998). Based on patterns illustrated by the experimental data, maximum rooting depth was assumed to be 70 cm, consequently, the maximum rooting depth to the fourth soil layer (50~70 cm). Root vertical distribution was dynamical, which varied with root growth and death in every soil layer. The initial ratios of roots in the four soil layers were set as 40% (0~10 cm), 40% (10~30 cm), 15% (30~50 cm), and 5% (50~70 cm). The variations were limited below 20% of the initial ratios.

Carbon transfer sub-model considers the transfer of carbon from roots and litters to soil and decomposition rates in soil and litter pools (Luo and Reynolds, 1999; Barrett, 2002). In this sub-model, a soil profile is divided into three layers with carbon movement from upper to lower layers. Carbon inputs to the soil from plant residues are partitioned into these three layers.

2.2.3 Model calibration

The TECO model was calibrated against the measured data from the field site of the Kessler Farm Field Laboratory of University of Oklahoma, which is located at the Great Plains Apiaries in McClain County, Oklahoma (34^{o}59' N, 97^{o}31' W), approximately 40 km southwest of the Norman campus of the University of Oklahoma, USA. It is an upland tallgrass prairie dominated mainly by four C_4 grasses. A silt loam soil in the grassland includes 35.3% sand, 55.0% silt, and 9.7% clay. The soil belongs to part of the

Nsh-Lucien complex with high water holding capacity (around 37%) and a deep, moderately penetrable root zone (Zhou et al., 2007). The measured data included soil respiration, soil moisture, above ground and below ground biomass during 2000~2005. The model was driven by the meteorological data from the nearest meteorological station, the MESONET station of Washington, Oklahoma. The soil texture was assigned a field capacity of 37% and a wilting point of 10%. Thus, the available water capacity is 27%. The model was run for 1200 years to reach equilibrium state. And then, the simulated daily soil moisture, soil respiration, and aboveground biomass from 01/01/2000 to 12/31/2005 were output and used to calibrate against the observed data.

Model predictions and observations were contrasted with a number of statistical approaches following Hanson et al. (2004). Linear regression slopes, intercepts, and R^2 outputs were provided as a common initial comparison between observations and predictions. Relative bias (RB) and mean absolute bias (ABS) were used to measure the magnitude of bias and the deviation from the observed values, respectively, which were calculated by the following equations.

$$RB = \frac{\sum(\hat{y}_i - y_i)}{\sum y_i} \times 100 \qquad (2.1)$$

$$ABS = \frac{\sum|\hat{y}_i - y_i|}{n} \qquad (2.2)$$

where, $\hat{y}_i$ is simulated value and y_i is measured value.

2.2.4 Scenarios

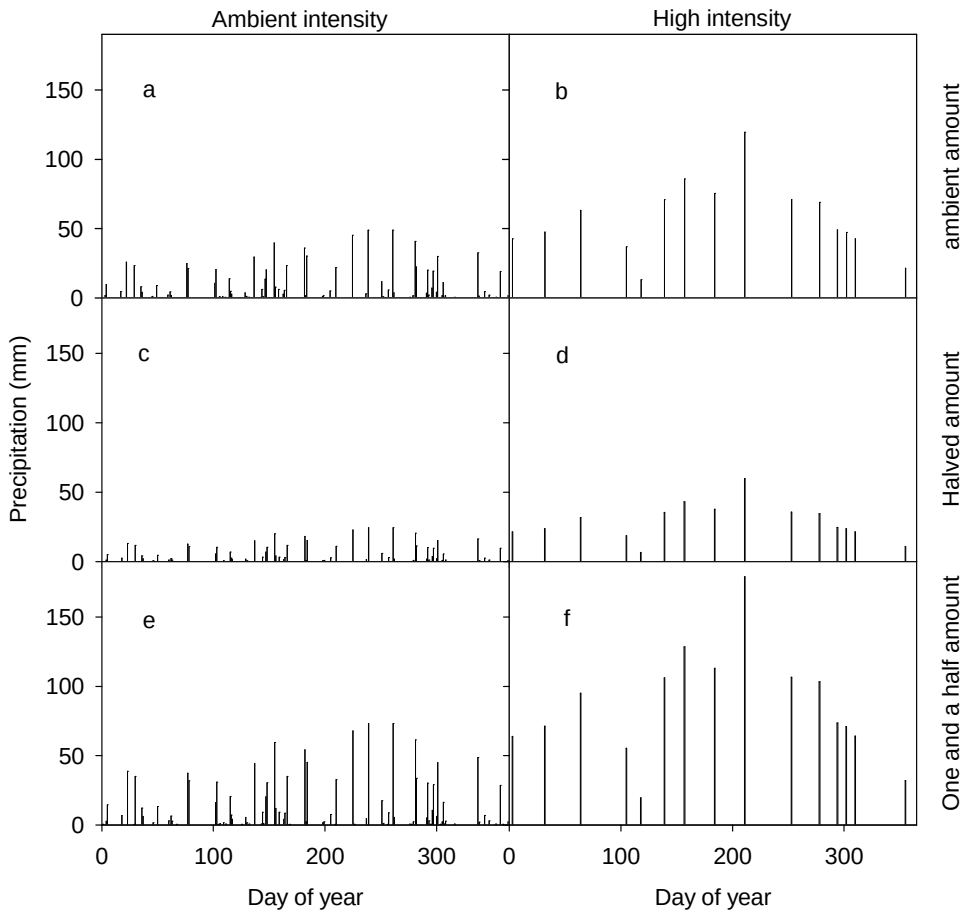

Figure 2.2 Scenarios of precipitation intensity and frequency. a. ambient precipitation (1.0 P); b. precipitation with high intensity (the neighboring 6 times precipitation events were merged into one precipitation) (1.0 P); c. halved precipitation with ambient frequency (0.5P); d. halved precipitation with high intensity (0.5 P); e. one and one half precipitation with ambient intensity (1.5 P); f. one and one half precipitation with high intensity (1.5 P)

The climatic scenarios were set according to current meteorological data, which included the records of temperature, precipitation, solar radiation, soil temperature, and relative humidity. According to the data, the mean annual precipitation was 804 mm

during 2000~2005. The mean number of the days with precipitation in a year was 95. The precipitation from April to October was 582 mm, 72% of the annual precipitation. The highest daily precipitation was 76.7 mm, occurred on Aug. 30th, 2003. Most of the precipitation events were below 10 mm (413 of 568 precipitation events in the six years). The daily precipitation that was above 50 mm only occurred 8 times in the six years. The mean temperature was 16 °C. The highest mean daily temperature was 32 °C, and the lowest mean daily temperature was -9.9 °C in these 6 years.

The meteorological data of 2002 were used as the ambient climatic data. In this year, the total precipitation was 854.5 mm and there were 89 rainfall days, which were treated as 89 rainfall events. The mean precipitation per rainfall event of ambient intensity was 9.6mm. The mean length of intervals between rainfall events was 5 days. The precipitation regime in 2002 was denoted as precipitation with ambient intensity. The scenario of precipitation with high intensity was achieved by merging the neighboring 6 times rainfall events into one. By doing so, the 89 rainfall events were merged to 15 rainfall events. Mean precipitation intensity was 56.9 mm and mean length of intervals between rainfall events increased to 24 days. Based on the frequency of precipitation, we set another 2 precipitation amount levels by timing 0.5 and 1.5 for every rainfall events. Thus, we obtained 3 precipitation amount levels: ambient (854.5mm·yr^{-1}, denoted as 1.0P), halved (427 mm·yr^{-1}, 0.5 P), and one and a half (1283 mm·yr^{-1}, 1.5 P) at ambient frequency and high intensity respectively (Fig.2.2). The mean temperature of 2002 was 15.4 °C. The temperature scenario was achieved by adding 2°C to daily temperatures.

The ambient atmospheric CO_2 concentration ($[CO_2]$) was assumed to be 360 ppm according published literatures (IPCC, 2001). Thus, the doubled $[CO_2]$ was 720 ppm.

Table 2.1 Field capacities, wilting points, and available water capacities of five soil texture types.

Soil texture	Sand	Sandy Loam	Loam	Silt Loam	Clay Loam
Field Capacity (%)	10	15	25	35	45
Wilting Point (%)	5	7.5	10	12	15
Available water capacity (%)	5	7.5	15	23	30

Grasslands have diverse soil texture types. In Central Grassland region of the U.S., the soil texture ranged from sand, sandy loam, to silt loam and silt clay loam and soil water holding capacity ranged from 0.062 to 0.33 g water/g soil (Lane et al., 1998). We assigned five soil texture types to cover the whole range in nature. These soil texture types were sand, sandy loam, loam, silt loam, and clay loam with field capacities ranging from10%to 45% (volumetric water content) and wilting point from 5% to 15%. So, the available water capacities (AWC) for the five soil texture types were 5% (sand), 7.5% (sandy loam), 15% (silt loam), 23% (loam), and 30% (clay loam) (Table 1). Thereafter, AWC would be used as an aggregate variable for soil texture. Usually, soil texture varied slightly with depth (Dodd and Lauenroth, 1997). In scenario designation, for the sake of

simplicity of interpretation of modeling results, all of the soil layers were assumed have the same field capacity and wilting point. Thus, we obtained 120 scenarios in total (Table 2). The model was run 1200 years to reach equilibrium state firstly. And then, the scenarios were used to drive model runs.

Table 2.2 Treatment levels of five variables examined in this study. We used full factorial combinations of all the treatment levels of the five variables to define 120 scenarios to drive model simulations

Variables	Treatments
Precipitation amount	Ambient (1.0P), halved (0.5P), one and one half(1.5P),
Precipitation intensity	Ambient intensity, high intensity
Temperature	Ambient, +2°C increased
CO_2 concentration	Ambient concentration (360 ppm), doubled concentration (720 ppm)
Available water capacity	5%, 7.5%, 15%, 25%, 35%

An index of drought-stressed days was used to show levels of drought stress for plants in a year. It is defined as the number of days with normalized soil moisture below 0.3 in a year. Normalized soil moisture (ω) was defined by equation 3.

$$\omega = \frac{W_{soil} - W_{\min}}{W_{\max} - W_{\min}} \qquad (2.3)$$

where, W_{max} was soil water holding capacity, W_{min} was wilting point, W_{soil} was soil moisture. In TECO model, if ω was below 0.3, photosynthesis and plant growth rate would be stressed.

2.3 Results

2.3.1 Data – model comparison

At equilibrium state, the simulated soil carbon content was around 8500 g·m^{-2}, which agreed with the measured soil carbon content 1.42% well (Luo et al., 2001). The simulated litter was 370 g·m^{-2}, which was very close to the measured value 384 ± 21 g·m^{-2}. The soil moisture dynamics, soil respiration, and aboveground biomass are generally consistent well with measurements too (Fig. 2.3). Simulated soil moisture was correlated with the observed values by $y = 0.72x + 6.6,\ R^2 = 0.50$ (x is observation and y is simulation) with a mean absolute bias (ABS) 5.11 and a relative bias (RB) -2.5%. Simulated soil moisture was slightly higher than the measured values when soil is very dry. Simulated and observed soil respirations had a regression equation $y = 0.83x + 0.77,\ R^2 = 0.57$, and ABS was 0.82 and the RB was 17.6%. In winter, the simulated soil respiration was slightly higher than the measured values. The ABS between simulated and observed aboveground biomass was 0.57 and RB is -3.4 % ($y = 0.43x + 140.36,\ R^2 = 0.57$).

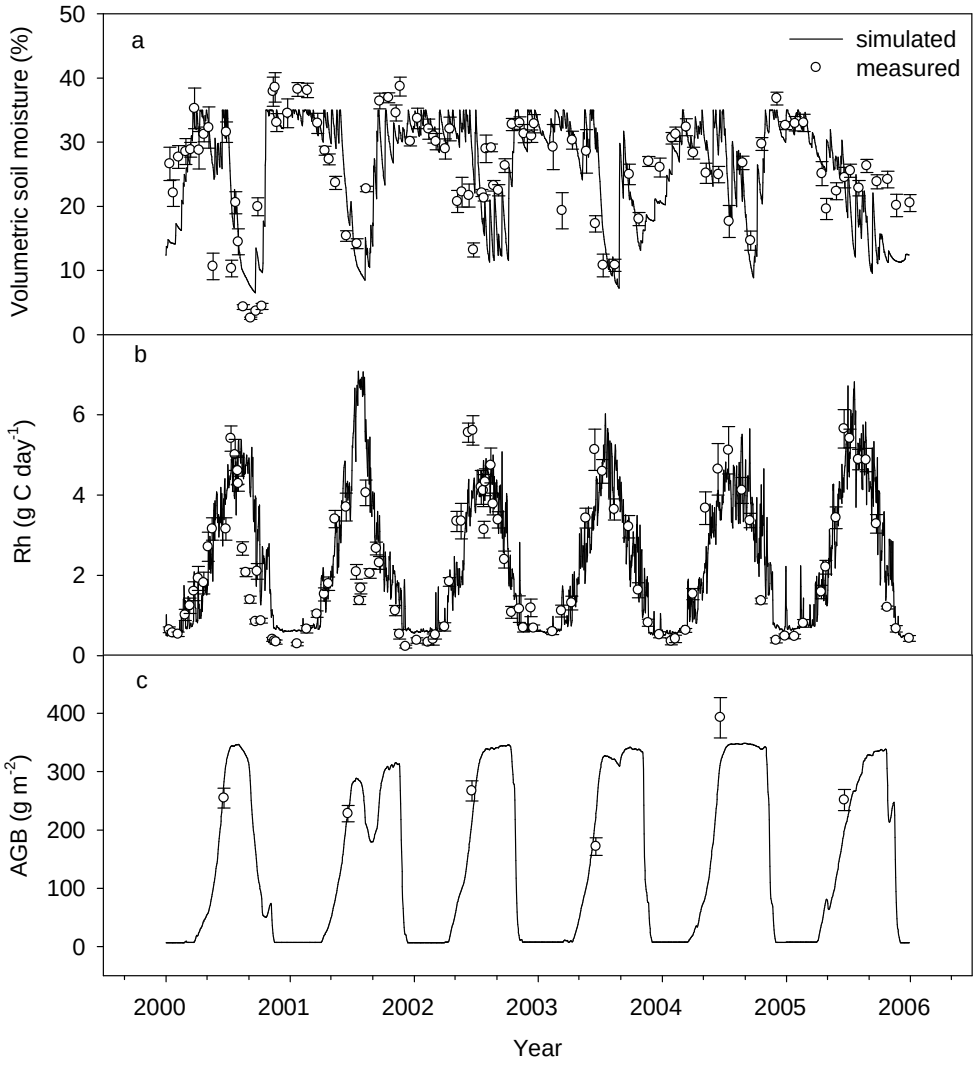

Figure 2.3 Model validations. a. soil moisture; b. soil respiration; c. above-ground biomass. R_h stands for heterotrophic respiration (g C m^{-2}·day^{-1}); AGB stands for above ground biomass (g·m^{-2}). The solid lines show simulated results. The open dots show the measured values.

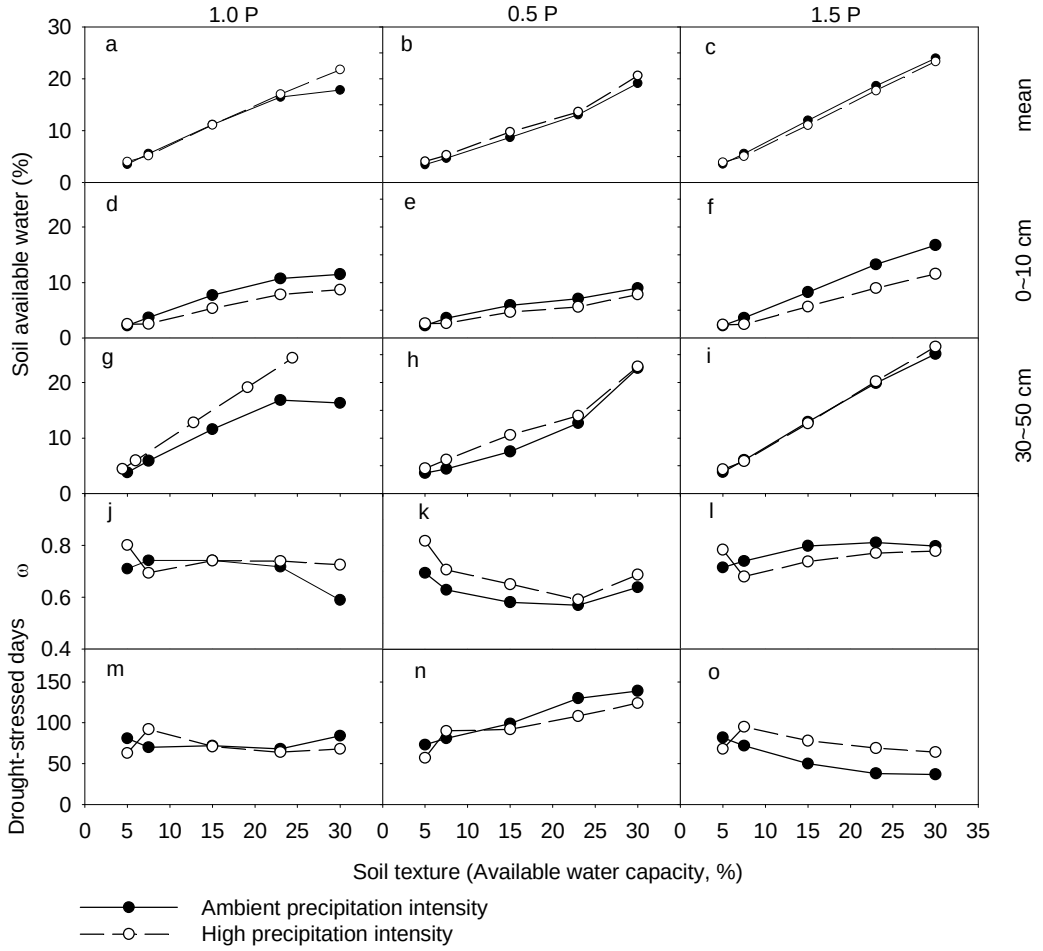

Figure 2.4 The soil available water (the difference between soil water content and wilting point), drought stressed index, and drought-stressed days with available water capacity (the difference between field capacity and wilting point) at three precipitation amount levels and two precipitation frequencies. Filled circles with solid lines represent ambient precipitation frequency. Open circles with dashed lines represent high precipitation intensity. Panels a, b, and c show the mean value of the three layers. Panels d, e, and f show soil available water of the surface layer (0~10 cm). Panels g, h, and i show soil available water of the third layer (30~50 cm). Panels j, k, and l' show normalized soil moisture ($\omega = (\theta - \theta_{\min})/(\theta_{\max} - \theta_{\min})$, where, θ is soil moisture, $\theta_{\max}$ and $\theta_{\min}$ are field capacity and wilting point, respectively). Panels m, n, and o show the drought-stressed days.

2.3.2 Ecosystem responses to changes of precipitation regime with soil texture

The annual mean soil available water (the difference between soil moisture and wilting point, %) increased with soil AWC (difference of field capacity and wilting point, %) under three precipitation scenarios (Fig. 2.4: a-c). The soil available water in deep layers increased with AWC more than that in the surface layer (Fig. 2.4: d-i). In the surface layer, soil available water increased from 3% to 12% with soil AWC, whereas it increased from 5% to 18% in the third layer at the ambient precipitation amount (1.0P) (Fig. 2.4 d and g). The same pattern occurred when precipitation increased by 50% (1.5P) (Fig. 2.4 f and i) or decreased 50% (0.5 P) (Fig. 2.4 e and h). At 1.5 P, the annual mean soil available water at AWC of 23% and 30% was higher than that at 0.5 P or 1.0 P.

The normalized soil moisture showed different patterns with AWC at the three precipitation levels. At 1.0 P, it nearly kept a constant around 0.73 along soil AWC. It decreased from 0.70 to 0.56 at 0.5 P and increased from 0.71 to 0.81 at 1.5 P (Fig. 2.4: j~l). As a consequence, the drought-stressed days showed identical pattern. At 1.0P there were not obvious changes with soil AWC (Fig. 2.4 m). At 0.5 P, drought-stressed days increased from 60 days to 135 days with AWC increasing from 5% to 30% (Fig.4: n). At 1.5P, drought-stressed days decreased from 82 days to 37 days (Fig. 2.4: o).

Precipitation intensity influenced soil moisture along the gradient of soil AWC. With 1.0 P, the annual mean soil available water was lower at ambient than high precipitation intensity when AWC was 30% (Fig. 2.4: a). At 0.5 P, high precipitation

intensity led to higher annual mean soil moisture than that of ambient intensity (Fig. 2.4b). The opposite occurred at 1.5 P. With all three precipitation amount, high precipitation intensity resulted in lower water content in the surface layer than the ambient intensity. While at the same time, high precipitation intensity led to higher soil water content in the deep layer than the ambient intensity at 1.0 P and 0.5 P. At 1.5 P, precipitation intensity showed little effects on soil moisture (Fig. 2.4: i).

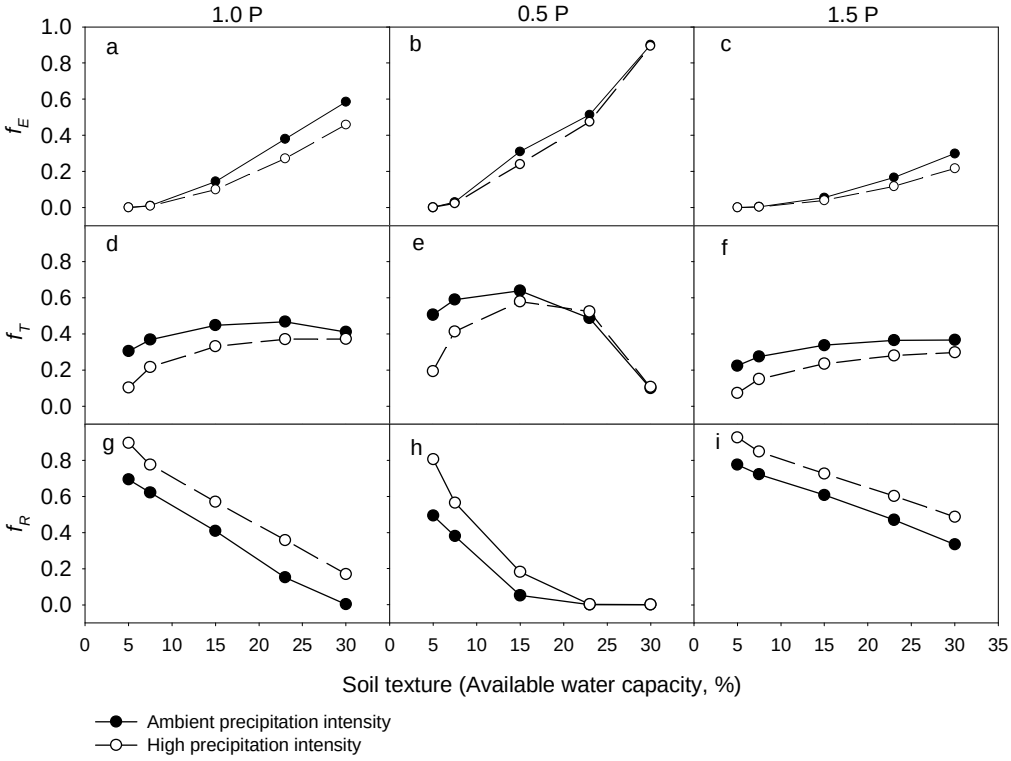

Figure 2.5 Fractions of water loss via Evaporation, Transpiration and Runoff. f_E: Evaporation/Precipitation; f_T: Transpiration/Precipitation; f_R: Runoff/Precipitation; E/ET: the ratio of evaporation to evapotranspiration

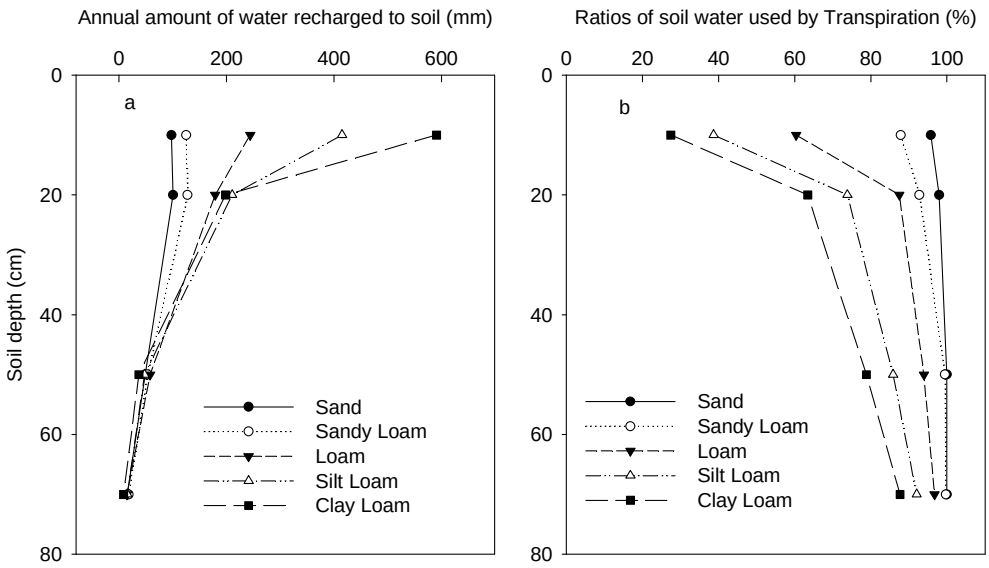

Figure 2.6 The water contributions to transpiration along soil depth by the five soil texture types. (a) The water recharged to soil layers every year, which is equal to the water used by evapotranspiration in these layers at equilibrium state. (b) The ratios of the water transpired through plants in every layer.

The fractions of precipitation used for evaporation and transpiration increased generally with AWC but decreased for runoff (Fig. 2.5). Fractions of precipitation used for evaporation increased continuously with AWC (Fig. 2.5 a, b, and c). Transpiration increased with soil AWC at its low range and gradually leveled off at the high range of AWC at the 1.0 P and 1.5 P precipitation amounts (Fig. 2.5 d and f). At 0.5 P, transpiration increased firstly, and then decrease sharply at the AWC of 23% and 30% (Fig. 2.5e). Runoff decreased with soil AWC continuously (Fig. 2.5 g~i). At 0.5 P, runoff approached to 0 at the 23% of AWC. In general, high precipitation intensity led to higher runoff, lower evaporation and transpiration than the ambient precipitation intensity with

the three precipitation amounts. The vertical distribution of the water recharged to soil could explain the changes in partitioning between transpiration and evaporation with AWC. With increase of soil AWC, more water was recharged to the surface layer (Fig. 2.6a), and the ratio of the water in these layers used by transpiration decreased with AWC (Fig. 2.6b).

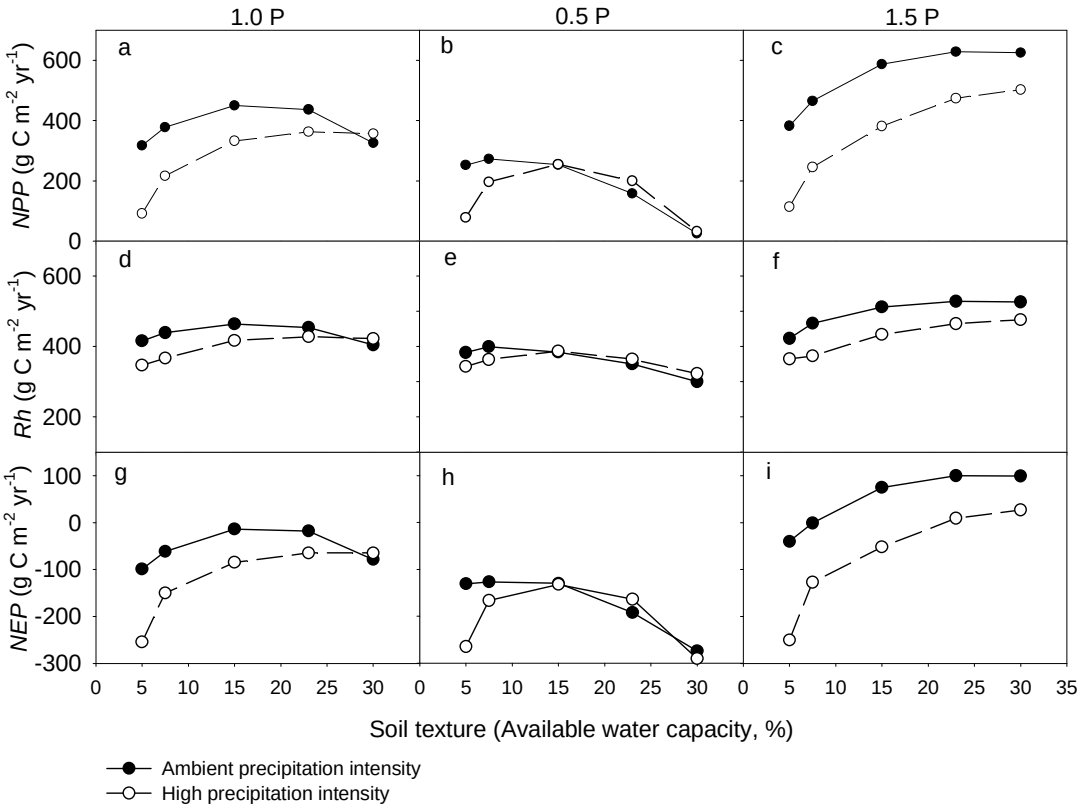

Figure 2.7 Soil texture effects on NPP, R_h, and NEP at three precipitation amount levels and two frequencies.

NPP, R_h, and NEP usually increased along the gradient of soil texture (Fig. 2.7). At 1.0 P, NPP, R_h, and NEP were the highest at soil AWC of 23% and lower at either low or

high AWC (Fig. 2.7a, d, and g). At 0.5 P, NPP, R_h, and NEP reached their peak points at AWC of 7.5% and then decreased with AWC (Fig. 2.7 b, e, and h). At 1.5 P, NPP, R_h, and NEP increased along the whole range of soil AWC (Fig. 2.7 c, f, and i). High precipitation intensity generally led to lower NPP, R_h, and NEP than the ambient intensity at 1.0P and 1.5P. At 0.5 P, NPP and Rh are slightly higher at high range of soil AWC than them at ambient intensity (Fig. 2.7: b, e). Differences in NPP, R_h, and NEP between ambient and high precipitation intensities were larger at coarse than fine textured soil (Fig. 2.7).

2.3.3 Responses of ecosystem to warming with different soil texture types

Simulated warming decreased soil moisture at all of the five soil texture types (Fig. 2.8 a~c). The relative decrease in soil moisture became larger at 1.0 P along the gradient of soil AWC (Fig. 2.8 a). At 0.5 P, the largest relative decrease occurred at AWC equal to 15% (Fig. 2.8b). At 1.0 P and 0.5 P, evaporation decreased under warming, especially at high soil AWC (Fig. 2.8 d and e). At 1.5 P, warming resulted in a decrease in evaporation at low AWC but an increase at high AWC (Fig. 2.8 f). Transpiration under warming increased by 10~25% with the three precipitation amounts (Fig. 2.8 g~i). Warming resulted in decreases in runoff (Fig. 2.8 j~l). The relative decrease of runoff was smaller at low AWC than high AWC with all of the three precipitation levels. High precipitation intensity usually led to less warming effects on ecohydrological processes than the ambient intensity (Fig. 2.8a~l).

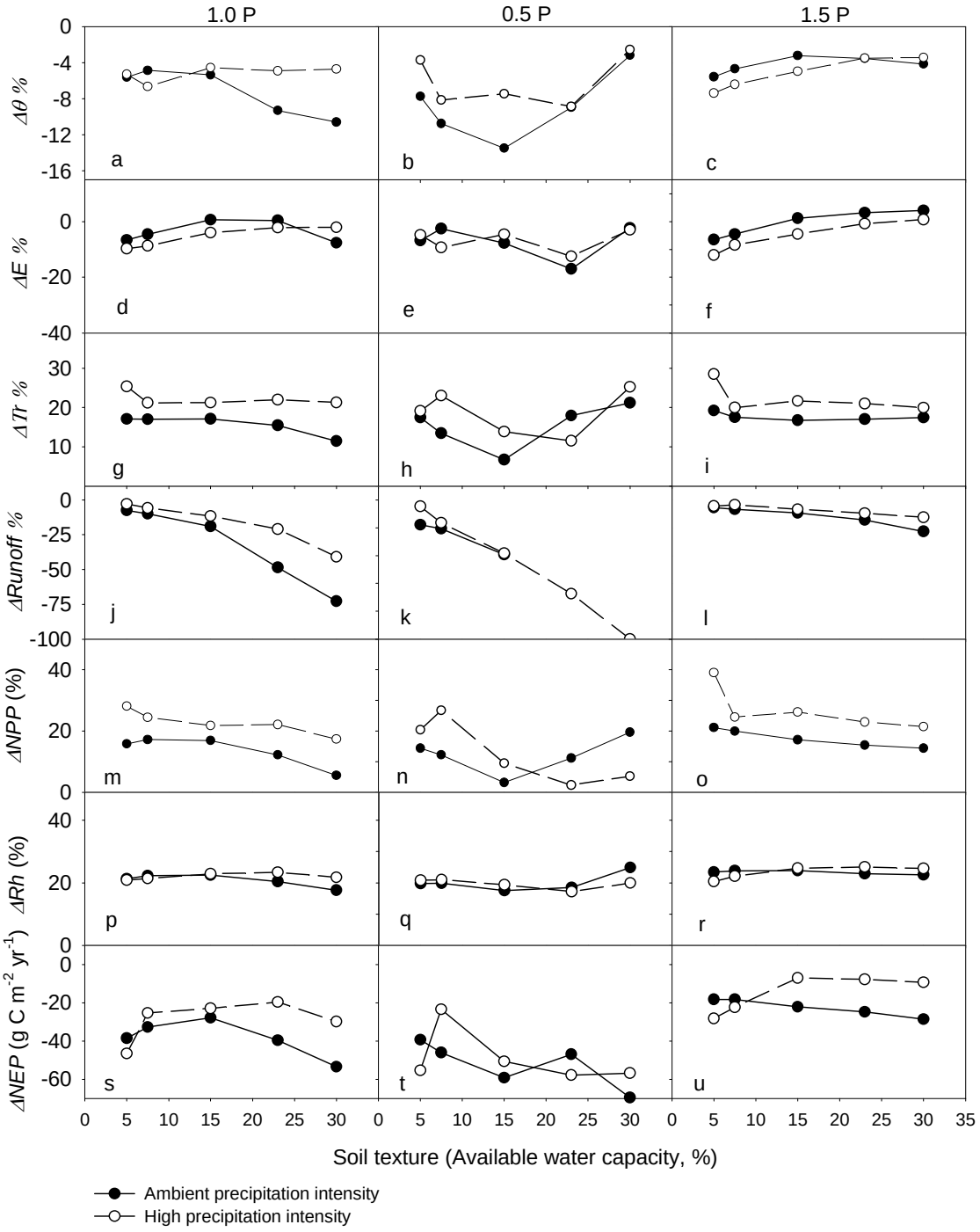

Figure 2.8 Effects of soil texture on the grassland responses to warming (2°C increased). Show the relative changes in soil water content, evaporation, transpiration, runoff, NPP, Rh, and NET with available water capacity. ***Δ* θ%**: percentage change of soil water content at warming treatments ($\Delta\ \theta\% = (\theta_{2°C} - \theta_{amb.})/\ \theta_{amb} \times 100$). ***Δ* E%**: percentage change

of evaporation at warming treatments (ΔE%=($E_{2°C}$−$E_{amb.}$)/ E_{amb}×100). ***Δ*Tr%**: percentage change of transpiration at warming treatments (ΔTr%=($Tr_{2°C}$−$Tr_{amb.}$)/ Tr_{amb}×100). ***Δ* Runoff%**: percentage change of runoff at warming treatments (ΔRunoff%=($Runoff_{2°C}$−$Runoff_{amb.}$)/ $Runoff_{amb}$×100). ***Δ* NPP%**: percentage change of NPP at warming treatments (ΔNPP%=($NPP_{2°C}$−$NPP_{amb.}$)/ NPP_{amb} × 100).

***Δ* Rh%**: percentage change of Rh at warming treatments (ΔRh%=($Rh_{2°C}$−$RH_{amb.}$)/ Rh_{amb} × 100).

***Δ* NEP%**: percentage change of NEP at warming treatments (Δ NEP%=($NEP_{2°C}$−$NEP_{amb.}$)/ NEP_{amb} × 100).

Warming usually resulted in increases in NPP and R_h but decreases in NEP (Fig. 2.8 m~u). Warming-induced relative increases in NPP generally were higher at high precipitation amount. The increase of NPP varied with AWC (Fig. 2.8 m, n, and o). R_h under warming increased by about 20% at all of the five soil texture types with the three precipitation amounts (Fig. 2.8 p, q, and r). Relative decreases in NEP under warming were least at AWC of 7.5-15% at 1.0 P (Fig. 2.8s). The high precipitation intensity led to higher relative increases in NPP and R_h but less relative decreases in NEP in most cases than ambient intensity along the soil texture gradient (Fig. 2.8m~u).

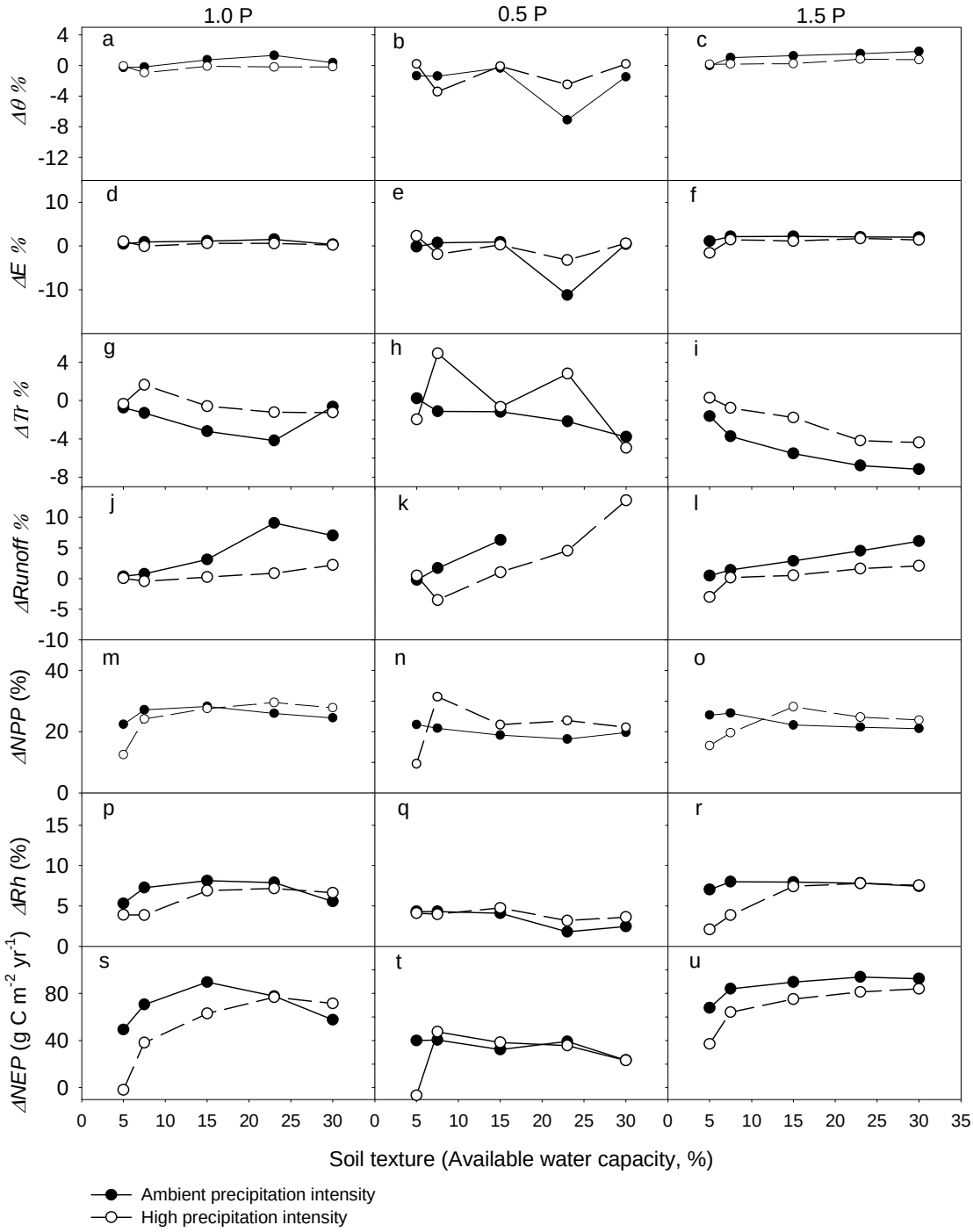

Figure 2.9 Effects of soil texture on the grassland responses to elevated [CO2]. Show the relative changes in soil water content, evaporation, transpiration, runoff, NPP, Rh, and NET with available water capacity. ***Δ* θ%**: percentage change of soil water content at elevated [CO2] ($\Delta\theta\% = (\theta_{2CO2} - \theta_{amb.})/\ \theta_{amb} \times 100$). ***Δ* E%**: percentage change of evaporation

at elevated [CO2] (Δ E%=(E_{2CO2}−$E_{amb.}$)/ E_{amb}×100). ***Δ* Tr%**: percentage change of transpiration at elevated [CO2] (ΔTr%=(Tr_{2CO2}−$Tr_{amb.}$)/ Tr_{amb}×100). ***Δ* Runoff%**: percentage change of runoff at elevated [CO2] (ΔRunoff%=($Runoff_{2CO2}$−$Runoff_{amb.}$)/ $Runoff_{amb}$×100).

2.3.4 Responses of ecosystem to doubled atmospheric [CO_2]

At 1.0 P and 1.5 P, doubled [CO_2] usually resulted in increases in soil moisture, evaporation, and runoff but decreases in transpiration in comparison to that under ambient [CO2] (Fig. 2.9 a~l). The relative increases or decreases in ecophydrological processes at doubled [CO_2] became larger at high AWC. At 0.5 P, changes in evaporation and transpiration showed no apparent trend with AWC, while soil moisture decreased slightly (Fig. 2.9b) and runoff generally increased under elevated [CO_2] with AWC (Fig. 2.9k). High precipitation intensity led to less changes in soil moisture, evaporation, transpiration, and runoff under elevated [CO_2] than ambient intensity at 1.0 P and 1.5 P.

CO_2-induced relative increases in NPP, R_h, and NEP were generally lower at low than high soil AWC at 1.0 P and 1.5 P (Fig. 2.9 m~u). Doubled [CO_2] usually increased NPP by 10-25% and R_h by 2-8%, leading to substantial increases in NEP. CO_2-induced changes in NPP, R_h, and NEP at 0.5 P were less than at 1.0 P and 1.5 P. Generally, CO_2 effects on NPP, R_h, and NEP were higher with high than ambient precipitation intensity at high AWC, and lower at low soil AWC.

2.4 Discussion

2.4.1 Water partitioning among runoff, evaporation, and transpiration

Soil texture regulates runoff and evaporation by changing soil water storage and the vertical distribution of soil water (Noy-Meir, 1973). Our results showed that runoff decreased and evaporation increased with AWC (Fig. 2.5). Transpiration increased with AWC quickly in the low range and leveled off in the high range of AWC (Fig. 2.5). The results indicated that the partitioning of precipitation water among runoff, evaporation, and transpiration could be regulated by soil texture. Soil hydrological properties control water infiltration and the depth to which water percolates, and consequently affect water partitioning between evaporation and transpiration (McAuliffe, 2003).

Water partitioning between evaporation and transpiration has been an important issue in ecohydrological studies (Lauenroth and Bradford, 2006). Model results suggested that transpiration is the dominant component (53%) of the global terrestrial water vapor flux from the continents and may reach a maximum of 75% in densely vegetated regions (Choudhury et al., 1998). However, only a few empirical studies have quantified partitioning of ET in semiarid shrublands over limited time periods (Ferretti et al., 2003; Scott et al., 2006). Reynolds et al. (2000) found the T/ET ranges from 7% to 80% at a warm desert site in a modeling study. Many factors involve in water partitioning between evaporation and transpiration, e.g. vegetation covers, root systems, precipitation regimes, et al.. Our simulation showed that changes in soil texture can alter T/ET substantially.

When soil is fine textured, a large portion of water is kept in upper layers, leading to more water is available for evaporation. However, at coarse textured soil, rapid dehydration of the surface soil layer results in saving water in deep layers (Wythers et al., 1999) and available for plants. As shown by Fig. 6a, the fine textured soils can hold more water, and keep most of the water in the surface layer, which results in higher evaporation. Thus, the percentage of the water that can be used by transpiration decreased (Fig. 2.6 b).

In water-controlled ecosystems, high water availability leads to high productivity. At 0.5 P, as shown in our results, normalized soil moisture decreased with AWC and drought-stressed days increased with AWC. As a consequence, NEP and NPP decreased with AWC at halved precipitation amount. Whereas, at high precipitation amounts (eg. 1.5 P), normalized soil moisture increased and drought-stressed days decreased with AWC. And then, NPP increased with AWC. These results supported the inverse texture hypothesis, which states that ecosystems on coarse-textured soils have higher net primary productivity than the ecosystems on fine-textured soils at low precipitation; the reverse is predicted to occur in humid regions (Noy-Meir, 1973). Field data measured in the central grassland region of the United States showed similar patterns (Sala, et al., 1988; Epstein et al., 1997; Lane et al., 1998).

2.4.2 Soil texture and effects of precipitation intensity on ecosystem

An increase in precipitation intensity with decreased frequency has been projected as a possible scenario of climate change (Easterling et al., 2000). Field experiments

showed that more extreme rainfall patterns, without concurrent changes in total rainfall quantity, increase temporal variability in soil moisture (Fay et al., 2003; Knapp et al., 2002). Carbon cycling processes such as soil respiration (Christopher et al., 2005), photosynthesis, and above ground net primary productivity (ANPP) (Fay et al., 2003; Knapp et al., 2002) are also reduced because of high soil moisture variability caused by increased rainfall variability. Consistent with the results from field experiments, our modeling results showed that high precipitation intensity led to more drought-stressed days than the ambient intensity in most cases (Fig. 2.4m~o).

Our modeling study also enriches experimental results from Knapp et al. (2002) by circumscribing conditions under which increased precipitation intensity with reduced frequency leads to either decreases or increases in ecosystem production. If precipitation amount is low (0.5P), for example, the high precipitation intensity led to higher soil moisture and less drought-stressed days than the ambient intensity when AWC was 15% or higher. At 1.0 P, the high precipitation intensity also decreased drought-stressed days when AWC was 30%, (Fig. 2.4). The reason is that the fine textured soils can store rain water from large precipitation events with high field capacity. Additionally, more water can be stored in deep layers at high precipitation intensity than that at the ambient intensity, which reduces the water used by evaporation. Thus, runoff and evaporation decreased, and water that was available to plants increased. Changes in soil moisture and drought-stressed days resulted in changes in NPP. As shown by our simulations, when precipitation amount was low (0.5P) and soil AWC was high, NPP at high precipitation

intensity was higher than that at ambient precipitation intensity. However, with increase of precipitation amounts (e.g., 1.5 P), high precipitation intensity led to lower NPP than that at ambient intensity. Therefore, soil texture can strongly regulate effects of precipitation intensity on soil moisture content and ecosystem carbon processes.

2.4.3 Soil texture and ecosystem responses to warming and elevated [CO_2]

Warming and elevated CO_2 both can alter plant production through their direct effects on plant physiology and indirect effects mediated by changes in soil water content (Parton et al. 2007; Shaver et al. 2000; Morgan et al. 2004). Experimental studies have shown that the indirect effects induced by changes in soil moisture play a critical role in regulating ecosystem responses to warming and elevated [CO_2] (Morgan et al., 2004; Nowak et al., 2004; Volk et al. 2000; Wullschleger et al., 2002). As a result, the factors that affect soil water dynamics (e.g., soil AWC) can regulate ecosystem responses to warming and elevated CO_2. Warming-induced decreases in soil moisture usually aggravate drought stress on ecosystems (Harte et al., 1995; Saleska et al., 1999; Wan et al., 2002). Although warming directly stimulates plant growth productivity in most field studies (Rustad et al., 2001), warming treatment may reduce NPP when negative effects of warming-induced soil drought override warming stimulation of plant growth (Saleska, et al., 1999). Experimental results have shown that warming improved plant growth in spring and fall but limited plant growth in summer because of drought stress induced by warming treatment (Wan et al., 2005). Soil texture can tip the balance between the negative and the positive effects of warming by regulating water partitioning

among runoff, evaporation, and transpiration. Our results showed that the percentage of warming-induced increases in NPP diminished with AWC when temperature increased by 2 °C degrees (Fig. 2.8: m-o), especially at 0.5 P. R_h shows a steady increase of around 20% regardless of changes in precipitation amount, intensity, and soil texture (Fig. 2.8 p, q, and r). The R_h strongly depends on the soil carbon content. At equilibrium state, the model developed a high soil carbon pool (about 8500 $g \cdot m^{-2}$), which did not change immediately when scenarios applied. Thus, R_h increased when soil temperature increased, leading to negative values of NEP consequently.

In contrast to warming effects, elevated atmospheric [CO_2] usually results in increases in soil moisture content by decreasing stomatal conductance of many plant species (Morgan et al. 2004). As shown by our simulations, percent increases in soil moisture content under double [CO2] increased slightly soil AWC at 1.0 P and 1.5 P (Fig. 2.9 a and c) and so did NPP, R_h, and NEP. However, elevated [CO2] did not led to increases in soil moisture at 0.5 P. Similar results were obtained from field experiments conducted in dry areas (e.g., Nowak et al., 2004) because increased water consumption from increased primary productivity under elevated [CO_2] offset the decreased water consumption from reduced stomatal conductance and hence soil water was not saved under elevated [CO2]. Indeed, CO_2 stimulation of NPP at 0.5 P was highest at AWC of 10% and declined with soil AWC due to reduction in soil moisture.

Along the soil AWC gradient from 5% to 30%, stimulation of NPP by warming ranged from 5% to 30% (Fig. 2.8: m~o) and from 10% to 30% by doubled [CO2] (Fig.

2.9: m~o). The results indicate that soil texture can substantially regulate ecosystem responses to warming and elevated [CO2]. The sites where warming and/or CO_2 experiments were conducted have variable soil texture and different available water capacities (Morgan et al., 2004; Rustad et al., 2001). Analysis of this paper suggests that variation in soil texture with changes in soil availability can result in diverse responses of ecosystem production to experimental warming and elevated atmospheric [CO_2].

2.4.4 Uncertainties in vegetation dynamics and unrealistic scenarios

Vegetation dynamics and phenology can affect water partitioning among evaporation, transpiration, and runoff by altering transpiration and water uptake through roots. Zavaleta et al. (2003) showed that earlier senescence induce by warming treatment in a Mediterranean grassland can lead to increase of soil moisture by decreasing transpiration. Scott et al. (2006) found that ecosystem evapotranspiration increased with increasing woody-plant dominance. A modeling study (Reynolds et al., 2000) showed that annual evapotranspiration (ET) is highly correlated with precipitation. However, the percent of water lost as transpiration (T/ET) is different among plant functional types. In the TECO model, a fully dynamical plant growth model was used to simulate LAI and root dynamics, which could strongly affect soil moisture dynamics. A test run using a set of prescribed LAI showed the same patterns of changes in soil moisture, transpiration, and NPP with those from the simulated dynamics, which indicated that the main conclusions about the effects of soil texture on ecosystem responses to changes in temperature, precipitation, and [CO_2] were robust regardless of uncertainties in

vegetation dynamics. In the model, the transpiration was controlled by LAI and water uptake through roots. LAIs were always consistent with soil water availability by growth and senescence. Rooting depth was a constant (70 cm) and root vertical distribution was regulated by every layer's water availability and their intrinsic vertical distribution ratios. Thus, a prescribed LAI couldn't strongly influence our main conclusions.

Some of the climatic scenarios we explored in this study may have little chance to happen in the future, such as altering precipitation patterns without changes in solar radiation and elevated atmospheric [CO_2] without an increase of air temperature. Our modeling study was intended to explore different possibilities under 120 scenarios of climate change (Table 2) using a full factorial design. The factorial design is a commonly used method in experimental research and has been adopted by the modeling community as well. Many modeling studies at scales from ecosystems to regions and the globe often explore various scenarios with different combinations of factors (e.g. Cramer et al., 2001; Parton et al., 2007; VEMAP, 1995). Such an approach was intended to explore possibilities and may not say anything about actuality in a given scenario. Scenario-based modeling analysis has been done in all IPCC assessments partly because we have great uncertainties project future climatic conditions. What we can learn from our scenario-based analysis in this study is to explore how soil hydrological properties affect ecosystem responses to changes in global change factors. These full factorial scenarios are useful to separate effects of individual factors on ecosystems and results are relatively easy to interpret.

2.5 Conclusions

The modeling results indicate that soil hydrological properties can regulate ecosystem responses to changes in precipitation, warming, and elevated atmospheric [CO_2] by altering partitioning of rain water among runoff, evaporation, and transpiration. Water partitioning patterns along soil texture alter AWC for plants and then regulate ecosystem responses to altered precipitation amount and intensity, climate warming, and elevated [CO_2] indirectly. Considering high variations in soil texture at field sites where experiments are conducted, soil texture may be one of the major causes underlying variable responses of ecosystems to changes in precipitation, temperature, and atmospheric [CO_2] observed from field experiments. Thus, it is important to know how soil texture regulates soil water dynamics in order to evaluate ecosystem responses to climate change.

Our modeling analysis showed that NPP, R_h, and NEP usually increased with soil AWC. Such increases were amplified by precipitation amounts. Warming stimulation of NPP decreased with soil AWC, whereas warming effects on R_h did not vary much in different soil texture types. Stimulation of NPP, R_h, and NEP by elevated [CO_2] was usually lower at coarse than fine textured soils. These results indicate that the water properties of soil can be a key factor regulating grassland responses to warming, changes in precipitation, and elevated atmospheric [CO_2]. Thus, it is highly desirable to examine

soil hydrological properties in regulating ecosystem responses to global change in future experimental research.

Acknowledgements

We thank Drs Xuhui Zhou and Rebecca Sherry for providing measured soil respiration, biomass, and soil moisture data and Dr. Yingping Wang for providing the source code of photosynthesis model. This study was financially supported by U.S. National Science Foundation under DEB0078325 and DEB 0444518, and by the Office of Science (BER), Department of Energy, Grants No.: DE-FG03-99ER62800 and DE-FG02-06ER64319 and TERACC initiative (Terrestrial Ecosystem Responses to Atmospheric and Climatic Change, a research coordination network supported by the U.S. National Science Foundation under DEB 0090238).

Appendix I: Description of the Terrestrial ECOlogical model (TECO)

Terrestrial ECOlogical model (TECO) evolves from a terrestrial carbon sequestration (TCS) model (Luo and Reynolds, 1999) and is designed to examine ecosystem responses to perturbations in global change factors. A canopy model is incorporated into the model to simulate photosynthesis at hourly time scale. A soil water dynamic model also has been coupled for simulating water dynamics at hourly time scale. The model contains four major components: a canopy photosynthesis sub-model, a soil water dynamic sub-model, a plant growth sub-model, and a soil carbon transfer sub-model. The photosynthesis and soil moisture dynamics are simulated at hourly time step while the plant growth and the carbon transfer are simulated at daily step.

1 Canopy sub-model

Canopy sub-model is from a two-leaf photosynthesis model simulating canopy conductance, photosynthesis, transpiration, and energy partitioning (Wang and Leuning, 1998). It consists of two parts: 1) a radiation submodel which calculates photosynthesis active radiation (PAR), near infrared radiation (NIR), and thermal radiation absorbed by sunlit and shaded leaves and 2) a coupled model of stomatal conductance, photosynthesis and partitioning of absorbed net radiation into sensible and latent heat.

The coupled model of stomata-photosynthesis-transpiration

The coupled model of stomatal conductance, photosynthesis and transpiration for the big sunlit leaf (i=1) or big shaded leaf (i=2) is given by the following equations.

Energy balance

$$Q_{n,i} = \lambda E_{c,i} + H_{c,i} \qquad \text{(A2.1)}$$

Transpiration

$$E_{c,i} = G_{s,i} D_{s,i} = G_{w,i}(D_a + s\Delta T_i) \qquad \text{(A2.2)}$$

Sensible heat

$$H_{c,i} = G_{h,i} c_p \Delta T_i \qquad \text{(A2.3)}$$

Photosynthesis-gas diffusion

$$A_{c,i} = b_{sc} G_{s,i}(C_{s,i} - C_i) = G_{c,i}(C_a - C_i) \qquad \text{(A2.4)}$$

Stomatal conductance:

$$G_{s,i} = G_{0,i} + \frac{a_1 f_w S_{NSC} A_{c,i}}{(C_{s,i} - \Gamma)(1 + D_{s,i} / D_0)} \qquad \text{(A2.5)}$$

Photosynthesis-biochemistry

$$A_{c,i} = V_{n,i} - R_{d,i} \qquad \text{(A2.6)}$$

Where, $Q_{n,i}$ is net available energy, $E_{c,i}$ is transpiration, $H_{c,i}$ is sensible heat, λ is latent heat of vaporization for water. D_a and $D_{s,i}$ are saturated deficit of water vapor pressure (VPD) in the ambient air and at the leaf surface, respectively. $G_{s,i}$ is stomatal conductance of a leaf or big leaf for H_2O, $G_{0,i}$ is stomatal conductance of a leaf or big leaf for H_2O when net leaf photosynthesis is zero. $G_{w,i}$ and $G_{c,i}$ are total conductance from the intercellular space of the leaves to the reference height above the canopy for H_2O and CO_2, respectively. $G_{h,i}$ is the total conductance for the heat transfer from the leaf surface to the reference height above the canopy, c_p is the specific heat of the air, ΔT_i is the

temperature difference between the surface of the big leaf and that of the air at the reference height, *s* is the slope of the function relating saturated water vapor mol fraction to temperature and bsc is the ratio of diffusivity of CO_2 and H_2O through the stomata. $A_{c,i}$ is the net photosynthesis rate, $V_{n,i}$ is the net carboxylation rate, $R_{d,i}$ is the day respiration rate. C_a, $C_{s,i}$, and C_i are CO_2 mol fractions in the air, at the leaf surface, and intercellular spaces, respectively. Γ is CO_2 compensation point of leaf photosynthesis, D_0 is a parameter for stomatal sensitivity to VPD. a_1 is an experience constant, which is related to the intercellular CO_2 concentration by $C_i/C_{s,i} = 1\text{-}1/a_1$. *i* stands for sun or shaded leaves; f_w is soil moisture scaling factor, and S_{nsc} is scaling factor derived by the size of non-structural pool. Equation (6) is a biochemical model of photosynthesis which is used to calculate biochemical processes limited photosynthesis rate. More details are in Farquhar et al. (1980) and Wang and Leuning (1998).

Radiation absorption

The net energy available to the big leaf *i* in wave-band *j*, $Q_{n,i}$, is calculated as:

$$Q_{n,i} = \sum_{j=1}^{3} Q_{i,j} \qquad \text{(A2.7)}$$

Leaf temperature should be known for calculating absorbed long-wave radiation ($Q_{i,3}$). However, it can be skipped by using the isothermal net radiation ($Q_{n,i}^*$).

$$Q_{n,i}^* = Q_{n,i} + c_p G_{r,i} \Delta T_i \qquad \text{(A2.8)}$$

Loss of thermal radiation of the big leaf to the air under non-isothermal conditions is calculated by $G_{r,i}(=4\varepsilon_f \delta T_a^3 / c_p)$. Where, ε_f is the leaf emissivity, σ is the Steffan Boltzman constant and T_a is air temperature (K).

2 Soil water dynamics sub-model

Soil water is represented in 10 layers (the thickness of the first layer is 10 cm, all others are 20 cm). Infiltration adds water to soil layers in a cascading fashion according to soil AWC. When the ten layers of soil is filled, excessive water runs off. Evaporation is calculated by the evaporation equation in the SiB2 (Sellers et al., 1996). Its allocation in the ten layers follows the ALFALFA model (Denison and Loomis, 1989). The water transpired from the soil is partitioned among the soil layers according the fractions of roots. The soil water content is calculated as the budget between input (precipitation) and output (runoff, evaporation, and transpiration).

Infiltration Water flows to the next layer when the upper layer is filled. Water in precipitation penetrates to a soil depth that depends on precipitation amount, field capacity, and the current soil water content. The model iterates the water content of each soil layer after calculating evaporation, and transpiration.

Transpiration The amount of water transpired from soil (transpiration) is calculated in the canopy model by stomatal conductance and the relative humidity difference between the inside and outside of leaves. It is partitioned among the soil layers according to the fractions of roots in these soil layers.

Evaporation Soil surface evaporation is calculated by the following equation (Sellers et al., 1996):

$$E_s = \frac{e^*(T_{soil}) - e_a}{r_{soil} + r_d} \frac{\rho c_p}{\gamma} \frac{1}{\lambda} \qquad \text{(A2.9)}$$

where E_S is soil evaporation, e* (T_{soil}) is the saturation vapor pressure at the temperature of the soil, ea is the atmospheric vapor pressure, r_{soil} is a soil resistance term, r_d is the aerodynamic resistance between the ground and the canopy air space, ρ is the density of air, c_p is the specific heat of air, γ is the psychrometric constant; λ is the latent heat of sublimation (Sellers et al., 1996).

Runoff If soil water content is greater than soil water holding capacity, then runoff occurs

$$\begin{aligned} &Runoff = W_{soil} - W_{\max} \\ &\text{then,} \quad W_{soil} = W_{\max} \end{aligned} \qquad \text{(A2.10)}$$

Where, W_{max} is soil water holding capacity.

Soil water content Soil water content is updated hourly according to the budget between precipitation and evpotranspiration.

$$W_{soil} = W_{soil0} + P - ET \qquad \text{(A2.11)}$$

Where, *ET* is evapotranspiration.

Soil moisture scalar A soil moisture scalar is computed here, which is an important scalar in regulating photosynthesis, plant growth rate, and soil carbon turnover time.

$$f_w = \min\left(1.0, 3.33 \cdot \left(\frac{W_{soil} - W_{\min}}{W_{\max} - W_{\min}}\right)\right) \qquad \text{(A2.12)}$$

where, $W_{\min}$ is wilting point.

3 Plant growth sub-model

The plant growth sub-model simulates the processes of carbon allocation to leaves, stems, and roots (i.e. plant growth), and the production of litter fall. The model has six carbon pools, which are one non-structural carbon pool (NSC), one leaf carbon pool (Q_L), one stem carbon pool (Q_W), and three root carbon pools (Q_{R1}, Q_{R2}, Q_{R3}). The carbon fixed by photosynthesis enters into NSC firstly. And then, the carbon in NSC is used by autotrophic respiration and allocated to plant tissues via plant growth. The carbon allocation from NSC to the other five C-pools is determined by plant growth rates. In the processes of leaf growth and fall, phenology is presented at the same time.

Autotrophic respiration

Autotrophic respiration is calculated daily based on temperature (either air or soil temperatures, for above and below ground tissues, respectively), tissue biomass, and phenology by Arrhenius equation (Ryan, 1991; Lloyd and Taylor, 1994).

$$R_i = R_{i0} \cdot e^{a \cdot T} \qquad \text{(A2.13)}$$

Where, $R_{i0} = b \cdot BM$, T is temperature of air or soil, a and b are constants, BM is biomass.

Growth

The idea is mainly from the ALFALFA model (Denison and Loomis, 1989; Luo et al., 1995). The growth rate of plant is controlled by root/shoot ratio, scalar of NSC, and scalar of leaf area index.

$$G_i = G_{\max i} \cdot BM_i \cdot S_{r/s} \cdot S_{nsc} \cdot S_{LAI} \quad \text{(A2.14)}$$

Where, i= leaf, stem, or root. G_i is the growth rate, G_{maxi} is the maximum relative growth rate, BM_i is biomass of leaves, stems or roots. $S_{r/s}$, S_{nsc} and S_{LAI} are the scaling factors derived from root/shoot ratio, the size of NSC, and leaf area index, respectively.

Litter production

Leaf fall and root turnover is induced by soil drought and low air temperature in the autumn following the approach of Arora and Boer (2005). Stem fall is only controlled by turnover time.

$$\gamma_T = \gamma_{T_{\max}} (1-\beta_T)^{b_T}$$
$$\gamma_W = \gamma_{W_{\max}} (1-W)^{b_W} \quad \text{(A2.15)}$$

Where, $\gamma_{T_{\max}}$ and $\gamma_{W_{\max}}$ are maximum rates of leaf fall induced by low temperature and drought respectively. β_T and W are scaling factors controlling the rate of leaf fall.

Then, leaf fall (D_L), stem fall (D_S) and root turnover (D_R) are:

$$D_L = q_L(\gamma_T + \gamma_W)$$
$$D_S = q_W / \tau_W \quad \text{(A2.16)}$$
$$D_R = q_R(\gamma_T + \gamma_W)$$

Where, q_L , q_W and q_R are the C-pool sizes of leaves ,stems, and roots, respectively. τ_W is turnover time of carbon in stem C-pool.

Phenology

Phenology is represented by periodical variations of leaf area index (LAI) and two plant states, dormancy and growth. In winter, grasses remain in a dormant state until the arrival of the favorable weather conditions in spring. The growth state is initiated by a

certain growing degree days above 5 °C (GDD_5). During the first several days of growing season, leaf growth consumes the carbon stored in NSC last growing season, until the stored carbon is used up. And then, leaf growing is based on carbon from photosynthesis. LAI is controlled by the budget of leaf growth and senescence. If leaf growth overrides leaf senescence, LAI increases, and vice versa. In fall, when LAI meets a minimum value (<0.1), the dormant state comes.

4. Carbon transfer sub-model

The carbon transfer model is evolved from TCS (Luo and Reynolds, 1999) and VAST (Barret et al., 2002). The soil carbon model is used to simulate the carbon flow from plant tissues to litters and soils, and then to atmosphere. There are five carbon pools in the soil carbon model, which are fine litters (Q_F), coarse litters (Q_C), and three soil carbon pools defined by three soil layers (Q_{S1}, Q_{S2}, Q_{S3}) (Fig.1). The carbon allocated to leaves (Q_F), stems (Q_W), and roots (Q_{R1}, Q_{R2}, Q_{R3}) flows through these C-pools, and then returns to atmosphere as CO_2.

The turnover time of carbon in leaf C-pool (τ_L) is determined by the growth and fall of leaves. The turnover times of carbon in stem C-pool (τ_W) and root C-pool (τ_{R1}, τ_{R2}, τ_{R3}) are assumed to be constants. The turnover times of carbon in fine litter (τ_F), coarse litter (τ_C), and soil carbon pools (τ_{S1}, τ_{S2}, τ_{S3}) are given by the following equation:

$$\tau_k = \tau_k^* / S_T \cdot S_\omega \qquad \text{(A2.17)}$$

Where, τ_k^* is the moisture and temperature independent turnover time, S_T and S_ω are scalars of the moisture and temperature, which modify residence times of the carbon pools.

The dynamics of *k*th C-pool, dq_k / dt (gC $m^{-2} \cdot d^{-1}$), is calculated by eqn.18.

$$dq_k / dt = I_k - q_k / \tau_k \qquad \text{(A2.18)}$$

Where, I_k is the input flux of carbon from upstream C-pools, q_k is the size of *k*th C-pool, τ_k is the turnover time (days) of carbon in the *k*th C-pool, q_k / τ_k is the daily carbon out flux of the *k*th pool.

The daily carbon influx of the *k*th pool (I_k) is given by:

$$\begin{aligned} I_F &= L_{Fall} + \eta_C W_{Fall} \\ I_C &= W_{Fall}(1-\eta_C) \\ I_{S1} &= q_{R1} / \tau_{R1} + q_F / \tau_F \theta_F + q_C / \tau_C \theta_C \\ I_{S2} &= q_{R2} / \tau_{R2} + q_{S1} / \tau_{S1} \theta_{S1} \\ I_{S3} &= q_{R3} / \tau_{R3} + q_{S2} / \tau_{S2} \theta_{S2} \end{aligned} \qquad \text{(A2.19)}$$

Where, q_k is the size of the *k*th C-pool, η_C is the fragmentation coefficient of wood going to fine litter, τ_k is the turnover time of the carbon in the *k*th C-pool, and θ_k is the partitioning parameter of C-pools.

Heterotrophic respiration from litter and soil carbon pools is given by the following equation:

$$R_{hk} = \sum q_k / \tau_k \cdot f_k' \qquad \text{(A2.20)}$$

Where, f'_k is the fraction of carbon out flux which enters the atmosphere from the *k*th pool, which is given by:

$$
\begin{aligned}
f_F^{'} &= 1-\theta_F \\
f_C^{'} &= 1-\theta_C \\
f_{S1}^{'} &= 1-\theta_{S1} \\
f_{S2}^{'} &= 1-\theta_{S2} \\
f_{S3}^{'} &= 1
\end{aligned}
\qquad \text{(A2.21)}
$$

CHAPTER 3 Relative Information Contributions of Model vs. Data to Short- and Long-Term Forecasts of Forest Carbon Dynamics[2]

[2] This part has been accepted by Ecological Applications and published online.

Abstract

Biogeochemical models have been used to evaluate long-term ecosystem responses to global change on decadal and century time scales. Recently, data assimilation has been applied to improve these models for ecological forecasting. It is not clear what the relative information contributions of model (structure and parameters) vs. data are to constraints of short- and long-term forecasting. In this study, we assimilated eight sets of ten-year data (foliage, woody, and fine root biomass, litter fall, forest floor carbon (C), microbial C, soil C, and soil respiration) collected from Duke Forest into a Terrestrial ECOsystem model (TECO). The relative information contribution was measured by Shannon information index calculated from probability density functions (PDF) of carbon pool sizes. The *null* knowledge without a model or data was defined by the uniform PDF within a *prior* range. The relative model contribution was information content in the PDF of modeled carbon pools minus that in the uniform PDF while the relative data contribution was the information content in the PDF of modeled carbon pools after data was assimilated minus that before data assimilation. Our results showed that the information contribution of the model to constrain carbon dynamics increased with time whereas the data contribution declined. The eight data sets contributed more than the model to constrain C dynamics in foliage and fine root pools over the 100-year forecasts. The model, however, contributed more than the data sets to constrain the litter, fast soil organic matter (SOM), and passive SOM pools. For the two major C pools, woody biomass and slow SOM, the model contributed less information in the first few decades and then more in the following decades than

the data. The knowledge on relative information contributions of model vs. data is useful for model development, uncertainty analysis, future data collection, and evaluation of ecological forecasting.

Key words: data assimilation, information theory, carbon cycle, model uncertainty, Duke Forest FACE, ecological forecasting.

3.1 Introduction

Biogeochemical models have been widely used to project long-term ecosystem responses to climate change and evaluate feedback between climate and the carbon cycle on century and millennium time scales (e.g. Cramer et al. 1999, McGuire et al. 2001, Friedlingstein et al. 2006, Carpenter et al. 2009). These models have been also used to explore interactions of multiple global change factors (Luo et al. 2008), forest management (Schmid et al. 2006, Pretzsch et al. 2008), and ecosystem services (Schröter et al. 2005) on decadal or shorter time scales. Most biogeochemical models share a similar model structure in which photosynthetically fixed carbon is allocated to multiple plant and soil pools (VEMAP 1995, Kucharik et al. 2000, Sitch et al. 2003). Photosynthesis is usually simulated using the Farquhar model (Farquhar et al. 1980) as regulated by light, CO_2 concentration, temperature, and nutrients. Allocation of carbohydrates from photosynthesis is often determined by fixed fractions or regulated by functional balance among multiple resources (Luo et al. 1994, Friedlingstein et al. 1999). Carbon transfers among pools are generally governed by pool size and specific transfer coefficients as affected by

environmental variables (Luo et al. 2001a). Although most biogeochemical models share a similar structure, model intercomparison and data-model comparison studies show tremendous variations among models for either short-term forecasts or long-term projections even if models are calibrated against historical and/or contemporary conditions (e.g., Friedlingstein et al. 2006, Sitch et al. 2008).

High uncertainties of model projections generally result from differences in initial values, parameterizations, and response functions that link those key carbon processes to environmental and biological variables. For example, using the observed soil carbon content as model initial values could lead to a higher carbon accumulation rate than the assumption of equilibrium state over 100-year simulations at a beech forest (Wutzler and Reichstein 2007). Knorr and Heimann (2001) illustrated that the uncertainties of key parameters were too large for reliable predictions of global net primary production (NPP). Burke et al. (2003) found the response functions that represent the sensitivities of litter decomposition to temperature differed dramatically after comparing eight popular biogeochemical models.

To improve models for accurate projections, data assimilation approaches have recently been developed in ecology to inform initial conditions, constrain parameters, evaluate alternative response functions, and assess model uncertainties (Raupach et al. 2005, Williams et al. 2009, Luo et al. in review). Most data assimilation studies focused on estimation of fast-response parameters, i.e., photosynthesis, respiration and evapotranspiration with short-term data sets. For example, Knorr and Kattge (2005) estimated 29 parameters governing photosynthesis, respiration, stomata activity, and energy balance by assimilating eddy covariance data of seven

days into the BETHY model. Wang et al. (2007) examined three key parameters related to photosynthesis and respiration (maximum photosynthetic carboxylation rate, potential photosynthetic electron transport rate, and basal soil respiration rate) in the CBM model using a nonlinear estimation technique to assimilate eddy covariance data. Wu et al. (2009) estimated 16 parameters of a flux-based ecosystem model by assimilating one-year eddy covariance data using a conditional inversion method. Braswell et al. (2005) assimilated eddy covariance observations with a Markov Chain Monte Carlo approach to estimated 25 parameters in the SIPNET model, of which only one is related to long-term process (woody carbon turnover rate) but not constrained.

A few data assimilation studies have been conducted to constrain long-term processes and parameters with simplified carbon cycle models. Luo et al. (2003) assessed ecosystem carbon sequestration rates by assimilating biometric data into the TECO with 7 target parameters (i.e., residence times of the seven carbon pools). Xu et al. (2006) developed a probabilistic data assimilation to quantify uncertainties of the estimated parameters and forecasted carbon pools using the same data sets and model as in Luo et al. (2003). Williams et al. (2005) assimilated both eddy-flux data and carbon stock data into a simplified carbon pool model and evaluated the rates of carbon sink. Fox et al. (2009) compared ten data assimilation approaches based on the DALEC model and found that the parameters related to fast processes (e.g., photosynthesis, ecosystem respiration) were constrained well but those related to the allocation to and turnover of fine roots and woody biomass pools were constrained poorly. Over all, these studies demonstrated that assimilation of biomass and soil carbon data can improve the constraints of some parameters related to long-term processes.

Since biogeochemical models are often used to evaluate ecosystem responses to climate changes at decadal and century time scales (e.g., Fung et al. 2005, Friedlingstein et al. 2006, Jones et al. 2006), one key question that has not been addressed is how much improvement data assimilation can make for short- vs. long-term forecasts of ecosystem carbon sequestration. To address this issue, we have to first quantify how much information a given model contributes to short- and long-term forecasts because data contribute additional information to forecasts conditioned on the *prior* knowledge contained in the model structure and parameter ranges.

To measure relative model and data contributions to forecasts of carbon dynamics, this study used the TECO model (Luo et al. 2003, Xu et al. 2006) to assimilate eight sets of ten-year data (foliage, wood, and fine root biomass, litter fall, forest floor carbon (C), microbial C, soil C, and soil respiration) collected from the Duke Forest Free-Air CO_2 Enrichment (FACE) experimental site. The relative contributions of the TECO model and the eight data sets were measured by the Shannon information index (Shannon 1948, Jaynes 1957, Kolmogorov 1968), which quantifies the uncertainty associated with a random variable as represented by probability density functions (PDFs). We first defined the *null* knowledge without either a model or data by a uniform PDF within a *prior* range. The model's contribution was quantified by the information content in the PDF of modeled C pools by the TECO model without data assimilation minus that in the uniform PDF. The contribution of the eight data sets was the information content in the PDF of forecasted C pools after the eight sets of data were assimilated minus that before the data assimilation. We applied this approach to quantify the relative information contributions of assimilated data to constraints of forecasted forest carbon storage in the carbon pools of TECO

model. We also evaluated various types of parameters in controlling short- and long-term forecasting of forest carbon dynamics. Based on our evaluation of data vs. model contributions to short- and long-term forecasting, we provided recommendations on model improvement and future data collection to enhance long-term forecasting of carbon sequestration.

3.2 Methods

3.2.1 The ecosystem carbon pool model

The Terestrial ECOsystem (TECO) model is a variant of the CENTURY model (Parton et al. 1987) and is designed to simulate carbon input from photosynthesis, carbon transfer among plant and soil pools, and respiratory carbon releases to the atmosphere. The model has been applied to several studies of carbon sequestration process in Duke Forest in response to elevated CO_2 (Luo et al. 2003, Xu et al. 2006, White and Luo 2008). It has a similar carbon pool structure and parameters to most current biogeochemical models.

In this study, we slightly modified the TECO model by separating a fine root pool from the foliage pool. Thus, it has eight C pools (Fig. 3.1). In this model, the processes of carbon transfer and decomposition were represented by the following first-order ordinary differential equation:

$$\frac{dX(t)}{dt} = \xi(t) ACX(t) + BU(t) \qquad (3.1)$$
$$X(0) = X_0$$

where, $\xi(t)$ is an environmental scalar, depending on temperature (T) and soil moisture (ω) ($\xi(t) = f(T, \omega)$). There are a few parameters describing the environmental scalar as functions of temperature and moisture (Luo et al. 2003, i.e., **environmental response parameters**).

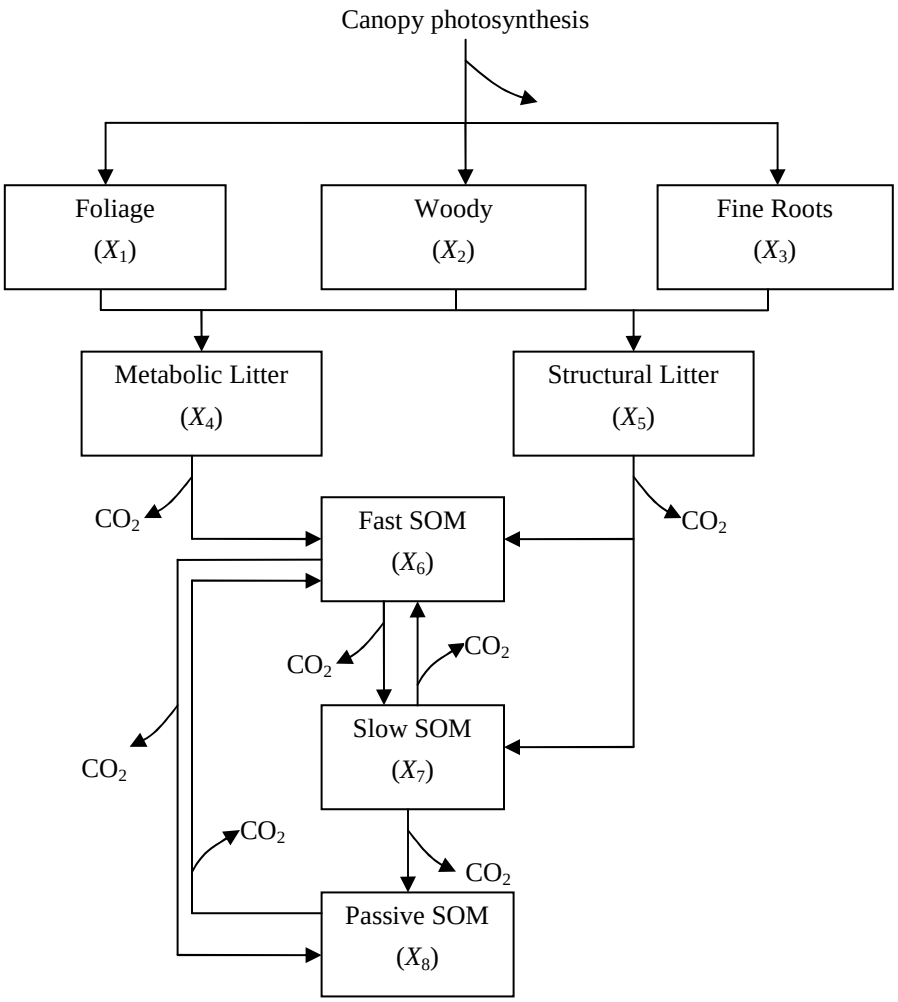

Figure 3.1 The schematic diagram of carbon allocation and transfers among the 8 pools of TECO model. The carbon allocation and transfers were described by equation (1) with 8×8 matrices *A* and *C*, and 8×1 vectors *B* and *X*. SOM stands for soil organic matter.

$X(t) = \left(X_1(t)\ X_2(t)\ X_3(t)\ ...\ X_8(t) \right)^{\mathrm{T}}$ is an 8 × 1 vector representing the carbon content of the eight carbon pools as depicted by Fig. 3.1. X_0 is an 8 × 1 vector of the initial values of $X(t)$. A is a matrix given by

$$A=\begin{pmatrix} -1 & 0 & 0 & 0 & 0 & 0 & 0 & 0 \\ 0 & -1 & 0 & 0 & 0 & 0 & 0 & 0 \\ 0 & 0 & -1 & 0 & 0 & 0 & 0 & 0 \\ f_{4,1} & f_{4,2} & f_{4,3} & -1 & 0 & 0 & 0 & 0 \\ f_{5,1} & f_{5,2} & f_{5,3} & 0 & -1 & 0 & 0 & 0 \\ 0 & 0 & 0 & f_{6,4} & f_{6,5} & -1 & f_{6,7} & f_{6,8} \\ 0 & 0 & 0 & 0 & f_{7,5} & f_{7,6} & -1 & 0 \\ 0 & 0 & 0 & 0 & 0 & f_{8,6} & f_{8,7} & -1 \end{pmatrix}$$

Matrix *A* defines C transfers among the C pools as illustrated by arrows in Fig. 3.1.The non-zero elements ($f_{i,j}$) in matrix *A* represent the fractions of the carbon entering i^{th} (row) pool from j^{th} (column) pool , termed ***carbon transfer coefficients***. The zero elements in matrix *A* mean no direct carbon flows between these two pools. Because $f_{4,1}+f_{5,1}=1$, $f_{4,2}+f_{5,2}=1$, and $f_{4,3}+f_{5,3}=1$, there are only 11 free parameters in matrix *A*. *C* is an 8 × 8 diagonal matrix, $C=diag(c)$ with elements $c=(c_1\ c_2\ c_3\ ...\ c_8)^T$, representing the amounts of carbon per unit mass leaving each of the pools per day, termed ***carbon exit rates***. $B=(b_1\ b_2\ b_3\ 0\ 0\ 0\ 0\ 0)^T$ is a vector of ***allocation coefficients*** of assimilated carbon by photosynthesis (gross primary production, GPP) partitioned to the three plant C pools. $U(t)$ is the C input (GPP) at time *t*.

This study estimated a total of 30 parameters: 8 initial values of carbon pools (X_0(i)), 8 exit rates (c_i), 3 allocation coefficients (b_i), and 11 transfer coefficients ($f_{j,i}$). We set the prior ranges of these 30 parameters (Table 1) according to the measurements at Duke Forest FACE project and/or published papers from literature. The initial values of the eight C pools were estimated mainly from the observations at Duke Forest (Lichter et al. 2005, Finzi et al. 2006). The ranges of exit rates were estimated from the residence times of different C pools at Duke Forest (Lichter et al. 2005), or the similar temperate forests (Harmon et al. 1986, Gaudinski et al. 2000).

Table 3.1 The free parameters of TECO model and their prior ranges.

Parameters	Description	Units	LL	UL
$X_0(1)$	Initial value of foliage pool	$gC \cdot m^{-2}$	100	400
$X_0(2)$	Initial value of woody pool	$gC \cdot m^{-2}$	3000	6000
$X_0(3)$	Initial value of fine roots pool	$gC \cdot m^{-2}$	100	400
$X_0(4)$	Initial value of metabolic pool	$gC \cdot m^{-2}$	40	120
$X_0(5)$	Initial value of structural pool	$gC \cdot m^{-2}$	400	700
$X_0(6)$	Initial value of fast SOM pool	$gC \cdot m^{-2}$	80	240
$X_0(7)$	Initial value of slow SOM pool	$gC \cdot m^{-2}$	1200	2400
$X_0(8)$	Initial value of passive SOM pool	$gC \cdot m^{-2}$	200	400
c_1	Exit rate of C from foliage pool	$gC \cdot gC^{-1} \cdot d^{-1}$	6.85×10^{-4}	5.48×10^{-3}
c_2	Exit rate of C from wood pool	$gC \cdot gC^{-1} \cdot d^{-1}$	3.42×10^{-6}	2.74×10^{-4}
c_3	Exit rate of C from fine root pool	$gC \cdot gC^{-1} \cdot d^{-1}$	1.37×10^{-3}	9.13×10^{-3}
c_4	Exit rate of C from metabolic litter pool	$gC \cdot gC^{-1} \cdot d^{-1}$	5.48×10^{-3}	2.74×10^{-2}
c_5	Exit rate of C from structural litter pool	$gC \cdot gC^{-1} \cdot d^{-1}$	1.37×10^{-4}	2.74×10^{-3}
c_6	Exit rate of C from fast SOM	$gC \cdot gC^{-1} \cdot d^{-1}$	5.48×10^{-3}	5.48×10^{-2}
c_7	Exit rate of C from slow SOM	$gC \cdot gC^{-1} \cdot d^{-1}$	5.48×10^{-6}	5.48×10^{-4}
c_8	Exit rate of C from passive SOM	$gC \cdot gC^{-1} \cdot d^{-1}$	1.37×10^{-6}	5.48×10^{-6}
b_1	Allocation of GPP to leaves	-	0.05	0.25
b_2	Allocation of GPP to woody biomass	-	0.10	0.40
b_3	Allocation of GPP to fine roots	-	0.05	0.25
$f_{4,1}$	Fraction of C in foliage pool transferring to metabolic litter	-	0.3	1.0
$f_{4,2}$	Fraction of C in woody pool transferring to metabolic litter	-	0.0	0.2
$f_{4,3}$	Fraction of C in fine roots transferring to metabolic litter	-	0.3	1.0
$f_{6,4}$	Fraction of C in metabolic litter transferring to fast SOM	-	0.3	0.7
$f_{6,5}$	Fraction of C in structural litter transferring to fast SOM	-	0.1	0.4
$f_{7,5}$	Fraction of C in structural litter transferring to slow SOM	-	0.1	0.4
$f_{7,6}$	Fraction of C in fast SOM transferring to slow SOM	-	0.3	0.7
$f_{8,6}$	Fraction of C in fast SOM transferring to slow SOM	-	0.0	0.008
$f_{6,7}$	Fraction of C in slow SOM transferring to fast SOM	-	0.1	0.6
$f_{8,7}$	Fraction of C in slow SOM transferring to passive SOM	-	0.0	0.02
$f_{6,8}$	Fraction of C in passive SOM transferring to fast SOM	-	0.3	0.7

LL = lower limit and UL = upper limit. SOM= soil organic matter. $X_0(1)$ - $X_0(8)$: initial values of the eight carbon pools; c_1 - c_8: exit rates; b_1 - b_3: allocation coefficients; $f_{i,j}$: carbon transfer coefficients.

Allocation coefficients were from the estimates of NPP of leaves, woody biomass, and fine roots during the experiment period (Palmroth et al. 2006, McCarthy et al. 2006). Transfer coefficients were estimated according to the carbon components of each pool and expert knowledge (Luo et al. 2003). It was assumed that the parameters distributed uniformly in their *prior* ranges. Since this research was to explore the model intrinsic properties not its responses to changes in climatic variables, fixed values were used for the environmental response parameters as described in Luo et al. (2001a, 2003).

3.2.2 Data from Duke forest FACE site

The data used in this analysis were obtained from the FACE experiment at the Blackwood Division, Duke Forest, Orange County, North Carolina (35˚58'N, 79˚5'W). The FACE site was a loblolly pine forest planted in 1983 after harvesting the similar vegetation and was not managed since planting (Hendrey et al. 2000). We used the data at the ambient atmospheric CO_2 concentration only. The ten years air temperature, precipitation, soil moisture, and GPP data (1996~2005) were used as input to drive the TECO model. Air temperature and precipitation were from the observations at Duke Forest FACE. Daily values of GPP were derived from the simulations of MAESTRA model (1996 and 1997) (Luo et al. 2001a) or gap-filled eddy flux data (1998~2005). A non-rectangular hyperbolic method (NRH) was used to derive GPP from eddy flux data (Stoy et al. 2006). Gap-filling might add uncertainty to the data. A comprehensive comparison on the methods differentiating GPP and ecosystem respiration (RE) showed that the gaps added an additional 6–7% variability, but did not result in additional bias and the estimates of both GPP and RE differed by less than 10% among the methods (Desai et al. 2008).

Table 3.2 The biometric data that were assimilated

Data type	Frequency	Number of observations	Mean standard deviation[1] (g C ·m^{-2})	Mean coefficient of variance (CV)	Reference
Foliage biomass	Yearly	9	62.04	15.3%	Pippen et al. unpublished[2]
Woody biomass	Yearly	9	1066.88	16.1%	Finzi et al. 2006
Fine roots	Yearly	9	21.56	7.0%	Pritchard et al. 2008
Litter fall	Yearly	10	65.61[3]	19.5%	Finzi et al. 2006
Forest floor carbon	Three years	4	216.19	24.6%	Lichter et al. 2008
Microbial carbon	Five times in total (1997~98)	5	20.67	21.5%	Allen et al. 2000
Soil total carbon	Three years	4	163.72	7.3%	Lichter et al. 2008
Soil respiration	Monthly	89	0.59[4]	65.7%	Bernhard et al. 2006 Jackson et al. 2009

[1]The standard deviation (SD) for each data point was calculated based on the data collected in the three ambient rings.

[2] On the website http://face.envi.duke.edu.

[3]The unit is g C ·m^{-2}·yr^{-1}.

[4]The unit is g C·m^{-2}·d^{-1}.

The 8 sets of biometric data that were assimilated into the TECO model for parameter estimation were foliage biomass, woody biomass (Finzi et al. 2006), fine root biomass (Pritchard et al. 2008), microbial C (Allen et al. 2000), litter fall, forest floor C, soil C (Lichter et al. 2005, 2008), and soil respiration (Bernhard et al. 2006, Jackson et al. 2009) (Table 2). The data were

collected in the years of 1996 through 2005. These data sets have been extensively described in the aforementioned papers in terms of instruments used for data collection, measurement methods, times and frequencies and are not repeated here.

3.2.3 Data assimilation

We used the probabilistic inversion approach developed by Xu et al. (2006) to assimilate the eight data sets into the TECO model. The probabilistic inversion is based on Bayes' theorem:

$$P(\theta|Z) = \frac{P(Z|\theta)P(\theta)}{P(Z)} \qquad (3.2)$$

where, the posterior probability distribution of the parameters (θ), $P(\theta|Z)$, is obtained from *prior* knowledge represented by a *prior* probability distribution $P(\theta)$ and information in the eight data sets represented by a likelihood function $P(Z|\theta)$. $p(Z)$ is the probability distribution function of observations. The *prior* probability distribution function of the estimated parameters $p(\theta)$ were specified as the uniform distributions over a set of specific intervals. The likelihood function $p(Z|\theta)$ was calculated with the assumption that each component is Gaussian and independently distributed according to the following equation.

$$P(Z|\theta) \propto \exp\left\{-\sum_{i=1}^{8}\sum_{t\in Z_i}\frac{\left[Z_i(t)-\varphi_i X(t)\right]^2}{2\sigma_i^2(t)}\right\} \qquad (3.3)$$

where, $Z(t)$ is data obtained from measurement and $\varphi X(t)$ is simulation, φ is the mapping vector that maps the simulated state variables (the carbon content of the eight pools) and fluxes to observational variables (i.e., plant biomass, litter fall, soil carbon, and soil respiration) (see Appendix B for details). σ is the observed standard deviation of measurements. According to Bayes' theorem, the posterior distribution of parameters was given by

$$P(\theta|Z) \propto P(Z|\theta)P(\theta) \quad (3.4)$$

The probabilistic inversion was carried on using a Metropolis-Hastings algorithm (M-H algorithm, thereafter) to construct posterior probability density functions of parameters. The detailed description of M-H algorithm was provided by Xu et al. (2006) with a brief summary here. M-H algorithm samples random variables in high-dimensional probability density functions in the parameter space via a sampling procedure based on Markov chain Monte Carlo (MCMC) theorems (Metropolis et al. 1953, Hastings, 1970, Gelfand and Smith 1990). In brief, the M-H algorithm was run by repeating two steps: a proposing step and a moving step. In each proposing step, the algorithm generated a new point θ^{new} for a parameter vector θ based on the previously accepted point θ^{old} with a proposal distribution $P(\theta^{new}|\theta^{old})$ (Equation 5).

$$\theta^{new} = \theta^{old} + r(\theta_{max} - \theta_{min}) \quad (3.5)$$

where, θ_{max} and θ_{min} are the maximum and minimum values in the *prior* range of the given parameter. r is a random variable between -0.5 and 0.5 with a uniform distribution. In each moving step, point θ^{new} was tested against the Metropolis criterion (Xu et al. 2006) to examine if it should be accepted or rejected. The accepted parameters were then used to simulate carbon contents of the 8 pools in the 100 years after 1996 using the same driving data of 1996~2005. The M-H algorithm then repeated the proposing and moving steps until approximately 300,000 sets of parameter values were accepted.

All the accepted parameter values were used to construct posterior PDFs. Meanwhile, the same number of sets was obtained for simulated carbon content in the eight pools during the 100-year forwarding runs of the model (namely the model forecasts after data assimilation). The

PDFs of the eight C pool obtained from data assimilation ($(PDFs)_{md}$) contained the information from both the model and the assimilated data. To generate another set of PDFs for the state variables (i.e., pool sizes) without the data assimilated, we ran the model for another 300,000 times by randomly sampling parameter values from their uniform distributions within their *prior* ranges. The generated PDFs of the eight C pools ($(PDFs)_{m}$) contained the information from the model only (including prior parameter ranges). Statistics describing relative information contributions of the model vs. the data was derived from these two sets of PDFs.

3.2.4 Relative information contribution of model and data

We used the Shannon information index (Shannon 1948, White et al. 2006) to measure the relative information contribution of model vs. data to constrain forecasts of short- and long-term carbon dynamics. According to information theory (Jaynes 1957, Kolmogorov 1968), the entropy H of a discrete random variable X in $\{x_1, \ldots, x_n\}$ is

$$H(X) = -\sum_{i=1}^{n} p(x_i) \log_b p(x_i) \qquad (3.6)$$

where $p(x_i)$ is probability of event x_i. For the base b equal to 2, the unit is bit. For a uniform distribution, the entropy is $\log_b n$.

The *null* knowledge on carbon dynamics of a pool (i.e., I_0=0) without either a model or data was defined by a uniform distribution $\pi(x)$ of the pool size within a range (Table 3). The minimum and maximum values of the range were assumed to be the same as those minimum and maximum carbon pool sizes of the $(PDFs)_{m}$ (Table 1). Thus, the entropy of null knowledge (H_0) is:

$$H_0 = \log_2 n \tag{3.7}$$

Model structure and prior parameter uncertainty constitute the "*prior* knowledge" on a system (model information). To estimate the relative information of the model (I_{m}), we obtained the entropy of $(\mathrm{PDFs})_{\mathrm{m}}$, $H(X_m)$, as:

$$H(X_m) = -\sum_{i=1}^{n} p(x_{m,i}) \log_2 p(x_{m,i}) \tag{3.8}$$

where X_m is state variables obtained by the model-only forecasts, $x_{m,i}$ is a value of X_m. n is the number of bins with equal width in the range between the minimum and maximum values of the $(\mathrm{PDFs})_{\mathrm{m}}$. The relative information contribution of the model (including model structure and prior parameter ranges), I_{m}, is:

$$I_m = H_0 - H(X_m) \tag{3.9}$$

Similarly, to estimate the relative information contribution of data assimilation (I_{d}), we first obtained the entropy of the $(\mathrm{PDFs})_{\mathrm{md}}$ derived from model forecasts after the data were assimilated, $H(X_{md})$, as:

$$H(X_{md}) = -\sum_{i=1}^{n} p(x_{md,i}) \log_2 p(x_{md,i}) \tag{3.10}$$

where X_{md} is state variables obtained by data assimilation with the model, $x_{md,i}$ is a value of X_{md}. Thus, the additional information contributed by the assimilated data, I_{d}, is:

$$I_d = H(X_m) - H(X_{md}) \tag{3.11}$$

The calculations of I_m and I_d are summarized in Table 3. $H0$, $H(X_m)$, and $H(X_{md})$ are dependent on the values of n but I_m and I_d change little with n if n is large enough (e.g., Stoy et al. 2006). A

value of 2400 was used in this study after a sensitivity test from 60 to 4800 bins. We calculated I_d and I_m for each of the eight C pools and total ecosystem C over 100 years of simulations.

Table 3.3 Definitions of relative information contribution

Symbol	Description	Contributor	Calculation
I_0	The information without either a model or data	Null knowledge	$I_0=H_0-H_0=0$
I_m	The relative information contributed by model structure and parameter prior ranges	Model	$I_m=H_0-H_m$
I_d	The relative information contributed by the assimilated data sets conditioned on the model structure and parameter *prior* ranges	Data	$I_d=H_m-H_{md}$

H_0 is the entropy of the uniform distribution defined as null knowledge. H_m is the entropy of $(PDFs)_m$ obtained by running the model using parameter values randomly sampled from their *prior* distributions. H_{md} is the entropy of $(PDFs)_{md}$ derived from model forecasts after the data sets were assimilated.

The index I_d only measures the decrease in the entropy of simulated carbon pools induced by data assimilation (i.e., the changes in shapes of PDFs). Assimilation of data may change both positions and shapes of the distributions of C pools. To measure the changes in pool size distributions caused by data assimilation, we used information gain (Kullback-Leibler divergence, $D_{KL}(p(X_{md}) \| q(X_m))$ (Kullback and Leibler 1951, Rényi 1961) to measure the

differences in the distributions of C pools between the model-only forecasts and the model + data forecasts (Equation 12).

$$D_{KL}(p(X_{md}) \,||\, q(X_m)) = \sum_{i=1}^{n} p(x_{md,i}) \log_2 \frac{p(x_{md,i})}{q(x_{m,i})} \qquad (3.12)$$

We also evaluated effects of measurement errors (i.e., standard deviations of the eight data sets), and *prior* ranges of exit rates and transfer coefficients on relative information contributions of the model and data and the Kullback-Leibler divergence induced by assimilation of data. In the analysis, we doubled the standard deviations for all the eight data sets and broadened ranges of the exit rates by doubling their upper limits and halving their lower limits. We used the full possible ranges (i.e., 0–1) for the transfer coefficients in comparison with those in Table 1.

3.2.5 Sensitivity of short- and long-term forecasts to parameters

The coefficients of determinant (R^2) between the forecasted sizes of the pools and the parameters were used as a measure of the sensitivity of the pools to the parameters. It represented the portion of variance of forecasted pool sizes induced by an individual parameter when all of the 30 parameters were varied randomly. We analyzed the sensitivity of each modeled C pool at the end of 2005 to each of the 30 parameters. The sensitivities of total ecosystem C content to the 30 parameters with forecasting years from 4 to 128 years were also calculated this way.

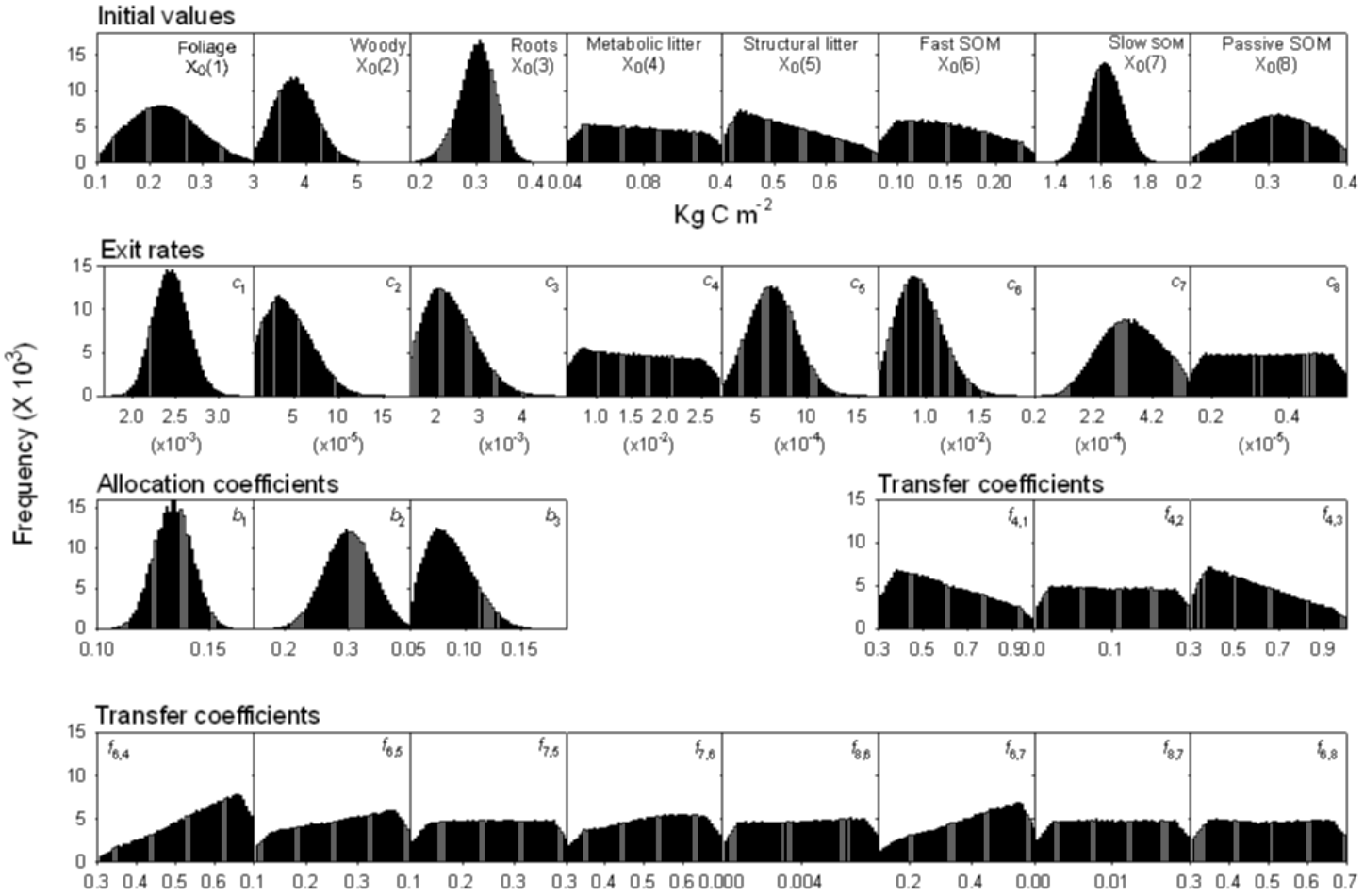

Figure 3.2 The posterior distributions of the 30 free parameters. $X_0(1)$ - $X_0(8)$ are initial values of carbon content in pools corresponding to X_1 - X_8 on Fig. 3.1. c_1 - c_8 are exit rates of the eight carbon pools. b_1 - b_3 are the allocation coefficients of GPP to leaves, woody biomass, and fine roots, respectively. $f_{j,i}$ is the carbon transfer coefficient from pool i to pool j.

3.3 Results

3.3.1 Posterior distributions of parameters

Assimilation of the eight data sets constrained, among the 30 target parameters, five initial values for the foliage biomass (X_0 (1)), woody biomass (X_0 (2)), fine root biomass (X_0 (3)), slow (X_0(7)) and passive(X_0(8)) soil organic matter (SOM) pools; six exit rates from three biomass pools (c_1, c_2, and c_3), structural litter (c_5), fast (c_6) and slow SOM pools (c_7); and two allocation coefficients for wood and fine root pools (b_2 and b_3). None of the transfer coefficients ($f_{i,j}$) were well constrained (Fig. 3.2). Thus, the eight data sets contained information for less than a half of the 30 target parameters.

3.3.2 Modeled carbon contents with and without data assimilation

Distributions of the simulated eight C pools at the end of 2005 without (Model only) and with data assimilation (Model + Data) are shown in Fig. 3.3. The model without assimilation of the eight data sets generated PDFs of carbon pool sizes (i.e., state variables) that were somewhat bell-shaped for long-term pools of woody biomass (X_2), structural litter (X_5), slow SOM (X_7), and passive SOM (X_8) but skewed to their low carbon content ends for short-term pools of foliage biomass (X_1), fine roots (X_3), metabolic litter (X_4) and fast SOM (X_6). The PDFs of carbon pools suggest that the model structure, together with the *prior* ranges of parameters, contains information on ecosystem carbon dynamics, particularly in the long-term pools. With assimilation of the

eight data sets, the simulated carbon content in foliage (X_1), woody (X_2), fine roots (X_3), structural litter (X_5), fast SOM (X_6), slow SOM (X_7), and passive SOM (X_8) pools were all well constrained. The metabolic litter pool (X_4) was still not constrained. Improved modeling of carbon contents indicated that the eight data sets provided a substantial amount of additional information on carbon processes.

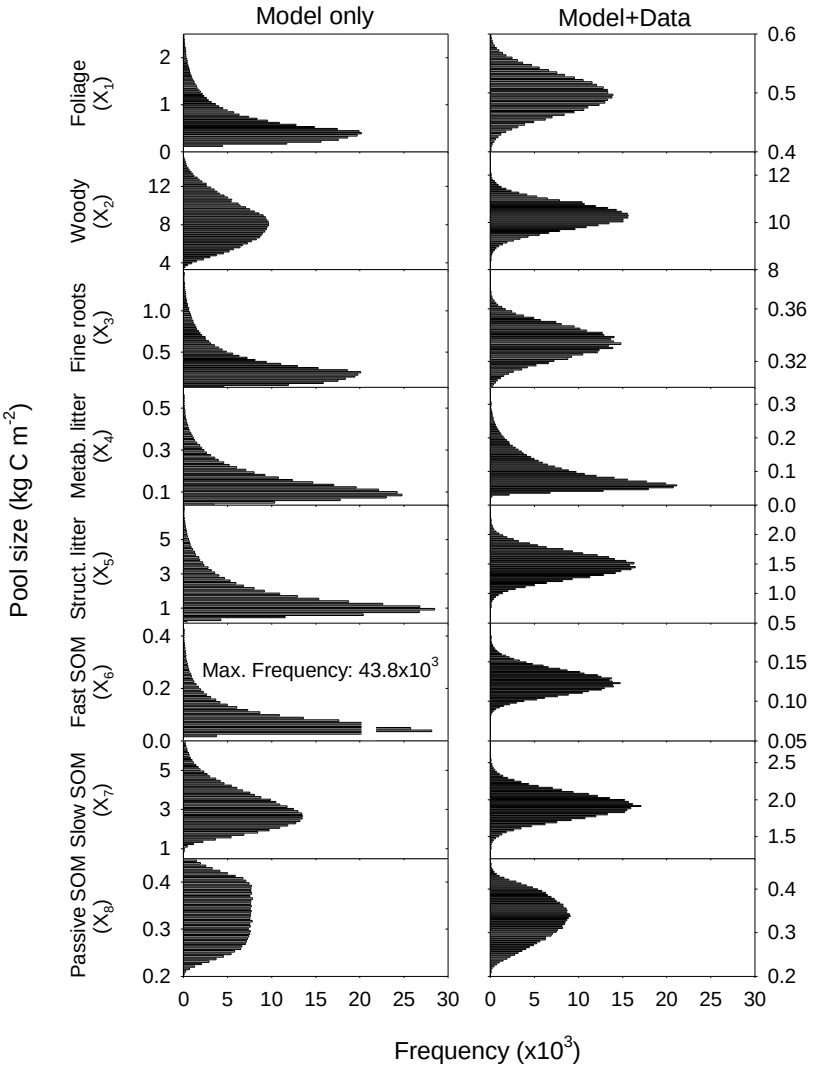

Figure 3.3 Simulated carbon contents at the end of 2005 with parameters sampled in *prior* distributions (Model only) and posterior distributions (Model + Data), respectively.

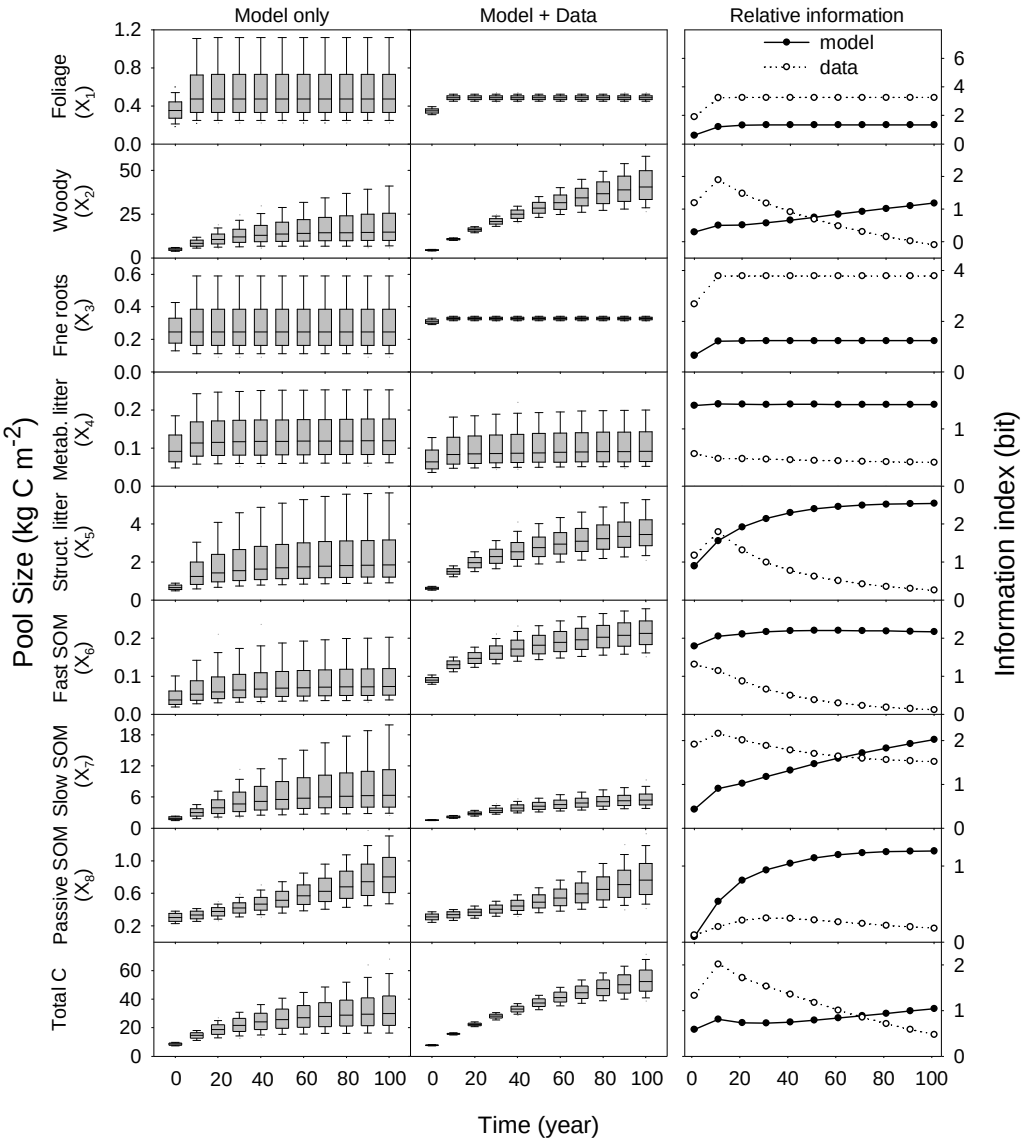

Figure 3.4 The projected carbon content (left and middle columns) and the relative information contributed by model and data (right column) over 100-year forecasts after 1996. Box plots show visual summaries of carbon content distributions in the 5% (bottom bar), 25% (bottom hinge of the box), 50% (the lined across the box), 75% (upper hinge of the box), and 95% (upper bar) intervals. Closed circles with solid lines are the relative information contribution of the model; open circles with dotted lines are the relative information contribution of data.

3.3.3 Long-term forecasts of C contents and information contributions of model and data

Either with or without assimilation of data, carbon contents were quickly stabilized in the fast turnover pools, such as foliage biomass (X_1), fine roots (X_3), and metabolic litter (X_4), but substantially increased in slow turnover pools, such as woody biomass (X_2), slow and passive SOM pools (X_7 and X_8), over the 100 years of forecasting (left and middle columns of Fig. 3.4). Corresponding variances of probability density distributions were also stabilized for the fast turnover pools (X_1, X_3, and X_4) in the second decade but kept growing for the slow turnover pools (e.g., X_2, X_7, and X_8). Assimilation of the eight data sets substantially reduced variations of forecasted C contents, especially in those fast turnover pools (Model + Data), in comparison with those without data assimilation (Model only) (Fig. 3.4). This indicates that data provide substantial information to constrain forecasts of carbon dynamics. Data assimilation also considerably altered the maximum likelihood estimates of carbon content in most of the eight pools.

The relative information contribution by the model (including model structure and parameter prior ranges) steadily increased whereas the data contribution decreased for the slow turnover pools and ecosystem total C during the 100-year forecasting (right column of Fig. 3.4). For the two major C pools, woody biomass (X_2) and slow SOM (X_7), the model contributed less information in the first few decades and more in the last decades than the assimilated data in the course of the 100-year forecasting. For foliage biomass (X_1) and fine roots (X_3) pools, the eight data sets contributed more information than the

model during the entire period of forecasting. The model contributed more information than the data in the litter pools (X_4 and X_5), fast(X_6) and passive (X_8) SOM pools.

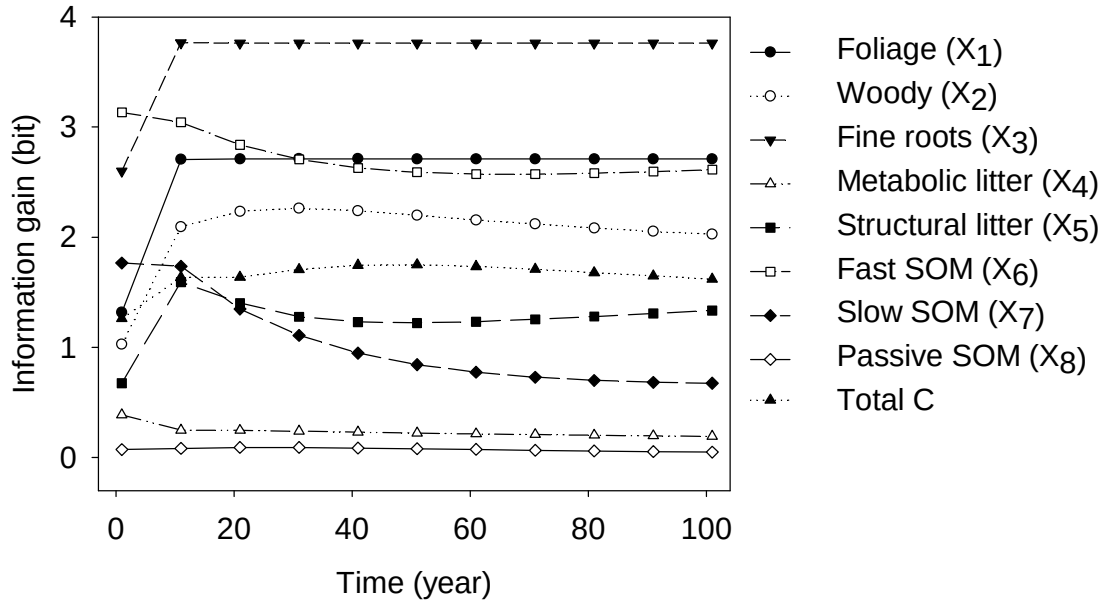

Figure 3.5 The changes in the distributions of the carbon content of the eight carbon pools and total ecosystem carbon at the assimilation of data into the model, measured by the information gains derived from the distributions of carbon content simulated by model only and those simulated by model plus data.

The information gain of data assimilation was the highest for the foliage biomass (X_1), fast SOM (X_6), and fine roots (X_3), and the lowest for the passive SOM (X_8) (Fig. 3.5). The information gain increased first and then decreased gradually for the woody biomass (X_2) and total C. The information gain declined with time for the fast and slow SOM pools (X_6 and X_7), and metabolic litter(X_4). The information gain for the structural litter (X_5) and fast SOM (X_6) pools was also substantial although data assimilation only

slightly reduced their uncertainties toward the end of the 100-year forecasting (Fig. 3.5 vs. Fig. 3.4).

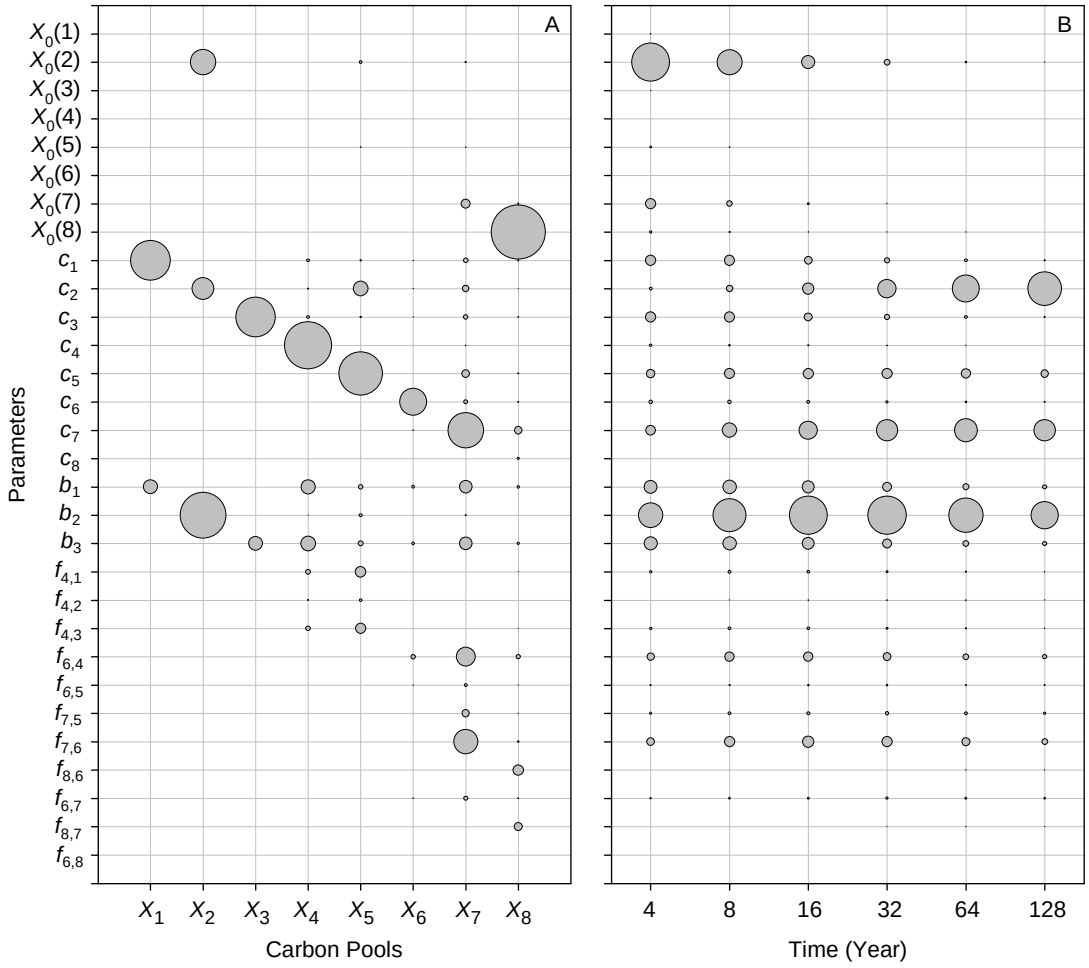

Figure 3.6 The sensitivity of the eight carbon pools at ten years' simulation (A) and the sensitivity of ecosystem total carbon in long-term simulations (B) to the 30 parameters. X_1 - X_8 are the eight carbon pools as shown in Fig. 3.1. $X_0(1)$ - $X_0(8)$ are initial values of the eight carbon pools. c_1 - c_8 are exit rates of the eight carbon pools. b_1 - b_3 are the allocation coefficients of GPP to leaves, woody biomass, and fine roots, respectively. $f_{i,j}$'s are the carbon transfer coefficients from pool *j* to pool *i*. The area of circle represents the value of the coefficient of determinant.

3.3.4 Parameters that determine short- vs. long-term forecasting

The simulated carbon content of the eight pools at the end of 2005 had different sensitivities to the 30 parameters (Fig. 3.6: A). The foliage biomass (X_1) and fine root pools (X_3) were highly sensitive to their respective exit rates (c_1 and c_3) and modest to allocation coefficients to themselves (b_1 and b_3). The woody biomass (X_2) was sensitive to its exit rate (c_2), allocation coefficient to itself (b_2), and its initial value (X_0 (2)). The metabolic litter (X_4) was highly sensitive to its exit rate (c_4), and modest to allocation coefficients b_1 and b_3. The structural litter (X_5) was highly sensitive to c_5 and modest to c_2. The fast SOM (X_6) was sensitive to c_6 only. The slow SOM (X_7) was sensitive to c_7, $f_{7,6}$, and $f_{6,4}$. The passive SOM (X_8) was sensitive to $X_0(8)$ only. In general, the modeled C pools were most sensitive to the parameters that governed the carbon input into or output out of themselves or their neighbor pools that directly affected them. Plant carbon pools (X_1, X_2 and X_3) were not sensitive to any of the transfer coefficients ($f_{i,j}$'s), which only regulate carbon dynamics in the downstream pools. The fast turnover pools (X_1, X_3, X_4, and X_6) were not sensitive to their initial values ($X_0(i)$, i = 1, 3, 4, or 6). The downstream pools were sensitive to more parameters than the upstream pools (e.g., X_7 vs. X_2) because the C dynamics in the downstream pools were influenced by behaviors of the upstream pools. The opposite did not occur.

The sensitivity of forecasted total ecosystem C content to parameters varied with time (Fig. 3.6: B). For example, the highest sensitive parameter for the total ecosystem C content was the initial value of woody biomass ($X_0(2)$) for the 4-year forecast. For the

128-year forecast, the highest sensitive parameter was the exit rate of C from the woody biomass pool (c_2), which gradually became more important over time in determining ecosystem C dynamics. The order of the six most sensitive parameters for the forecasted total ecosystem C content was $X_0(2)$, b_2, b_3, b_1, $X_0(7)$, and c_3 at the 4th year but it was c_2, b_2, c_7, c_5, $f_{7,6}$, and $f_{6,4}$ at the 128th year.

3.3.5 Effects of *prior* ranges and measurement errors on information contribution

The data contributed more information to constrain forecasts of forest carbon dynamics when the *prior* ranges of parameters were enlarged (Fig. 3.7 B vs. A). The enlarged parameter ranges also resulted in slight increases in the relative information contribution of the model since the *null* information was lowered due to changes in the minima and maxima of simulated carbon contents, which were used to define the *null* information. The relative information contribution of data increased at low model priors (Fig. 3.7: B vs. A). The information contribution by the data substantially decreased but did not change for the model component at doubled measurement errors (Fig. 3.7 C vs. A). However, the temporal patterns of information contribution did not change. The information gain was high at enlarged parameter ranges (low model *prior*) (Fig. 3.7: E), and it was low at doubled measurement errors (Fig. 3.7: F).

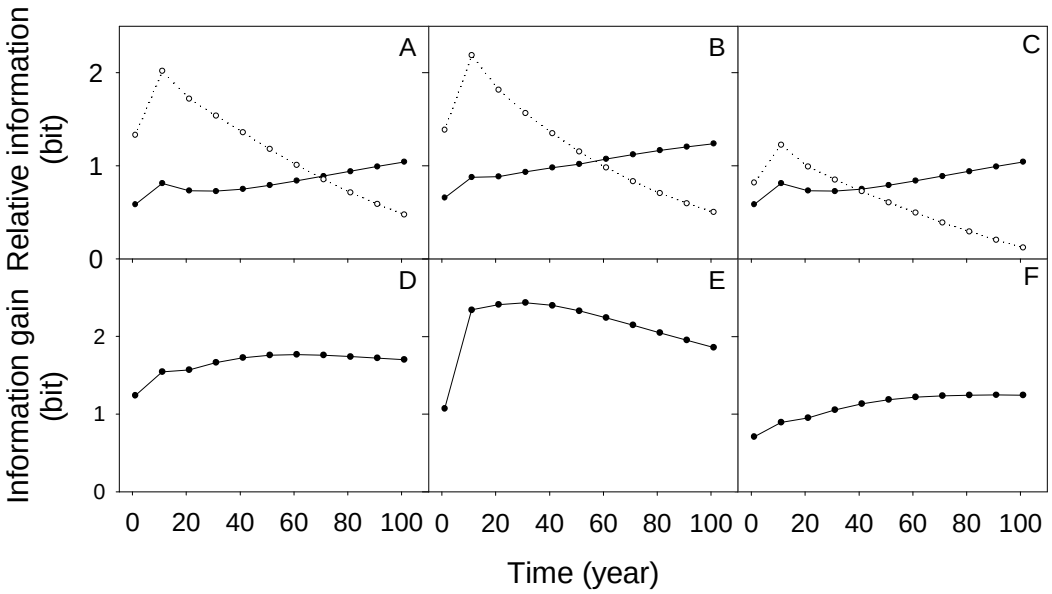

Figure 3.7 Information contribution of model vs. data and information gain with different parameter priors and measurement errors. Panels A, B, and C show relative information contributions with original parameter ranges and original measurement errors (A), full ranges of transfer coefficients and broadened ranges of exit rates (doubled upper limits, halved lower limits) with original measurement errors (B), and doubled measurement errors with original parameter ranges (C), respectively. Closed circles with solid lines are relative information contributions of the TECO model; open circles with dotted lines are the relative information contributions of the data. Panels D, E, and F are the information gains with the same order of the combinations of parameter ranges and measurement errors as panels A, B, and C.

3.4 Discussion

In this study, we evaluated relative information contributions of the TECO model and the eight data sets to the constraints of 100-year forecasts of carbon dynamics in Duke Forest. The sensitivities of short and long-term forecasts to model parameters were

analyzed to explain how the information contributions of the model and the data varied over time. The temporal changes in information contributions and parameter sensitivities have strong implications for the development and evaluation of current terrestrial biogeochemical models for regional and global assessment, and data collections in the future.

3.4.1 Short- vs. long-term forecasts of forest carbon dynamics

Parameters that influence uncertainty of carbon dynamics forecasts varied with time scale. Our analysis shows that the initial value of woody biomass ($X_0(2)$) and allocation coefficient to woody biomass (b_2) were the two most important parameters in influencing short-term forecasts of total ecosystem C dynamics (Fig. 3.7). The initial values of C pools define their positions on a trajectory of transient recovery, and therefore determine the rate of carbon accumulation and C storage potential (Carvalhais et al. 2008, Gough et al. 2008). The changes in C content of the eight C pools are different because their initial values are apart from their equilibrium states differently. The fast turnover pools, e.g., foliage and fine root C pools, are almost equilibrated at the initial states, while the slow turnover pools, e.g., woody biomass, slow SOM, and passive SOM, are far lower than their equilibrium states. So, woody biomass, slow SOM, and passive SOM have high carbon accumulate rates. The Duke forest was in its early stage of secondary succession after plantation in 1983 (Hendrey et al. 1999). Carbon in many pools, especially in the slow turnover pools, was accumulating. Thus, $X_0(2)$ and b_2, which determine the

trajectory of transient C dynamics in one of the long-term pools, are the two key parameters affecting short-term forecasts of ecosystem C dynamics.

The results indicate that long-term forecasts of forest carbon dynamics were strongly influenced by the growth rate of woody biomass of trees (determined by exit rate, c_2 and the allocation coefficient, b_2, in the model), and the decomposition rate of slow SOM (c_7) (Fig. 3.7). Theoretically, the long-term C storage in an ecosystem is determined by C influx and residence time (Luo et al. 2001a). In this study, the C influx was input from simulation results of another photosynthesis model based on the eddy covariance data (Luo et al. 2003, Stoy et al. 2006), while the parameters that determine C influx were not evaluated. The ecosystem carbon residence time is determined by carbon residence times in individual pools, carbon allocation of GPP to plant pools, and transfer coefficients among soil C pools (Zhou and Luo 2008). Thus, we mainly evaluated the ecosystem residence time in influencing the long-term C storage in this study. The inverses of c_2 and c_7 are the residence times of the woody biomass and slow soil C pools, respectively. Parameter b_2 controls the amount of photosynthetically fixed C to be allocated to the wood pool and subsequently influences C transfer to other long-term pools, such as structural litter, slow and passive SOM pools. Therefore, these three parameters are most important in determining the long-term carbon dynamics of forest ecosystems. Parameter b_2 is important for both short- and long- term forecasts of forest C dynamics partially because it controls C allocation to the largest, long-term C pool in this particular forest, therefore, influences the C dynamics of the downstream pools.

Terrestrial biogeochemical models are usually tested against short-term data (e.g., Stöckli et al. 2008, Randerson et al. 2009) and the evaluations of parameterization are mainly on the parameters controlling short-term processes (e.g., Knorr and Heimann 2001, Zaehle et al. 2005). Whereas, these models are widely used in long-term predictions (e.g., Fung et al., 2005, Friedlingstein et al. 2006, Sitch et al. 2008). Rastetter (1996) had proposed that long-term processes must be tested against long-term data after examining the performance of a photosynthesis model at multiple temporal scales. Parameter sensitivity analysis in this study shows that the long-term process related parameters are still important for short-term forecasts (e.g., initial value ($X_0(2)$) and allocation coefficient (b_2) of woody biomass, and exit rate of soil slow C (c_7)) (Fig. 3.7). Therefore, the emphasis of parameterization for a biogeochemical model used to predict C storage should be on the long-term related parameters, especially on initial values for short-term forecasts and residence times for long-term forecasts.

3.4.2 Relative information contribution of model and data

Our analysis shows that the relative information contributed by the data declined over time but that contributed by the model increased slightly for the slow C pools (i.e., woody biomass, slow and passive SOM pools) and total ecosystem C (right column of Fig. 3.4). This means the model with the *prior* knowledge it represented plays an important role in forecasting long-term carbon dynamics. The processes (e.g, the compartmentalized pools and donor pool controlled carbon transfers for the TECO

model) defined the behavior of a model, therefore the spaces of its projections. This may probably be true for all process-based biogeochemical models. Statistical models can sometimes generate better results than the process-based models by deriving the relationships between climate variables and carbon dynamics. Artificial neural networks, for example, can fit the observations better than sophisticated process-based models after training by data (Abramowitz 2005). An experience model with the relationships between NPP and climate variables can reproduce the pattern of global NPP (Del Grosso et al. 2008). A well calibrated climate-vegetation relationship model can capture the vegetation distribution pattern globally or regionally (e.g., BIOME model, Prentice et al. 1992, Weng and Zhou 2006). But the statistical relationships may be different with changes in climate, since ecosystems may not always be on equilibrium states because of lag effects (Sherry et al. 2008), vegetation shifts (Bachelet et al. 2001, Harrison and Prentice 2003), acclimation (Luo et al. 2001b), or ecosystem development (Chadwick et al. 1999). The process-based biogeochemical models can represent these mechanisms by incorporating simple or complex processes. Thus, the analysis of the relationships between climate variables and carbon dynamics should be confined in the framework defined by the *prior* knowledge on ecological mechanisms.

The eight data sets provided high information for upper stream pools (i.e., foliage, woody, and fine root pools) but low for down stream pools (litters and soil carbon pools) generally (right column of Fig. 3.4). This may be a result of the consistency between data types and model carbon pools. Three data sets (foliage, woody, and fine root biomass) are

directly accordant with the three plant C pools. But none of the litter and soil C data is accordant with the two litter pools and the slow and passive SOM pools. Fox et al. (2009) explored the constraints of parameters in a TECO-like model, DALEC model, with assimilation of net ecosystem exchange (NEE) and leaf area index (LAI) data. The difference between these two models is that the DALEC model has one litter pool and one soil C pool, while the TECO has two and three, respectively. They found that the parameters related to photosynthesis and ecosystem respiration processes were constrained well. But the parameters related to roots and woody C pools (turnover rates and allocation coefficients) were constrained poorly. Therefore, their predictions on C stock diverged broadly in the third year. These results indicate collecting biometric data (e.g., woody biomass and soil carbon) is important for both short- and long-term forecasts on ecosystem C content and it is necessary for researchers to constrain long term pools and fluxes using short term observations.

3.4.3 Factors influencing information contributions

The *null* knowledge of pool sizes, model *prior*, and data uncertainties can affect relative information contributions of the model and data. Uniform distribution is usually used to represent *null* knowledge and the ranges are consequently the same with the corresponding PDFs. The way that uses the ranges of simulated carbon contents of the eight pools by the model with prior parameters can provide a wide enough space that all simulated results lie. And, the changes in the shapes of the PDFs induced by the model with prior or with posterior parameters can be effectively measured by relative

information indices (I_m or I_m+I_d). By doing so, the information contribution of the model (I_m) is independent on the number of bins (n).

Model *prior*, including model structure and quantitative estimates of parameter uncertainties, is a quantitative measure on what we have known about the system. In this study, the model structure is well established. The parameter ranges are also well recognized from qualitative aspect, e.g., woody biomass's residence time is much longer than the leaf's; the carbon flowing to passive SOM is much lower than that to slow SOM. However, they are still varied among researchers when putting each of the parameters into a numerical range. We thoroughly reviewed the literature and proposed a set of parameter ranges that are believed to cover the right values. Uniform distributions are used to represent parameter uncertainties, since we did not want to put our judgment that some values were likely or unlikely to be the right ones. The sensitivity test on parameter ranges showed that the enlarged ranges led to little changes in the relative information contributions of the model. However, the data contributed more information at wider *prior* parameter ranges (Fig. 3.7: B). These indicate model-only results are not sensitive to parameter ranges if these ranges are reasonable.

Measurement errors determine the weighting between observations and simulated results and the weighting of each observation. A thorough evaluation of measurement errors is necessary for assimilation of multiple sourced data sets. In this study, the standard deviations (SD) of assimilated data were calculated for each observation based on the data collected in the three ambient rings. The coefficient of variation (CV) is the

highest for the soil respiration data (66%) and lowest for the fine root data (7%). The number of data points of each data set is also a factor affecting its weight in cost function. Among the eight data sets, soil respiration has the highest points, 89, while the forest floor C and soil total C are the lowest, 4 only (Table 2). Thus, it is desirable to explore the weight of each data set for multiple sourced data assimilation. We tested the effects of magnitudes of measurement errors on information contribution. Less information contributed by data at doubled measurement errors, but the pattern that model's contribution increases while data's decreases remains (Fig. 3.7: C and F).

In this study, GPP is derived from another model or eddy-flux data and used as an input to the model. The given GPP may influence the constraints of modeled carbon pool sizes and total ecosystem C content. In most biogeochemical models, GPP is modeled by an independent photosynthesis model with influences of the dynamic of the foliage pool, and is usually stabilized within one or a couple of decades. Thus, the uncertainties in simulated GPP do not affect the relative information contributions of model and data in the framework of a carbon pool model.

The processes that are not considered in the model may also affect long-term forecasts of ecosystem states. For example, the current version of TECO model does not have the processes representing disturbances and carbon-nitrogen interactions. These two processes are considered to affect forest ecosystem C storage at long temporal scales (Luo et al. 2003, Gough et al. 2007). Since the woody biomass related parameters (c_2 and b_2) have high sensitivity to disturbances and nitrogen availability, the uncertainties in

long-term forecasts may be higher than simulated. Therefore, the effects of disturbances and nitrogen on the long-term forecast sensitive parameters, i.e., c_2, b_2, and c_7) should be evaluated carefully in long-term forecasting. Overall, the accuracy of 100-year forecasts is essentially un-testable. But, the assimilation of data did reduce the uncertainties in the model and its forecasts based on the processes considered in the model.

3.5 Conclusions

Our results showed the information contribution of the model generally increased with time whereas the data's contribution declined. The eight data sets contributed more than the model to constrain C dynamics in foliage and fine root pools over the 100-year forecasts. The model, however, contributed more than the data sets to constrain litter, fast SOM, and passive SOM pools. For the two major C pools, woody biomass and slow SOM, the model contributed less information in the first several decades and then more in the last decades than the data. Parameter sensitivity analysis showed that the initial value of woody carbon pool ($X_0(2)$) and allocation coefficient to woody biomass (b_2) were the two most important parameters for short-term forecasts of ecosystem total C, while the key parameters for the long-term forecasts were the exit rate (c_2) and allocation coefficient (b_2) of woody biomass, and exit rate of slow SOM (c_7).

These results indicate data assimilation is very useful in constraining short and long-term forecasts of forest carbon dynamics, while a good forward model is still fundamental to long-term forecasts. The test against short-term data cannot guarantee

improving the parameters governing long-term processes since the important parameters for short-term forecasts may be different from those for long-term forecasts. Incorporating the processes affecting long-term ecosystem carbon dynamics into biogeochemical models, such as disturbances and carbon-nitrogen interaction processes, and collecting more long-term data related to soil carbon dynamics are required for reducing the uncertainties in the forecasts of long-term ecosystem carbon dynamics.

3.6 Acknowledgments

This research was financially supported by the Office of Science, Department of Energy, Grants No.: DE-FG02-006ER64319 and through the Midwestern Regional Center of the National Institute for Climatic Change Research at Michigan Technological University, under Award Number DE-FC02-06ER64158, and by National Science Foundation under DBI 0850290, DEB 0840964, and DEB 0743778. The data are from Duke FACE facility, which was supported by the Office of Science, U.S. Department of Energy, Grant No. DE-FG02-95ER62083, and through its Southeast Regional Center of the National Institute for Global Environmental Change under Cooperative Agreement No. DE-FC02-03ER63613. The runs for this research were performed at the OU Supercomputing Center for Education & Research at the University of Oklahoma. We thank Dr. Henry Neeman for his help with using super computer. We appreciate Wendy M. Martin and Oleksandra Hararuk for their help in writing.

CHAPTER 4 Carbon Storage Capacity under Varying Disturbance Regimes[3]

[3] This part is from a manuscript coauthored by Yiqi Luo, Nikola Petrov, Weile Wang, Han Wang, Daniel J. Hayes, A. David McGuire, Alan Hastings, and David S. Schimel

Abstract:

Disturbance has been recognized as a key factor affecting terrestrial carbon storage and dynamics. Most observational studies have focused on quantifying impacts of individual disturbance events on ecosystem carbon processes. Modeling studies mostly link specific disturbance events with ecosystem processes to characterize carbon sink dynamics. However, the quantitative relationship between carbon storage capacity and disturbance regimes has not yet been explored. Here we developed a mathematical model to quantify carbon storage capacity of ecosystems with varying disturbance regimes. The latter is defined in this study by the mean disturbance interval (MDI, λ, an index of disturbance frequency) and the mean disturbance severity ($E[s]$). Thus, expected carbon storage capacity ($E[X]$) under the disturbance regime can be described by $E[X] = U \cdot \tau_E \cdot \frac{\lambda}{\lambda + E[s]\tau_1}$, where U is ecosystem carbon influx, τ_E is ecosystem carbon residence time, and τ_1 is the residence time of live biomass pool. Our model shows that carbon storage capacity decreases with disturbance severity but increases with mean disturbance intervals, carbon influx and residence time. This model, for the first time to our knowledge, analytically integrates biogeochemical processes (carbon input and residence time) with disturbance regimes (MDI and severity) to reveal general patterns of terrestrial carbon sink dynamics under varying disturbance regimes.

Key words: Ecosystem carbon storage,disturbance, carbon cycle, dynamic disequilibrium

4.1 Introduction

Disturbances can profoundly affect ecosystem carbon (C) storage and dynamics by generating spatial heterogeneous landscapes, altering ecosystem species compositions, reducing ecosystem production, depleting one or more C pools, and relocating C distribution among the C pools (Goetz et al. 2007, Turner et al. 2010) and leave legacies strongly influencing future carbon sources or sinks (Houghton et al. 1983, Balshi et al. 2007). Climate warming can cause increases in frequencies, severities, and the spatial coverage of disturbance events, such as fires (Bowman et al. 2009, Turetsky et al. 2011), storms (Webster et al. 2005, Emanuel 2005), and insect outbreaks (Kurz et al. 2008), and therefore increase the vulnerability of C storage of terrestrial ecosystems (Balshi et al. 2009). Better understanding of ecosystem C storage responses to disturbances in the context of climate change is required for accurately estimating the feedbacks between C cycle and climate change.

Impacts of individual disturbance events on ecosystem carbon processes have been extensively studied. For example, the effects of fire on landscape heterogeneity (Turner et al. 1994), ecosystem recovery patterns (Kashian et al. 2005, Kashian et al. 2006), and C and nitrogen dynamics (Kashian et al. 2006, Smithwick et al. 2009) have been systematically investigated following the 1988 Yellowstone Fires. Insect outbreaks can

substantially reduce ecosystem C gross primary production, transforming Canadian boreal forests from C sinks to sources (Kurz et al. 2008). Many modeling studies that link specific disturbance events with ecosystem processes to characterize and project ecosystem C dynamics have been conducted to reveal mechanisms of disturbances affecting C processes and possible changes of C dynamics in the future. Bond-Lamberty et al. (2007) found that disturbance events were the dominant driver of central Canadian boreal forest carbon balance by modeling analysis with Biome-BGC model. Balshi et al. (2007, 2009) analyzed the effects of historical fires on current C dynamics of the high latitude regions of North America and proposed that fires could substantially increase the vulnerability of the C storage in the boreal forests with in the 21st century.

However, terrestrial ecosystems can rapidly recover from individual disturbance events, even like the great fires of Yellowstone 1988 (Turner et al. 2010), making them carbon neutral from a long-term view (Kashian et al. 2006). The structure and functions of main terrestrial ecosystems, and therefore their C storage, are strongly shaped by disturbance regimes, which is the summary of the frequencies, severities, and the spatial coverage of disturbance events (Turner et al. 1994, White and Jentsch 2001). Disturbance regimes vary among the major terrestrial ecosystem types of the world. Tropical rain forests have a low frequency and severity of fires (Bowman et al. 2009) but a high frequency of storms (Zeng et al. 2009). Fires occur frequently with low severity in Savanna but of intermediate frequency and high severity in boreal forests (Bowman et al. 2009, Chuvieco et al. 2008). Climate change is altering the disturbance regimes of these

ecosystems (Turetsky et al. 2010) and triggering ecosystem state shifts (Johnstone et al. 2010), and inducing a large amount of C release to atmosphere (Beck et al. 2011). But, we still lack theoretical understanding of ecosystem C storage as a function of disturbance regimes and ecosystem internal processes. Thus, it is necessary to generalize the quantitative patterns of ecosystem C dynamics in response to changes in disturbance regimes and the rates of C input and output for improving our predictive understanding of ecosystem responses to changing climate.

In this study, we derived a general quantitative description of ecosystem C storage changing with disturbance regimes based on explicit descriptions of spatial and temporal patterns of C dynamics of ecosystems induced by disturbances generalized from event-based studies. At temporal scales, ecosystem C content usually decreases sharply at the occurrence of disturbance events and then gradually recovers, as documented from chronosequence studies and long-term observations in most of the terrestrial biomes across the world (Hughes et al. 1999, Law et al. 2003, Vargas et al. 2008). The recovery patterns encompass the fluxes of ecosystem C input (i.e., net primary production, NPP) and output (e.g., decompositions of litter and soil organic matters), controlled by internal ecosystem processes that equilibrate ecosystem C storage (Luo and Weng 2011). While at large spatial scales, ecosystems are usually at different recovery stages due to random disturbances, leading to mosaics of C content in a large region. The mean C storage therefore is always lower than the equilibrium state defined by ecosystem internal processes (Luo and Weng 2011). We integrated the spatial and temporal patterns of

ecosystem C dynamics with a few key assumptions about the probability density distribution of disturbance occurrence and the pattern of ecosystem C recovery and thus developed a theoretical model to quantify ecosystem C storage capacity as affected by disturbance regimes at large spatial scales. This model was then tested against the simulations of TEM model in the high latitude areas of North America. The model can improve our predictive understanding of C storage with changes in disturbance regime and ecosystem internal properties.

4.2 Materials and Methods

4.2.1 Ecosystem Model

A three-pool model was used in numerical simulations and mathematical reasoning. The model has biomass, litter, and soil organic matter (SOM) carbon pools (Fig. 4.1). For an ecosystem developed from bare ground, it can be represented by Eqn 4.1.

$$\frac{dX(t)}{dt} = AT^{-1}X(t) + BU(t)$$
$$X(0) = \begin{pmatrix} 0 & 0 & 0 \end{pmatrix}' \qquad (4.1)$$

where, $X(t)$ is ecosystem carbon content at time t; A is a 3 × 3 matrix representing carbon transfer among the three pools, $A = \begin{pmatrix} -1 & 0 & 0 \\ 1 & -1 & 0 \\ 0 & \eta & -1 \end{pmatrix}$ and η is carbon transfer coefficient from the litter pool to the SOM pool. T is an 3 × 3 diagonal matrix, $\mathrm{T} = diag(\tau)$. The diagonal elements are $\mathrm{T} = (\tau_1\ \tau_2\ \tau_3)'$. τ_1, τ_2, and τ_3 are the residence times of the carbon in

biomass, litter, and SOM, respectively. B is the allocation coefficients of carbon influx (i.e., NPP) to the three pools, $(1 \quad 0 \quad 0)'$. $U(t)$ is the carbon influx at time t.

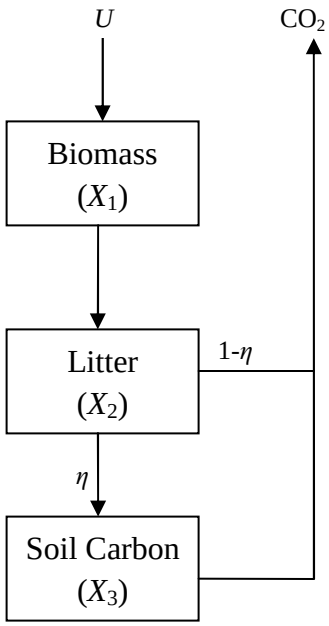

Figure 4.1 Ecosystem model Structure U is the ecosystem carbon input from photosynthesis (net primary production). The model has three carbon pools: Biomass (X_1), Litter (X_2), and Soil Organic Matter (SOM) (X_3). η is the ratio of carbon transferred to the SOM pool from the litter pool. In simulation tests, we let τ_1 =20 yrs, τ_2=5 yrs, τ_3=60 yrs, and η=0.25. Thus, the ecosystem carbon residence time $\tau_E=\tau_1+\tau_2+\tau_3 \cdot \eta$=40 yrs.

Two characters of disturbance regime, the mean disturbance interval (MDI) and the disturbance severity, were considered. The disturbance events were assumed as Poisson events. The ecosystem carbon dynamics with effects of disturbance was represented by the following equation:

$$\frac{dX(t)}{dt} = AT^{-1}X(t) + BU(t) + r \cdot s \cdot \Xi X(t) \qquad (4.2)$$

where r is a discrete random variable taking the value either 0 or 1. $P(r=1)=1/\lambda$ is the probability that disturbance happens in a year and λ is the MDI. Matrix Ξ represents carbon losses and transfer among the three carbon pools induced by a disturbance event. It was assumed that the disturbance events could only remove biomass with a fraction of s and had no effects on the litter and the SOM pools. So, $\Xi = \begin{pmatrix} -1 & 0 & 0 \\ 0 & 0 & 0 \\ 0 & 0 & 0 \end{pmatrix}$. The NPP was 1.2 Kg C $m^{-2} \cdot yr^{-1}$, τ_1 20 yrs, τ_2 5 yrs, τ_3 60 yrs, and η was 0.25 for numerical simulations. Thus, the ecosystem carbon residence time, τ_E, was 40 yrs ($\tau_E=\tau_1+\tau_2+\tau_3 \cdot \eta=40$).

4.2.2 Sensitivity tests

Probability density functions of disturbance interval Both Weibull distribution and exponential distribution are widely used to describe disturbance intervals (Katz et al. 2005, Johnson and Gutsell 1994). Weibull distribution is usually used in the disturbances that depend on the conditions of ecosystems (e.g., fire) for its flexibility to represent the changes of the disturbance occurrence probability over time by varying its shape factor (Clark 1990, Grissino-Mayer 1999).

$$f(T;\lambda,k)=\begin{cases} \frac{k}{\lambda}\left(\frac{T}{\lambda}\right)^{k-1} e^{-(T/\lambda)^k} & (T \geq 0) \\ 0 & (T<0) \end{cases} \quad (4.3)$$

where k is shape factor. Exponential distribution is a special case of Weibull distribution with k=1, and is usually used to describe the intervals of the disturbance events that are Poissonian (the probability of disturbance occurrence is constant over time). It is

applicable to many disturbances, e.g., storm and landslide with their occurrence being independent on the state of ecosystems. We simulated ecosystem C content by the ecosystem model with disturbance severity equal to 1 and intervals were sampled from a Weibull distribution with the shape factor varying from 1.0 (exponential distribution) to 2.0. The mean simulated carbon content was generated by running the model at 65000 grids.

Dynamics of NPP after disturbances Forest NPP usually decreases sharply at disturbances and then increases with age. After approaching the highest level, it decreases slightly and is stable at a certain level with the development of a stand (Gower et al. 1996, Ryan et al. 1997), although it is still in debate for natural forests (Wirth 2009). We conducted a simulation test to illustrate the biases of ecosystem carbon storage resulted from the assumption of constant NPP. The realistic NPP pattern was simulated by the following equations:

$$\begin{aligned} GPP(t) &= GPP_{\max} \cdot \left(1 - e^{-[X_1(t)/L + a]}\right) \\ U(t) &= (1-b) \cdot GPP(t) - f \cdot X_1(t) \end{aligned} \tag{4.4}$$

where, $GPP_{\max}$ is the maximum GPP, 2.4 Kg C $m^{-2} \cdot yr^{-1}$. L is an experience value controlling the recovery rate of NPP. a is a small number for determining the initial NPP when biomass (X_1) is zero. We used 2.4 Kg C m^{-2} and 0.2 for L and a, respectively. b is 0.3 and f is 0.02. A NPP recovery curve was generated with NPP increasing in the first 10 years and then decreasing slightly.

4.2.3 Comparison with the simulations of TEM model

The yearly vegetation C content, net primary production (NPP), litter fall, fire-induced carbon loss, and harvest in the high latitude regions (Latitudes>45°) of North America from 1900 to 2006 were from the simulations of the TEM model (Balshi et al. 2007, McGuire et al. 2010). The simulations considered changes in climatic variables, atmospheric CO_2 concentration, fire regimes, and harvests since 1959. The whole area was divided into 24 regions according to the states in the United States and provinces in Canada. Region averaged NPP (U), litter fall (L), heterotrophic respiration (RH), vegetation and soil C content (C_{veg}, C_{soil}), fire-induced C loss ($C_{fire,veg}$, $C_{fire,soil}$), and harvest ($C_{production}$) were calculated by averaging the values at each grid for the recent 30 years (1977~2006). Vegetation C residence time (τ_{veg}) was calculated by current vegetation C content divided by annual litter fall (C_{veg}/L). Potential vegetation C content is calculated by $U \times \tau_{veg}$. Disturbance regime (σ) was calculated by $(C_{fire}+C_{production})/C_{veg}$, which was equivalent to s/λ. Soil C residence time (τ_{soil}) was calculated by current soil C content divided by annual heterotrophic respiration (C_{soil}/RH). The potential soil C content ($C_{soil,potential}$) was calculated by $U \times \tau_{soil}$. The soil C content with impacts of disturbances was calculated by the following equation:

$$C_{soil,cal} = U \cdot \tau_{soil} \cdot \frac{1}{1+\sigma_{veg} \cdot \tau_{veg}} \cdot \frac{1}{1+\sigma_{soil} \cdot \tau_{soil}} \quad (4.5)$$

4.3 Results

4.3.1 The derived model

We begin by looking at the simplest description of disturbance frequency and assume that it is independent of the state of the ecosystem, with a constant probability through time of a disturbance. We treat this exponential or Poisson regime in depth with our mathematical approach and examine sensitivity to changes in the description through simulation (e.g. a Weibull description which has been used to describe fire frequency (Katz et al. 2005, Clark 1990)). We used the exponential distribution to describe intervals between disturbances:

$$f(T;\lambda) = \begin{cases} \frac{1}{\lambda} \cdot e^{-\frac{1}{\lambda}T}, T \geq 0 \\ 0 \qquad\quad , T < 0 \end{cases} \tag{4.6}$$

where T is the interval of two consecutive disturbance events and λ is the mean disturbance interval (MDI).

A three-pool model with biomass, litter, and soil carbon pools (Fig. 4.1) was used to represent the carbon dynamics of ecosystems. With the assumption that carbon influx and residence are not affected by disturbances, the recovery pattern of biomass pool can be described by:

$$X_1 = x_{1,0} \cdot e^{-t/\tau_1} + U\tau_1(1 - e^{-t/\tau_1}) \tag{4.7}$$

where X_1 is carbon content of the biomass pool, $x_{1,0}$ is the legacy carbon of the biomass pool right after a disturbance event, U is carbon influx, τ_1 is carbon residence time of the

biomass pool, and *t* is the time since last disturbance event. Equation 2 is the solution to the differential equation describing carbon accumulation at a constant input rate *U* and decay at rate ($1/\tau_1$). The first term of the right side ($x_{1,0} \cdot e^{-t/\tau_1}$) shows the decay of legacy carbon and the second term [$U\tau_1(1-e^{-t/\tau_1})$] represents the accumulation of new carbon.

Integration of the exponential distribution of disturbance intervals with the ecosystem carbon recovery curve (Eqn 4.7) at a given disturbance severity, *s*, yields the expected biomass, $E[X_1]$ (see mathematical derivations in Supplemental materials B for details) as:

$$E[X_1] = U \cdot \tau_1 \cdot \frac{\lambda}{\lambda + s\tau_1} \qquad (4.8)$$

The disturbance severity, *s*, ranging from 0 to 1, represents the fraction of biomass removed by a disturbance event. Here the disturbance severity is assumed to be independent of the current biomass. Incorporation of the biomass dynamics into the three-pool model produces the expectation of ecosystem total carbon (*X*):

$$E[X] = U \cdot \tau_E \cdot \frac{\lambda}{\lambda + s\tau_1} \qquad (4.9)$$

where, τ_E is ecosystem carbon residence time. If the disturbance severity (*s*) is a random variable, the expectation of total ecosystem carbon (*X*) is:

$$E[X] = U \cdot \tau_E \cdot \frac{\lambda}{\lambda + E[s] \cdot \tau_1} \qquad (4.10)$$

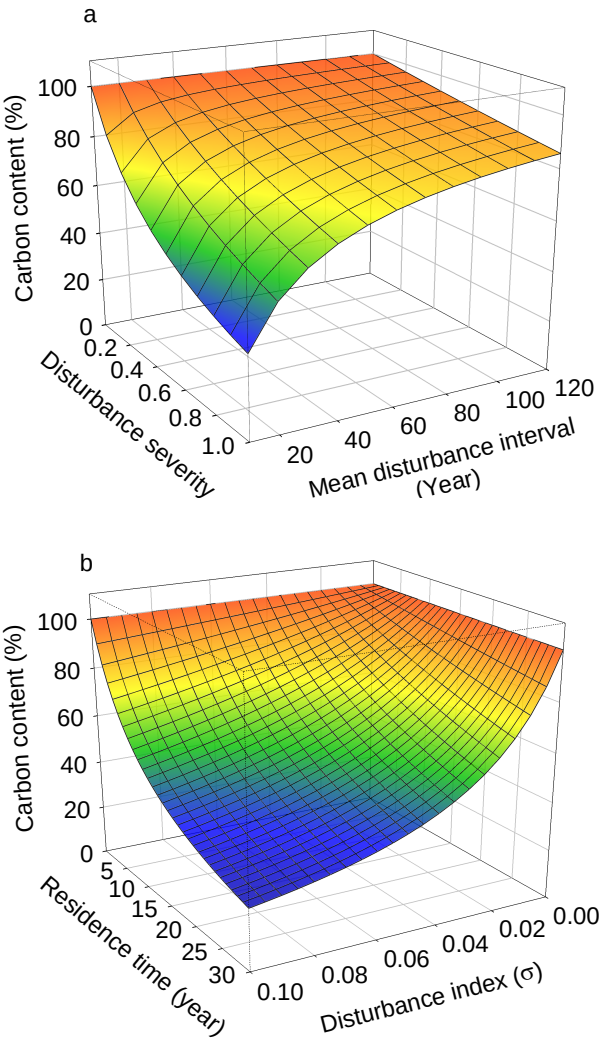

Figure 4.2 Ecosystem carbon contents with a) changes in mean disturbance interval and severity, and b) changes in residence time and disturbance index (σ=s/λ) based on the Eqn 4.8.

where, $E(s)$ is the expectation of disturbance severity. This equation contains two parts, the potential C storage ($U\tau$) and the disturbance effect ($\frac{\lambda}{\lambda + E[s]\cdot\tau_1}$). The former is determined by ecosystem internal processes and the latter is determined by disturbance severity, mean disturbance intervals, and the residence time of biomass pool. If we define

a disturbance index, σ, as E(*s*)/λ, the equation can be written as $E[X] = U \cdot \tau_E \cdot \frac{1}{1+\sigma\tau_1}$.

Equation (5) shows that expected carbon storage increases with carbon influx, residence time, MDI but decreases with disturbance severity (Fig. 4.2: a). The sensitivity of ecosystem C storage to disturbance is determined by the residence time of biomass C pool that is directly affected by disturbances (Fig. 4.2: b).

4.3.2 Sensitivity analysis to the assumptions

The sensitivity analysis showed the biases incurred by the assumptions used to derive these equations were low (Fig. 4.3). Simulated ecosystem C storage was not sensitive when the shape factor *k* of Weibull distribution changes from 1 (i.e., the exponential distribution) to 2 (a usual value for fires, Grissino-Mayer 1999) (Fig. 4.3: a). The assumption of constant carbon influx results in very small biases in comparison with the variable carbon influx even if disturbances occur frequently (Fig. 4.3: b and c).

4.3.3 Validation and application

Based on the framework defined by these equations (Eqns 4.8~4.10), we analyzed the simulated vegetation and soil C dynamics of the high latitude regions (>45°N) of North America by the Terrestrial Ecosystem Model (TEM) considering the impacts of fires and harvests (Balshi et al. 2007, McGuire et al. 2010). The whole region was separated into 24 sub-regions according to the provinces in Canada and states in the US.

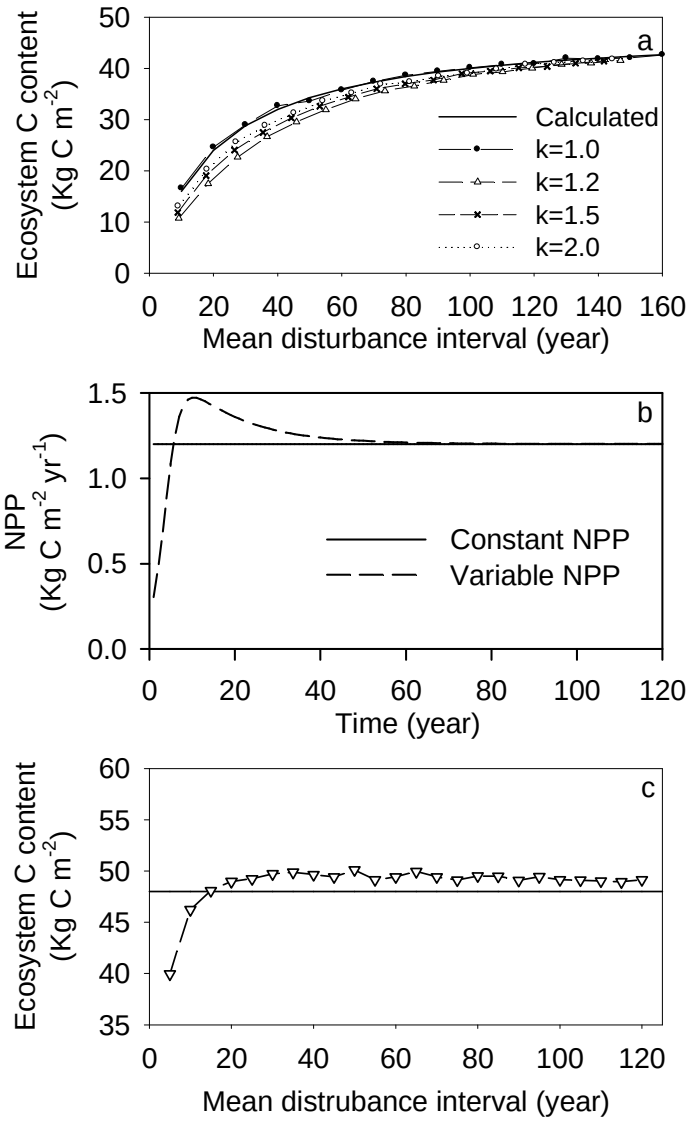

Figure 4.3 Sensitivity tests to the assumptions of constant NPP and exponential distribution of disturbance intervals. Panel *a* illustrates the differences of simulated C content induced by the different distributions (Weibull distribution with different shape factor) with the mean disturbance intervals ranging from 10 to 160 years. Panel *b* shows the pattern of realistic NPP simulated by the Eqn 4.4. Panel *c* shows the simulated carbon content at variable NPP to those at constant NPP with mean disturbance interval ranging from 5 to 120 years (dashed line with open triangles).

The ratios of vegetation (Fig. 4.4: a, b) and soil C storage (Fig. 4.4: c, d) to their corresponding potential values calculated by this equation fit the simulated ones well. The correlations between the ratios of actual C content to the potential and disturbance regimes (s/λ) of the 24 districts follow the disturbance effect factor $\frac{1}{1+\sigma \cdot \tau_1}$ (Fig. 4.4: b and d). For the regions with low disturbances (e.g., Canada), the simulated C content in vegetation and soil C pools is very close to its potential level ($U\tau$). While, in the regions with frequent and severe disturbances, such as the states of United States, the C content is much lower than the potential.

The pattern represented by Eqn 4.10 is also supported by many lines of experimental evidence. Forests in dry lands can have high net primary production (NPP) (Rotenberg and Yakir 2010) but low carbon storage likely due to frequent fire (Peterson and Reich 2001). Suppression of fires leads to increases in carbon stock in forests (Tilman et al. 2000), while increases in disturbance frequencies reduced Canadian forest biomass during 1980s (Kurz et al. 1999). The biomass of a Savanna ecosystem decreases with fire severity and increases with fire return intervals nonlinearly based on observation and modeling results from a 50-year fire experiment (Ryan and Williams 2010).

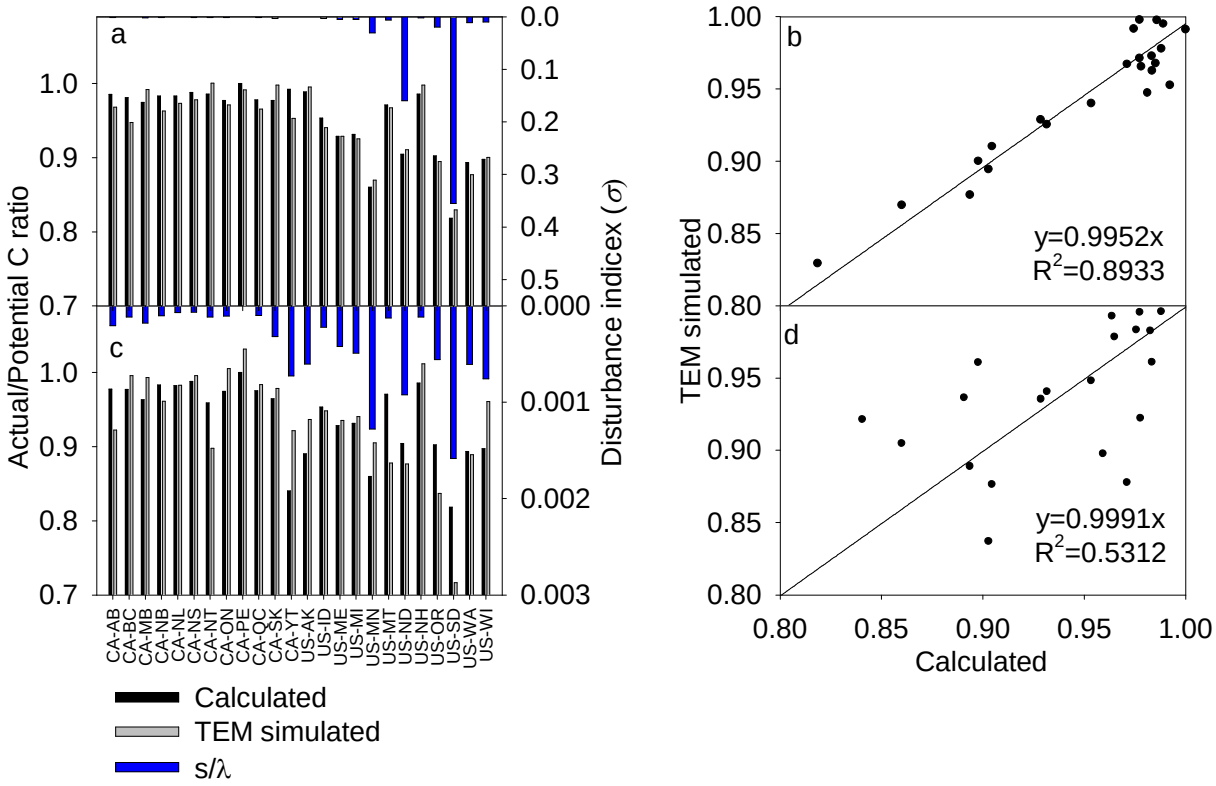

Figure 4.4 Calculated and simulated C storage in the high latitude regions of North America. The black bars of panel *a* are the ratios of calculated vegetation C content to the potential C storage defined by NPP and vegetation C residence time in the 24 regions. The gray bars are the TEM simulated. The blue bars are the indices of disturbance to vegetation (σ=s/λ) in the 24 regions. Panel *b* shows the relationship between the ratios of calculated and simulated C content to the potential vegetation C storage. Panels *c* and *d* are for soil C. Black bars are the calculated by the equation and Grey bars are simulated by the TEM model. The blue bars are the indices of disturbance to ecosystem (vegetation and soil) C.

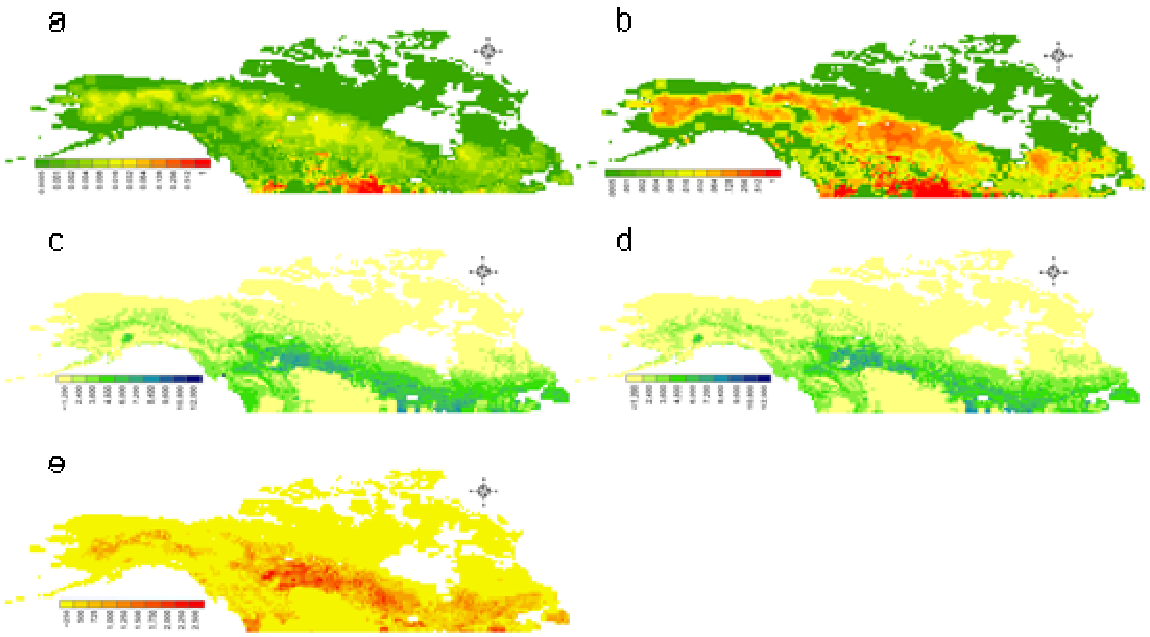

Figure 4.5 Simulated changes of the vegetation C storage in the boreal area (>45°N) of North America in response to changes in disturbance regime. Panel a is the current disturbance regime from Balshi et al. 2007 (the fraction of vegetation C that is removed by fires and harvests per year), b is the predicted disturbance regime in the last decade of 21st century (5.7 times of current disturbance index, following Balshi et al. 2009). c is the current vegetation C storage, d is vegetation C storage in the last decade of 21st century with changes in disturbance only calculated by equation 5, and e is the C loss of vegetation alone induced by changes in disturbance regimes.

We applied this model to analyze the possible vegetation C storage changes in the high latitudes of North America by this model in the last decade of 21st century due to changes in disturbance regime (Fig.4.5: a, b) based on the simulated NPP and C residence times by the TEM (McGuire et al. 2010). Around 1.8 Pg C would be released at the 5.7 times of current disturbance index given NPP and residence time were constant (Fig. 4.5 c, d, and e), which was comparable with the simulated predictions (Balshi et al. 2009).

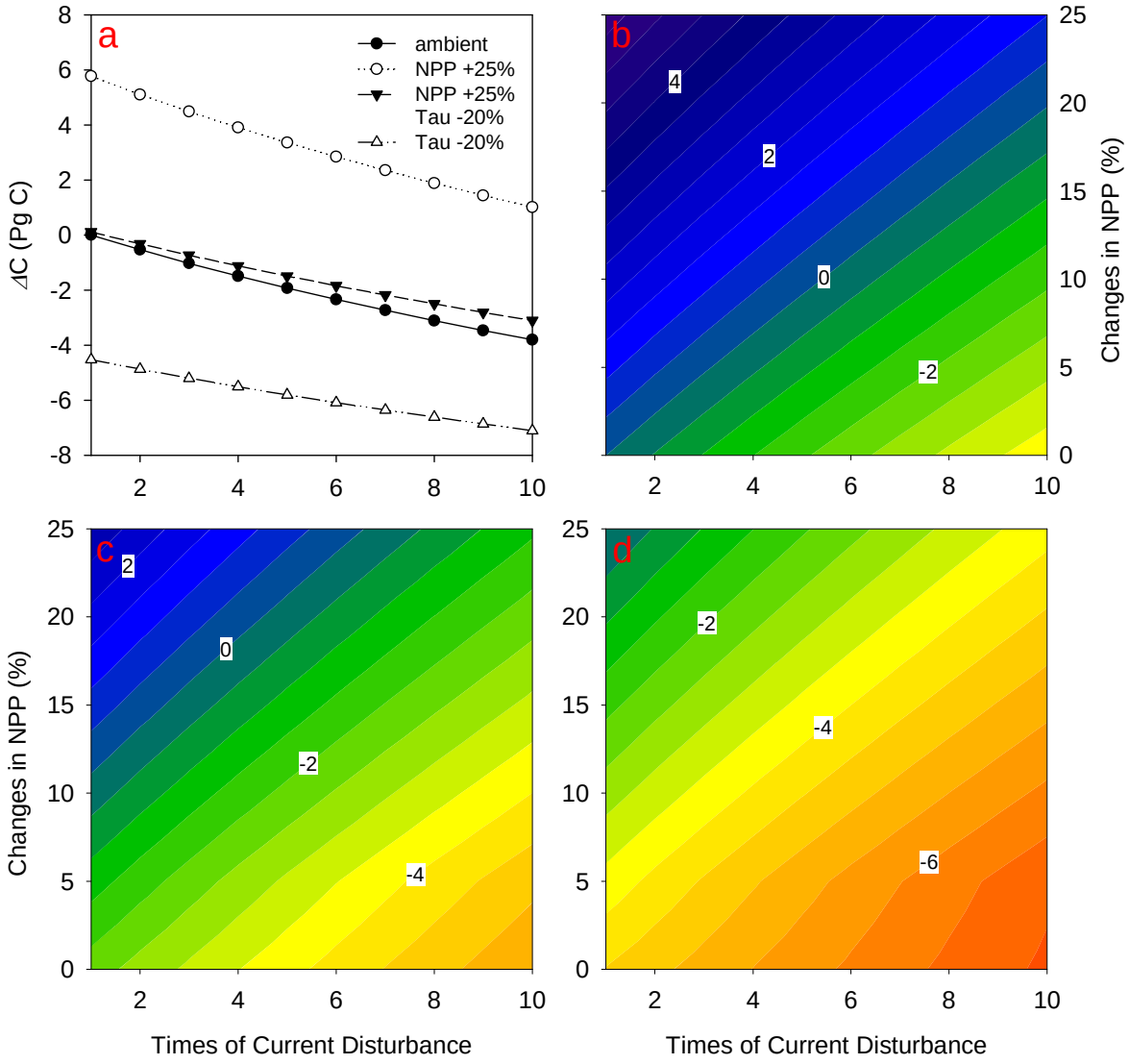

Figure 4.6 Ensemble analyses of changes in vegetation carbon storage in the high latitude regions of North America. Panel a shows the C stock changes with disturbance intensity at ambient NPP and residence time (solid line with closed circles), increased NPP (dotted line with open circles), decreased residence time (dashed line with open triangles), or both (long-dashed line with closed triangles). Panels b-d show the isometric lines of vegetation C stock changes (Pg C) with changes in NPP and disturbance intensity at ambient (b), 10% reduced (c), and 20% reduced (d) residence times.

Considering the simultaneous changes in NPP and residence time, we explored more possibilities of vegetation C storage changes in this area with combined changes in NPP and residence time. A 25% increase in NPP could compensate the C loss induced by 10 times increases in disturbance. A 25% increase in NPP with a 20% decrease in residence time didn't change the potential (equilibrium) vegetation C storage, but the C loss induced by disturbance was decreased, since the lower residence time reduced the sensitivity of C storage to disturbance. Lowered residence time with constant NPP led to more carbon loss (Fig. 4.6: a). This model enabled us to analytically analyze C storage changes with NPP, residence time, and disturbance regime. For the high latitude areas of North America, each fold of current disturbance intensity increase required 2% of increase in NPP to keep C storage at current level if residence times didn't change (Fig. 4.6: b). Thus, 6 times of increases in disturbance required 12% increase in NPP (Fig. 4.5: b), which could happen with increases in temperature and fertilization of elevated CO_2. While if residence time decreased 10%, that along required 12.5% increase in NPP for maintaining current vegetation C stock. And, 6 times of increase in disturbance required additional 10% increase in NPP (Fig. 4.6: c). A 20% decrease in residence time required 25% increase of NPP to keep vegetation C stock at current level and any increases in disturbance would induce decreases in C stock (Fig. 4.6:d). Future climate change will induce increases in mortality, decomposition rates, fires, and more drought stress. So, the chance of vegetation C pool to be a sustaining C sink is very narrow when the three factors change simultaneously.

4.4 Discussion

This model is an integration of the temporal patterns of ecosystem C recovery and the spatial heterogeneity of landscapes induced by disturbances, representing a quantitative description of the dynamic equilibrium states of ecosystem C dynamics at large spatial scales with effects of disturbances (Luo and Weng, 2011). It quantifies the nonlinear relationships of ecosystem C storage with ecosystem internal properties and disturbance regime, which are usually explored by model simulations. The derivatives of this model illustrate the different properties of C storage of an ecosystem in such dynamic disequilibrium states with those at equilibrium states and thus provided an overarching mathematical framework to quantitatively analyze the possibilities of ecosystem carbon storage responses to changes in NPP, decomposition/mortality rates, and disturbance regimes induced by changes in climate and disturbance in the future.

4.4.1 Model properties and derivatives

In this model, as shown by Eqn 5, NPP, decomposition rates, and disturbance regimes define a multiple (3 or 4) dimensional space to determine ecosystem carbon storage. For the vegetation C pool, it is a three dimensional space. Changes of ecosystem carbon depend on the relative changes of the three variables. Increases of disturbance can be compensated linearly by increases in NPP. Decreases in residence time and increases in disturbance result in more C loss than any one of them, but the effects are not additive

since lowered residence time alleviated the effects of disturbances. The carbon gain from increased NPP can be offset by decreasing residence time.

Eqn 4.10 also indicates that the sensitivity of ecosystem C storage capacity to disturbances is determined by the residence times of the C pools affected by disturbances. Disturbances have higher impacts on forests than on grasslands, since trees have longer residence time and need more time to recover to the pre-disturbance states than grasses. The recovery rate of carbon influx (i.e., NPP) also affects the impact of disturbances on carbon storage capacity. If disturbance occurs very frequently (short MDI) so that carbon influx does not have enough time to fully recover, the actual carbon storage will be lower than that estimated by this model (Fig. 4.2: c).

When the Eqn 4.10 is written as $E[X] = U \cdot \tau_E \cdot \frac{1}{1+\sigma \cdot \tau_1}$, the disturbance regime can be represented by only one parameter, σ. This parameter has multiple meanings. It can be the fraction of C that is removed by disturbances per time unit (e.g., year) in a region and can also be the area that is burned or harvested with the assumption that disturbance severity is 1. The inverse of σ is the MDI of the equivalent disturbances with severity 1. σX is the C efflux induced by disturbances that counteracts part of NPP or increases C outflow (litter fall for biomass or heterotrophic respiration for soil organic matters). The decreases in C residence time in ecosystems or net primary production induced by disturbances can be quantified by the factor $\frac{1}{1+\sigma \cdot \tau_1}$. The parameter σ can

simplify and standardize the description of diverse disturbances when evaluating their effects on ecosystem C dynamics.

4.4.2 Applications

This model provides a unique angle to the analysis of the data collected from observational studies based on paradigm of dynamic disequilibrium, which is more close to reality than that of equilibrium. Eqn 5 suggests that ecosystem C storage capacity can approach the potential level ($U\tau_E$) only when there are no disturbances (i.e., as s approaches zero or λ approaches infinite), which is unlikely in most regions of the Earth. Therefore, there will be a mean growth rate of vegetation C pool (or net ecosystem production) $U\frac{\sigma\cdot\tau_1}{1+\sigma\cdot\tau_1}$ (σ=s/λ) when the whole region is actually carbon neutral, rather than zero in the paradigm of static equilibrium. For example, the ecosystem C storage will keep constant at large spatial scales while the mean observed biomass growth rate is 100 g C m^{-2} yr^{-1} for a forest with 600 g C m^{-2} yr^{-1} of NPP, 20 yrs of biomass C residence time, and a disturbance index (s/τ) of 0.01, since the large amount of C removed by occasionally happened disturbances counteracted the continuous C accumulation with a rate of 100 g C m^{-2} yr^{-1} ($U\frac{\sigma\cdot\tau_1}{1+\sigma\cdot\tau_1}=600\cdot\frac{0.01\cdot 20}{1+0.01\cdot 20}=100(\mathrm{gCm^{-2}yr^{-1}})$). This property demands an integrated assessment of carbon sink dynamics at large spatial or temporal scales with consideration of disturbance regimes. Forests at individual sites slowly accumulate carbon most time while lose large amounts of it quickly when a disturbance

event happens. Thus, the probability of observing carbon uptake is high. Old growth forests have been shown to be carbon sinks (Luyssaert et al. 2008, Lewis et al. 2009) likely because most forests take up carbon continuously between disturbance events.

It also can improve the representation of ecosystem states and processes for modeling studies. Most global modeling analyses, for example, are initialized with the carbon pools equilibrated to historical climate data (Schimel et al. 1997, McGuire et al. 2001, Sitch et al. 2008). This may overestimate the initial terrestrial C storage, leading to misunderstanding on the mechanisms of terrestrial carbon sink. For example, C storage will be overestimated by approximately 20% if disturbance occurs, on average, once every 40 years with a severity of 0.5 according to this model. Lack of representation of disturbances in models also results in overestimation of terrestrial carbon sequestration in response to climate change, since the increases in disturbances can incur a large amount of carbon lose (Schimel et al. 1997). Eqn 4.10 provides a way to reevaluate these model predictions with information on disturbance regimes.

4.4.3 Uncertainties

Our derivation is based on a few simplifying assumptions about disturbance regimes and ecosystem processes to succinctly describe dynamics of C storage capacity as affected by ecosystem carbon processes (i.e., influx and residence time) and disturbance regimes (represented by frequency and severity). These assumptions include (1) no effects of disturbance on NPP and residence times, (2) independence of the

fraction of carbon removed by a disturbance event from current carbon content of biomass, and (3) representation of disturbance intervals by exponential distribution. These assumptions define a dynamic equilibrium system (Turner et al. 1993, Perry et al. 2002) at a large spatial scale, where ecosystems at each sub-grid can eventually recover to their original states after disturbances. They are acceptable if we only explore the rough picture of C storage at large spatial or temporal scales. For example, even for stand-replacing disturbances (fires or harvests), the recovery period of NPP is only five to ten years (Hicke et al. 2003, Hughes et al. 1999, Law et al. 2003), which is very short compared to the recovery of carbon stocks. The high agreement with simulations of TEM also indicates current mainstream biogeochemical models are employing the philosophy of dynamic equilibrium.

Many studies have shown the assumptions of dynamic equilibrium of a landscape may not be true especially when disturbance is frequent and ecosystems are undergoing climate change (Turner et al. 1993, Johnstone et al. 2010). With the trends of climate change, for example, ecosystem state shifts can be triggered by fires that initiate a recovery process leading to the changes forest types (Johnstone et al. 2010). Disturbances of terrestrial ecosystems are diverse and there are complicated interactions among them (Miao et al. 2009). Their impacts on ecosystems are far more complex than the assumptions of this study. Our study provides a benchmark for disturbance modeling with clear assumptions and tractable processes. Further study should be conducted to understand and model these complex facets.

4.5 Conclusions

In conclusion, the model developed in this study provides an analytical description on the relationships between ecosystem carbon storage and NPP, C residence time, and disturbance intervals and severity. The model represents a disequilibrium perspective for examining C storage dynamics in light of impacts of disturbances and improves our predictive understanding on regional C dynamics (Luo and Weng 2011). C cycling at the scale of ecosystem is almost always in dynamic disequilibrium with most ecosystems accumulating carbon at various stages of recovery with intermittent disturbances to release large amounts of carbon. At a regional or landscape scale at which disturbances occur, carbon cycle is in dynamic equilibrium and carbon storage capacity does not change over time when disturbance regime in a region does not vary over time. Carbon cycle is in dynamic disequilibrium when the disturbance regime in the region varies in response to global change. This disequilibrium perspective is critical for scaling of site-level observations to estimate regional and global carbon sink, for modeling studies on carbon-climate feedbacks, and for design of field experiments and observation networks.

4.6 Acknowledgements

This research was financially supported by the Office of Science, Department of Energy, Grants No.: DE-FG02-006ER64319 and through the Midwestern Regional Center of the

National Institute for Climatic Change Research at Michigan Technological University, under Award Number DE-FC02-06ER64158, and by National Science Foundation under DBI 0850290, DEB 0840964, DEB 0743778 and EPS 0919466.

Supplemental Materials

Table A1: Notations

Symbol	*Meaning*	*Symbol*	*Meaning*
A	Carbon transfer matrix	$X(t)$	Vector for carbon pools at time t
B	Allocation vector of net primary production (NPP)	η	The ratio of carbon transferred to SOM from litter pool
r	A random variable representing the occurrence of large-disturbances (1 for the occurrence, 0 for null)	λ	The mean disturbance interval (MDI)
s	The fraction of biomass removed by a large-disturbance event (0~1)	Ξ	Disturbance carbon transfer matrix
U_0	Reference NPP	τ_1	Carbon residence time of biomass
$U(t)$	NPP at time t	τ_2	Carbon residence time of litter
X_1	Biomass carbon pool	τ_3	Carbon residence time of SOM
X_2	Litter carbon pool	τ_E	Ecosystem carbon residence time
X_3	Soil organic matter (SOM) carbon pool	T	Diagonal matrix for carbon residence times

B: Mathematical Derivations

The carbon cycle model is described by the following equation:

$$\frac{dX(t)}{dt} = AT^{-1}X(t) + BU(t) \quad \textbf{(B1)}$$

where, $X(t)$ is ecosystem carbon content at time t, A is a 3 × 3 matrix representing carbon transfer among the three pools, $A = \begin{pmatrix} -1 & 0 & 0 \\ 1 & -1 & 0 \\ 0 & \eta & -1 \end{pmatrix}$ and η is the ratio of carbon transferred to the SOM pool from the litter pool. T is an 3 × 3 diagonal matrix, $\mathrm{T} = diag(\tau)$. The diagonal elements are τ_1, τ_2, and τ_3, which are the residence times of the carbon in biomass, litter, and SOM, respectively. B is the allocation ratios of carbon input to the three pools, $(1 \quad 0 \quad 0)'$. $U(t)$ is the carbon input (net primary production, NPP) at time t. We assumed it was a constant in model simulations and mathematical derivations.

Carbon storage capacity at the disturbances with severity is 1.0 (all biomass was removed):

According to the Equation B1, the carbon content of biomass with an initial value of zero follows the following equation:

$$X_1 = U\tau_1(1 - e^{-t/\tau_1}) \quad \textbf{(B2)}$$

where, t is time.

Fore each disturbance cycle, the mean C content over a disturbance interval T can be taken as the height of a rectangle with the length T and the same area with that

enclosed by the recovery cure (Supplemental Figure S4: a). Thus, the mean carbon content of biomass ($X_{1,avg}$) in a disturbance cycle with interval T:

$$X_{1,avg} = \frac{\left[\int_0^T U\tau_1(1-e^{-\frac{t}{\tau_1}})dt\right]}{T} = U\tau_1 \cdot \left[1-\frac{\tau_1}{T}\cdot(1-e^{-\frac{T}{\tau_1}})\right] \quad \textbf{(B3)}$$

Note, the interval T is in distribution:

$$f(T;\lambda) = \begin{cases} \frac{1}{\lambda}\cdot e^{-\frac{1}{\lambda}T}, T \geq 0 \\ 0 \qquad\quad , T < 0 \end{cases} \quad \textbf{(B4)}$$

The mean carbon content in an infinite time series with numerous disturbance events and any kinds of interval T can be calculated as the total area enclosed by the recovery curves divided by the sum of T's. Taking the probability density function of interval T into account, the mean carbon content is:

$$\begin{aligned} E[X_1] &= \frac{\int_0^\infty T\cdot U\tau_1\cdot\left[1-\frac{\tau_1}{T}\cdot(1-e^{-\frac{T}{\tau_1}})\right]\cdot\frac{1}{\lambda}\cdot e^{-\frac{1}{\lambda}T}dT}{\int_0^\infty T\cdot\frac{1}{\lambda}\cdot e^{-\frac{1}{\lambda}T}dT} \\ &= U\tau_1\frac{\lambda}{\lambda+\tau_1} \end{aligned} \quad \textbf{(B5)}$$

For the pools of litter and SOM, the changes are only their inputs. For a long period, the whole ecosystem carbon content can be represented by:

$$
\begin{aligned}
E[X] &= E[X_1] + E[X_2] + E[X_3] \\
&= U\tau_1 \cdot \frac{\lambda}{\lambda+\tau_1} + \frac{E[X_1]}{\tau_1} \cdot \tau_2 + \frac{E[X_2]}{\tau_2} \cdot \eta \cdot \tau_3 \\
&= U\tau_1 \cdot \frac{\lambda}{\lambda+\tau_1} + U\tau_1 \cdot \frac{\lambda}{\lambda+\tau_1} \cdot \frac{1}{\tau_1} \cdot \tau_2 + U\tau_1 \cdot \frac{\lambda}{\lambda+\tau_1} \cdot \frac{1}{\tau_1} \cdot \tau_2 \cdot \frac{1}{\tau_2} \cdot \eta \cdot \tau_3 \\
&= U(\tau_1 + \tau_2 + \tau_3 \cdot \eta) \cdot \frac{\lambda}{\lambda+\tau_1} \\
&= U\tau_E \cdot \frac{\lambda}{\lambda+\tau_1}
\end{aligned}
\qquad \textbf{(B6)}
$$

Carbon storage capacity at the disturbances with severity is less than 1.0 (part of biomass was removed):

For each disturbance cycle, the carbon can be divided into two parts: the legacy carbon from the last rotation, the new carbon accumulated from zero since the disturbance event (see Supplemental Figure S4: b). The legacy carbon decomposes exponentially ($X_{1,old} = x_{1,0} \cdot e^{-t/\tau_1}$, where, $x_{1,0}$ is the initial value of legacy carbon just after a disturbance event); the new carbon accumulates following the equation $X_{1,new} = U\tau_1(1-e^{-t/\tau_1})$, the total carbon of biomass at time *t* since last disturbance is:

$$
X_1 = x_{1,0} \cdot e^{-t/\tau_1} + U\tau_1(1-e^{-t/\tau_1}) \qquad \textbf{(B7)}
$$

The mean carbon content of biomass in a disturbance rotation ($X_{1,\text{avg}}$) with given $x_{1,0}$ and disturbance interval *T*:

$$
\begin{aligned}
X_{1,avg} &= \left[\int_0^T U\tau_1(1-e^{-\frac{t}{\tau_1}})dt + \int_0^T x_{1,0} \cdot e^{-t/\tau_1} dt \right] / T \\
&= U \cdot \tau_1 \cdot \left[1 - \frac{\tau_1}{T} \cdot (1-e^{-\frac{T}{\tau_1}}) \right] + x_{1,0} \cdot \frac{\tau_1}{T} \cdot (1-e^{-\frac{T}{\tau_1}})
\end{aligned}
\qquad \textbf{(B8)}
$$

Since $x_{1,0}$ is determined by the previous disturbance event, it is independent on the interval of the next disturbance (here, the interval is assumed to be T). Thus, considering all kinds of T, the expectation of this rotation conditioned on $x_{1,0}$ is:

$$E[X_1 \mid x_{1,0}] = \frac{\int_0^\infty T \cdot U \cdot \tau_1 \cdot \left[1 - \frac{\tau_1}{T} \cdot (1 - e^{-\frac{T}{\tau_1}})\right] \cdot \frac{1}{\lambda} \cdot e^{-\frac{1}{\lambda}T} dT + \int_0^\infty T \cdot x_{1,0} \cdot \frac{\tau_1}{T} \cdot (1 - e^{-\frac{T}{\tau_1}}) \cdot \frac{1}{\lambda} \cdot e^{-\frac{1}{\lambda}T}}{\int_0^\infty T \cdot \frac{1}{\lambda} \cdot e^{-\frac{1}{\lambda}T} dT} \quad \textbf{(B9}$$

$$= U\tau_1 \cdot \frac{\lambda}{\lambda + \tau_1} + x_{1,0} \cdot \frac{\tau_1}{\lambda + \tau_1} \quad \textbf{)}$$

Then, the expectation of X_1 is:

$$\begin{aligned} E[X_1] &= E[E[X_1 \mid x_{1,0}]] \\ &= E[U\tau_1 \cdot \frac{\lambda}{\lambda + \tau_1} + x_{1,0} \cdot \frac{\tau_1}{\lambda + \tau_1}] \\ &= U\tau_1 \cdot \frac{\lambda}{\lambda + \tau_1} + E[x_{1,0}] \cdot \frac{\tau_1}{\lambda + \tau_1} \end{aligned} \quad \textbf{(B10)}$$

For solving the mean of $x_{1,0}$, we need to know the mean of the carbon content just before disturbance happens ($X_{1,0}^-$) ($X_{1,0}^- = x_{1,0} \cdot e^{-t/\tau_1} + U\tau_1(1 - e^{-t/\tau_1})$, where $x_{1,0}$ is the initial value of that disturbance cycle) (see Supplemental Figure S3: c for the definition of X_1, $X_{1,0}^-$, and $x_{1,0}$). Let t be the time that the disturbance happens since the last one. The distribution of t is an exponential distribution.

$$
\begin{aligned}
&E[\bar{X}_{1,0}] = E[x_{1,0} \cdot e^{-t/\tau_1}] + E[U\tau_1(1-e^{-t/\tau_1})] \\
&= E[x_{1,0}]\frac{1}{\lambda}\int_{t=0}^{t=\infty} e^{-t/\tau_1} \cdot e^{-\frac{1}{\lambda}t} dt + \frac{1}{\lambda}U\tau_1\int_{t=0}^{t=\infty} e^{-\frac{1}{\lambda}t} dt - \frac{1}{\lambda}U\tau_1\int_{t=0}^{t=\infty} e^{-t/\tau_1} \cdot e^{-\frac{1}{\lambda}t} dt \\
&= E[x_{1,0}]\frac{1}{\lambda}\int_{t=0}^{t=\infty} e^{-t/\tau_1} \cdot e^{-\frac{1}{\lambda}t} dt + \frac{1}{\lambda}U\tau_1\int_{t=0}^{t=\infty} e^{-\frac{1}{\lambda}t} dt - \frac{1}{\lambda}U\tau_1\int_{t=0}^{t=\infty} e^{-t/\tau_1} \cdot e^{-\frac{1}{\lambda}t} dt \\
&= (\frac{E[x_{1,0}]}{\lambda} - \frac{U\tau_1}{\lambda})\int_{t=0}^{t=\infty} e^{-(\frac{1}{\lambda}+\frac{1}{\tau_1})t} dt + \frac{1}{\lambda}U\tau_1\int_{t=0}^{t=\infty} e^{-\frac{1}{\lambda}t} dt \\
&= (\frac{E[x_{1,0}]}{\lambda} - \frac{U\tau_1}{\lambda}) \cdot \frac{\lambda\tau}{\lambda+\tau} + U\tau_1 \\
&= E[x_{1,0}] \cdot \frac{\tau_1}{\lambda+\tau_1} + U\tau_1 \cdot \frac{\lambda}{\lambda+\tau_1}
\end{aligned}
\qquad \textbf{(B11)}
$$

It indicates that $E[\bar{X}_{1,0}] = E[X_1]$.

For each $\bar{X}_{1,0}$, there is an $x_{1,0} = (1-s) \cdot \bar{X}_{1,0}$. Thus,

$$
\begin{aligned}
&\bar{x}_{1,0} = (1-s)E[\bar{X}_{1,0}] = (1-s)\left[\bar{x}_{1,0} \cdot \frac{\tau_1}{\lambda+\tau_1} + U\tau_1 \cdot \frac{\lambda}{\lambda+\tau_1}\right] \\
&\Rightarrow \bar{x}_{1,0} = (1-s) \cdot U\tau_1 \cdot \frac{1}{1+s\tau_1/\lambda}
\end{aligned}
\qquad \textbf{(B12)}
$$

Therefore, the expectation of X_1 (plant biomass) in disturbances with severity *s* and mean interval λ is:

$$
\begin{aligned}
&E[X_1] = U\tau_1 \cdot \frac{\lambda}{\lambda+\tau_1} + E[x_{1,0}] \cdot \frac{\tau_1}{\lambda+\tau_1} \\
&= U\tau_1 \cdot \frac{\lambda}{\lambda+\tau_1} + (1-s) \cdot U\tau_1 \cdot \frac{\lambda}{\lambda+s\tau_1} \cdot \frac{\tau_1}{\lambda+\tau_1} \\
&= U\tau_1 \cdot \left[\frac{\lambda}{\lambda+\tau_1} + \frac{(1-s)\cdot\lambda}{\lambda+s\tau_1} \cdot \frac{\tau_1}{\lambda+\tau_1}\right] \\
&= U\tau_1 \cdot \frac{1}{\lambda+\tau_1} \cdot \left[\lambda + \frac{(1-s)\cdot\lambda}{\lambda+s\tau_1} \cdot \tau_1\right] \\
&= U\tau_1 \cdot \frac{1}{\lambda+\tau_1} \cdot \left[\frac{(\lambda+\tau_1)\cdot\lambda}{\lambda+s\tau_1}\right] \\
&= U \cdot \tau_1 \cdot \frac{\lambda}{\lambda+s\tau_1}
\end{aligned}
\qquad \textbf{(B13)}
$$

And, for the expectation of ecosystem total carbon (X):

$$
\begin{aligned}
E[X] &= E[X_1] + E[X_2] + E[X_3] \\
&= U\tau_1 \cdot \frac{\lambda}{\lambda + \tau_1} + \frac{E[X_1]}{\tau_1} \cdot \tau_2 + \frac{E[X_2]}{\tau_2} \cdot \eta \cdot \tau_3 \\
&= U\tau_1 \cdot \frac{\lambda}{\lambda + s\tau_1} + U\tau_1 \cdot \frac{\lambda}{\lambda + s\tau_1} \cdot \frac{1}{\tau_1} \cdot \tau_2 + U\tau_1 \cdot \frac{\lambda}{\lambda + s\tau_1} \cdot \frac{1}{\tau_1} \cdot \tau_2 \cdot \frac{1}{\tau_2} \cdot \eta \cdot \tau_3 \\
&= U(\tau_1 + \tau_2 + \tau_3 \cdot \eta) \cdot \frac{\lambda}{\lambda + s\tau_1} \\
&= U\tau_E \cdot \frac{\lambda}{\lambda + s\tau_1}
\end{aligned}
\qquad \textbf{(B14)}
$$

According to the equation (B14), ecosystem carbon storage capacity can be estimated by its intrinsic properties (U and τ) and disturbance regime (λ and s). We also simulated carbon storage capacities with severities (s) ranging from 0 to 1. The calculated values agree with the simulated well (Fig. S4.2: a and b). The mean of carbon content just after disturbances events calculated by the equation B12 agree with the simulations well (Fig. S4.2: c).

Disturbance severity is a random variable:

If severity (s) is a random variable, say uniformly distributed in [0,1], then the mean carbon content can be calculated as following.

As we have known, the expectation of X_1 and $X_{1,0}^-$ is

$$E(X_1) = E[X_1^-] = U\tau_1 \cdot \frac{\lambda}{\lambda + \tau_1} + E[x_{1,0}] \cdot \frac{\tau_1}{\lambda + \tau_1}.$$

And, for each $X_{1,0}^-$, there is an $x_{1,0} = (1-s) \cdot X_{1,0}^-$, where s is a RV. Thus,

$$E[x_{1,0}] = E[(1-s)]E[X_{1,0}^{-}] = (1-E[s]) \cdot \left[\bar{x}_{1,0} \cdot \frac{\tau_1}{\lambda + \tau_1} + U\tau_1 \cdot \frac{\lambda}{\lambda + \tau_1} \right]$$
$$\Rightarrow E[x_{1,0}] = (1-E[s]) \cdot U\tau_1 \cdot \frac{1}{1 + E[s] \cdot \tau_1 / \lambda} \quad \textbf{(B15)}$$

Therefore, the expectation of X_1 is:

$$E[X_1] = U\tau_1 \cdot \frac{1}{1 + E[s] \cdot \tau_1 / \lambda}$$
$$= U\tau_1 \cdot \frac{\lambda}{\lambda + E[s] \cdot \tau_1} \quad \textbf{(B16)}$$

And, the expectation of total ecosystem carbon is:

$$E[X] = U\tau_E \cdot \frac{\lambda}{\lambda + E[s] \cdot \tau_1} \quad \textbf{(B17)}$$

This equation indicates for disturbances with random intervals and random severity, we should first calculate the expectations of disturbance interval (λ) and severity ($E[s]$), and then calculate mean carbon content. The carbon contents calculated by this equation (B17) agree with the simulations well (Fig. S4.2: d).

Figure S4.1 Diagrams for mathematical derivation

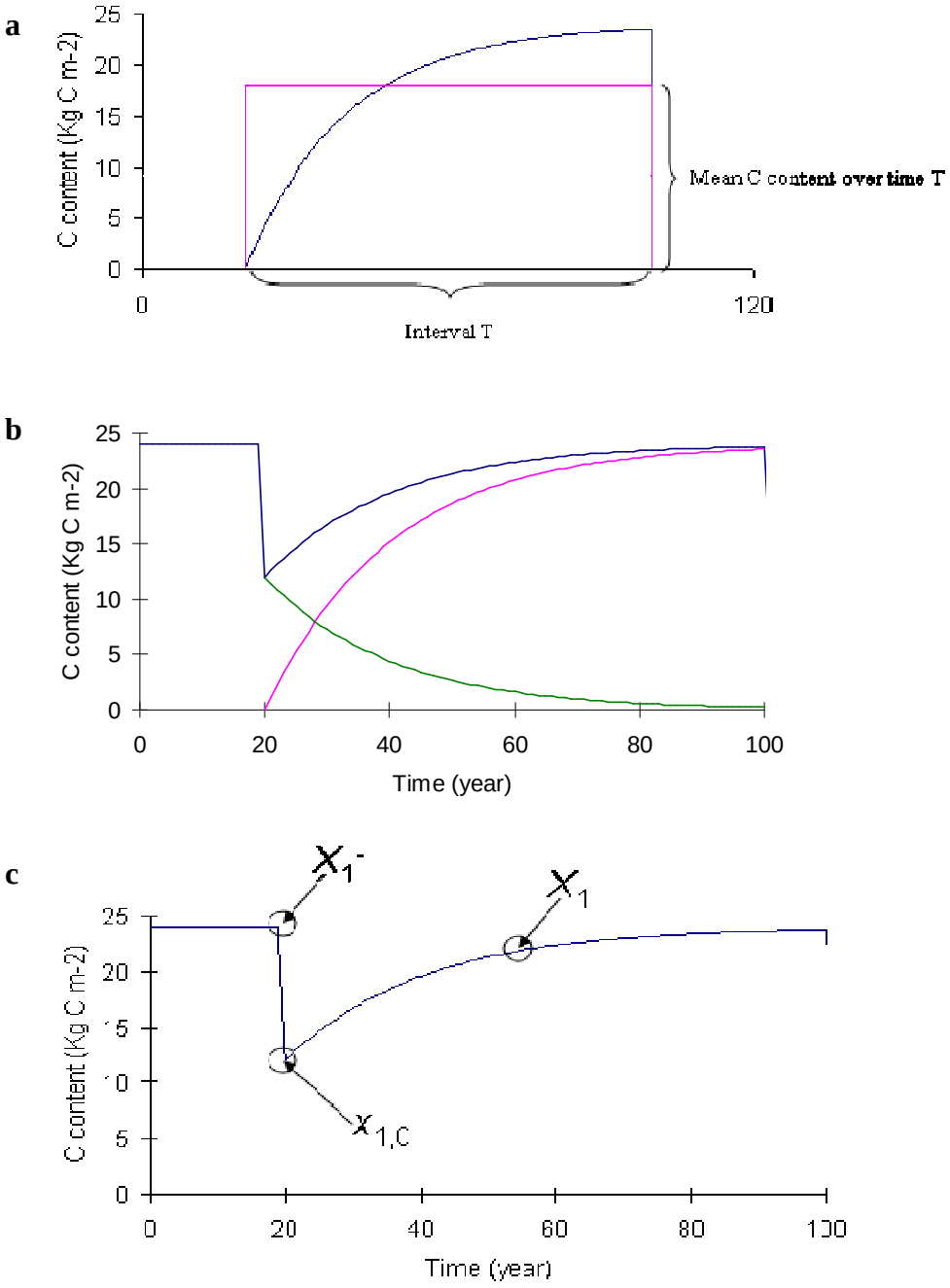

a. The height of the rectangle is the mean C content over disturbance interval T; b A recovery curve that can be decomposed into two curves: the accumulation of new carbon, and the decay of legacy carbon; c. The definitions of X_1, $X_{1,0}^-$, and $x_{1,0}$.

Figure S4.2 Comparison between the simulated and calculated carbon storage capacities at disturbances

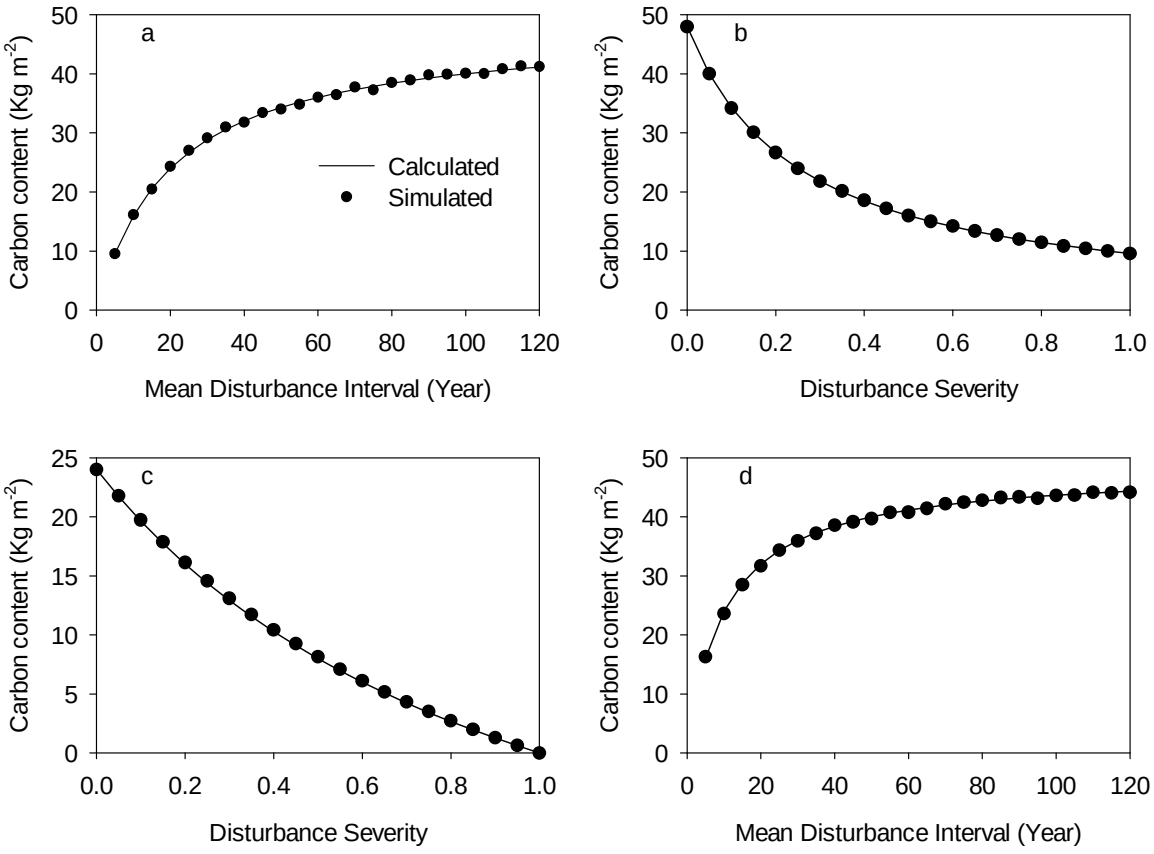

Carbon storage capacities at large disturbances with (a) changes in mean disturbance interval (MDI) while the severity is 1.0; (b) changes in severity while the MDI is 5 yrs. (c). Mean carbon content of the live biomass pool just after a disturbance event ($x_{1,0}$) with severity ranging from 0 to 1 and a MDI of 20 yrs. (d) Carbon storage capacity at large disturbances with severity uniformly distributed in [0,1] with MDI ranging from 5 to 120 years.The NPP is 1.2 Kg C $m^{-2}\cdot yr^{-1}$. τ_1, τ_2, and τ_3 are 20, 5, and 60 years, respectively. η is 0.25. Thus, the ecosystem carbon residence time is $\tau_E=\tau_1+\tau_2+\tau_3\cdot\eta=40$ years.

CHAPTER 5 Conclusions and Perspectives

5.1 Conclusions

These studies showed that current ecosystem C modeling schemes, i.e., a Farquhar model based canopy model simulating C input to the system and compartmentalized C pool model simulating C allocation, transfer, and decomposition, works well in simulating the short-term patterns of ecosystem C dynamics, but with high uncertainties and sensitivities to some parameters and boundary conditions. Our study (Chapter 2) showed that soil hydrologic properties could substantially change the effects of water dynamics on C processes and their responses to warming and elevated CO_2. How to correctly represent the sensitivities of these ecological processes to such conditions and parameters is an issue in model development and can affect our confidence on simulated results.

Data assimilation is an effective method to combine the information from model and data and therefore improve model parameterization and accuracy of predictions. However, once a model structure is given, optimizing parameters can only find out the best agreement with observations within the space defined by the given model. As shown by our data assimilation study (Chapter 3), the model with optimized parameters by data assimilation approach can give a subset of simulations of the given model structure. Due to the limitation of data, only short-term predictions can be improved while long-term

predictions are still dependent on the model structure, which represents our prior knowledge on ecosystem C dynamics.

These two studies indicate that improving our understanding of ecosystem dynamics is central to ecosystem modeling studies. Our theoretical analysis on the C storage capacity with effects of disturbances (Chapter 4) illustrates that new theories and paradigms for modeling ecosystems can fundamentally change the way that ecosystems are represented in models. This study is based on the knowledge of temporal patterns of biogeochemical cycles with ecosystem development and dynamic spatial patterns of ecosystem structure of landscape ecology. It proposes an analytical model to represent the relationships between ecosystem carbon storage and NPP, C residence time, and disturbance intervals and severity. The model represents a disequilibrium perspective for examining C storage dynamics in light of impacts of disturbances and improves our predictive understanding on regional C dynamics (Luo and Weng 2011). This disequilibrium perspective is critical for scaling of site-level observations to estimate regional and global carbon sink, for modeling studies on carbon-climate feedbacks, and for design of field experiments and observation networks.

5.2 Perspectives

Ecosystem C cycle modeling is still in its infant stage. Current C cycle models are based on the highly simplified representation of C processes. Only biophysical and biogeochemical processes are well represented. Photosynthesis controls C input;

Allocation schemes determine where the C goes and how long time they will stay in the system; decomposition processes release C back to atmosphere. Water, nutrients, and environmental conditions affect ecosystems via these C processes.

However, the overarching aim of organisms in ecosystems is to survive, rather than store C. Terrestrial plants use all available resources, such as water, carbon, light, and nutrients, to build themselves and choose the best strategies for them to survive and compete with their neighbors. They can respond to environmental changes by biological, ecological, and evolutionary processes (Parmesan 2006) in addition to biophysical and biogeochemical processes. These behaviors can change the processes of the C cycle of ecosystems when climate changes or disturbances happen. How to integrate these biogeochemical and biophysical processes within the framework of ecological processes and how to represent the interactions of plants at the community level in models are key steps to improving ecosystem models.

REFERENCES

Abramowitz, G. 2005. Towards a benchmark for land surface models. Geophysical Research Letters 32: L22702, doi:10.1029/2005/GL024419.

Ainsworth, E.A., and S. P. Long. 2005. What have we learned from 15 years of free-air CO2 enrichment (FACE)? A meta-analytic review of the responses of photosynthesis, canopy properties and plant production to rising CO_2. New Phytologist 165, 351-372.

Allen, A.S., J.A. Andrews, A.C. Finze, R. Matamala, D.D. Richter, and W.H. Schlesinger. 2000. Effects of free-air CO_2 enrichment (FACE) on belowground processes in a Pinus taeda Forest. Ecological Applications 10: 437 - 448.

Arora, V. K., and G. J. Boer. 2005. A parameterization of leaf phenology for the terrestrial ecosystem component of climate models, Global Change Biology 11: 39-59.

Bachelet, D., R. P. Neilson, J. M. Lenihan, and R. J. Drapek. 2001. Climate change effects on vegetation distribution and carbon budget in the United States. Ecosystems 4: 164 - 185.

Ball, J. T., I. E. Woodrow, and J.A. Berry. 1987. A model predicting stomatal conductance and its contribution to the control of photosynthesis under different environmental conditions, In Progress in Photosynthesis Research, edited by J. Biggens, pp. 221–224, Martinus Nijhoff Publishers, The Netherlands.

Balshi, M.S., A. D. McGuire, Q. Zhuang, J. Melillo, D. W. Kicklighter, E.S. Kasischke, C. Wirth, M. Flannigan, J. Harden, J. S. Clein, T. J. Burnside, J. McAllister, W. A. Kurz, M. Apps, A. Shvidenko. 2007. The role of historical fire disturbance in the carbon dynamics of the pan-boreal region : a process-based analysis. Journal of Geophysical Research 112: G02029, doi:10.1029/2006JG000380.

Balshi, M.S., A.D. McGuire, P. Duffy, D.W. Kicklighter, and J. Melillo. 2009. Vulnerability of carbon storage in North American boreal forests to wildfires during the 21st Century. Global Change Biology 15:1491-1510.

Barrett, D. J. 2002. Steady state turnover time of carbon in the Australian terrestrial biosphere, Global Biogeochemical Cycles 16: 1608, doi:10.1029/2002GB001860.

Bernhard, E. S., J. J. Barber, J. S. Pippen, L. Taneva, J. A. Andrews, and W. H. Schlesinger. 2006. Long-term effects of free air CO_2 enrichment (FACE) on soil respiration. Biogeochemistry 77: 91 - 116.

Bonan, G.B. 2008. Forests and climate change: forcings, feedbacks, and the climate benefits of forests. Science 320: 14444-1449.

Bond-Lamberty, B., Peckham, S. D., Ahl, D. E., and Gower, S. T. 2008. Fire as the dominant driver of central Canadian boreal forest carbon balance. Nature 450: 89-92.

Bowman, D.M.J.S., et al. 2009. Fire in the earth system. Science 324: 481-484.

Braswell, B. H., W. J. Sacks, E. Linder, and D. S. Shimel. 2005. Estimating diurnal to annual ecosystem parameters by synthesis of a carbon flux model with eddy covariance net ecosystem exchange observations. Global Change Biology 11: 335 - 355.

Buckman, H. O., and N. C. Brady. 1960. The nature and properties of soils. McMillan Company, New York.

Burke, I. C., J. P. Kaye, S. P. Bird, S. A. Hall, R. L. McCulley, and G. L. Sommerville. 2003. Evaluating and testing models of terrestrial biogeochemistry: the role of temperature in controlling decomposition. Pages 225 - 253 in Canham, C. D., J. J. Cole, W. K. Lauenroth, editors. Models in ecosystem science. Princeton University Press, Princeton, New Jersey, USA.

Carpenter, S. R., H. A. Mooney, J. Agard, D. Capistrano, R. S. Defries, S. Díaz, T. Dietz, A. K. Duraiappah, A. Oteng-Yeboah, H. M. Pereira, C. Perrings, W. V. Reid, J. Sarukhan, R. J. Scholes, and A. Whyte. 2009. Science for managing ecosystem services: Beyond the Millennium Ecosystem Assessment. Proceedings of the National Academy of Sciences (USA) 106: 1305-1312.

Carvalhais, N., M. Reichstein, J. Seixas, G. J. Collatz, J. S. Pereira, P. Berbigier, A. Carrara, A. Granier, L. Montagnani, D. Papale, S. Rambal, M. J. Sanz, and R. Valentini. 2008. Implications of the carbon cycle steady state assumption for biogeochemical modeling performance and inverse parameter retrieval, Global Biogeochemical Cycles 22: GB2007, doi:10.1029/2007GB003033.

Chadwick, O. A., L. A. Derry, P. M. Vitousek, B. J. Huebert, and L. O. Hedin. 1999. Changing sources of nutrients during four million years of ecosystem development. Nature 397: 491 - 497.

Choudhury, B.J., N. E. DiGirolamob, J. Susskindc, W. L. Darnelld, S.K. Guptae, and G. Asrar. 1998. A biophysical process-based estimate of global land surface evaporation using satellite and ancillary data II. Regional and global patterns of seasonal and annual variations, J. Hydrol., 205, 186–204

Chuvieco, E., L. Giglio, and C. Justice. 2008. Global characterization of fire activity: toward defining fire regimes from Earth observation data. Global Change Biololgy 14: 1488-1502.

Clark, J. M., 1990. Fire and climate change during the last 750 yr in Northwestern Minnesota. Ecology Monographs 60: 135-159.

Conant RT, et al. 2008. Sensitivity of organic matter decomposition to warming varies with its quality. Global Change Biology 14: 868~877.

Cramer, W., A. Bondeau, F. I. Woodward, I. C. Prentice, R. A. Betts, V. Brovkin, P. M. Cox, V. Fisher, J. Foley, A. D. Friend, C. Kucharik, M. R. Lomas, N. Ramankutty, S. Sitch, B. Smith, A. White, and C. Young-Molling. 2001. Global response of terrestrial ecosystem structure and function to CO_2 and climate change: results from six dynamic global vegetation models, Global Change Biology 7: 357-373.

Cramer, W., D. W. Kicklighter, A. Bondeau, B. Moore, G. Churkina, B. Nemry, A. Ruimy, A. L. Schloss, et al. 1999. Comparing global models of terrestrial net primary productivity (NPP): overview and key results. Global Change Biology 5 (Supplement 1): 1 - 15.

Davidson EA and Janssens IA, 2006. Temperature sensitivity of soil carbon decomposition and feedbacks to climate change. Nature 440: 165~173.

de Pury, D. G. G. and G. D. Farquhar. 1997. Simple scaling of photosynthesis from leaves to canopies without the errors of big-leaf models. Plant, Cell and Environment 20: 537-557.

Del Grosso, S., W. Parton, T. Stohlgren, D. Zheng, D. Bachelet, S. Prince, K. Hibbard, and R. Olson. 2008. Global potential net primary production predicted from vegetation class, precipitation, and temperature. Ecology 89: 2117 - 2126.

Denison, F., and B. Loomis, 1989. An Integrative Physiological Model of Alfalfa Growth and Development. UC ANR Publication 1926. University of California, Davis.

Desai, A.R., A.D. Richardson, A.M. Moffat, J. Kattge, D.Y. Hollinger, A. Barr, E. Falge, A. Noormets, D. Papale, M. Reichstein, V.J. Stauch, 2008. Cross site evaluation of eddy covariance GPP and RE decomposition techniques. Agricultural and Forest Meteorology, 148: 821-838

Dodd, M. B., and W. K. Lauenroth. 1997. The influence of soil texture on the soil water dynamics and vegetation structure of a shortgrass steppe ecosystem, Plant Ecololgy 133: 13-28.

Easterling, D.R., G. A. Meehl, C. Parmesan, S. A. Changnon, T. R. Kar, and L. O. Mearns. 2000. Climate extremes: observations, modeling, and impacts. Science, 289, 2068-2073.

Emanuel, K. 2005. Increasing destructiveness of tropical cyclones over the past 30 years. Nature 436, 686-688.

Epstein, H. E., W. K. Lauenroth, and I. C. Burke. 1997. Effects of temperature and soil texture on ANPP in the U.S. Great Plains, Ecology 78: 2628-2631.

Fang, C., P. Smith, J. B. Moncrieff, and J. U. Smith. 2005. Similar response of labile and resistant soil organic matter pools to changes in temperature. Nature 433: 57~59.

Farquhar, G. D., S. von Caemmerer, and J. A. Berry. 1980. A Biochemical Model of Photosynthetic CO2 Assimilation in Leaves of C3 species. Planta 149: 78 - 90.

Fay, P. A., J. D. Carlisle, A. K. Knapp, J. M. Blair, and S. L. Collins. 2003. Productivity responses to altered rainfall patterns in a C4-dominated grassland. Oecologia 137: 245–251.

Ferretti, D.F., E. Pendall, J.A. Morgan, J.A. Nelson, D. LeCain, and A.R. Mosier. 2003. Partitioning evapotranspiration fluxes from a Colorado grassland using stable isotopes: seasonal variation and ecosystem implications of elevated atmospheric CO_2. Plant and Soil 254: 291-303.

Field, C. B., D. B. Lobell, H. A. Peters, and N. R. Chiariello. 2007. Feedbacks of Terrestrial Ecosystems to Climate Change. Annual Review of Environment and Resources 32: 1-29.

Fierer, N., J. M. Craine, K. McLauchlan, and J. P. Schimel. 2005. Litter quality and the temperature sensitivity of decomposition. Ecology 86: 320~326.

Finzi, A.C., R.L. Sinsabaugh, T. M. Long, and M. P. Osgood. 2006. Microbial Community responses to atmospheric carbon dioxide enrichment in a warm-temperate forest. Ecosystems 9: 215 - 226.

Fissore C, C. P. Giardina, C. W. Swanston, G. M. King, R. K. Kolka. 2009. Variable temperature sensitivity of soil organic carbon in North American forests. Global Change Biology 15: 2295-2310.

Foley, J.A., et al. 2005. Global Consequences of Land Use. Science 309, 570-574.

Fox, A., M. Willianms, A.D. Richardson, D. Cameron, J. H. Gove, T. Quaife, D. Ricciuto, M. Reichstein, E. Tomelleri, C.M. Trudinger, M.T. van Wijk. 2009. The REFLEX project: comparing different algorithms and implementations for the inversion of a terrestrial ecosystem model against eddy covariance data. Agricultural and Forest Meteorology 149: 1597 - 1615.

Friedlingstein, P., G. Joel, C. B. Field, and I. Y. Fung. 1999. Toward an allocation scheme for global terrestrial carbon models. Global Change Biology 5: 755 - 770.

Friedlingstein, P., P. Cox, R. Betts, L. Bopp, W. von Bloh, V. Brovkin, P. Cadule, W. Doney, M. Eby, I. Fung, G. Bala, J. John et al. 2006. Climate-carbon cycle feedback analysis: results from the C4MIP model intercomparison. Journal of Climate 19: 3337 - 3353.

Fung, I.Y., S. C. Doney, K. Lindsay, and J. John. 2005. Evolution of carbon sinks in a changing climate. Proceedings of the National Academy of Sciences (USA) 102: 11201 - 11206.

Gaudinski, J. B., S. E. Trumbore1, E. A. Davidson, and S. Zheng. 2000. Soil carbon cycling in a temperate forest: radiocarbon-based estimates of residence times, sequestration rates and partitioning of fluxes. Biogeochemistry 51: 33 - 69.

Gelfand, A. E., and A. F. M. Smith. 1990. Sampling-based approaches to calculating marginal densities. Journal of the American Statistical Association 85: 398 - 409.

Gough, C. M., C. S. Vogel, H. P. Schmid, and P. S. Curtis. 2008. Controls on Annual Forest Carbon Storage: Lessons from the Past and Predictions for the Future. BioScience 58: 609 - 622.

Gough, C. M., C. S. Vogel, K. H. Harrold, K. George, and P. S. Curtis. 2007. The legacy of harvest and fire on ecosystem carbon storage in a north temperate forest, Global Change Biology 13: 1935 - 1949.

Gower, S. T., R. E. McMurtrie, and D. Murty. 1996. Aboveground net primary production decline with stand age: potential causes. Trends in Ecology and Evolution 11: 378-382.

Grissino-Mayer, H. D., 1999. Modeling fire interval data from the American Southwest with the Weibull distribution. International Journal of Wildland Fire 9: 37-50.

Hanson, P. J., J. S. Amthor, S. D. Wullschleger, K. B. Wilson, R. F. Grant, A. Hartley, D. F. Hui, E. R. Hunt, D.W. Johnson, J. S. Kimball, A. W. King, Y. Luo, S.G. McNulty, G. Sun, P. E. Thornton, S. Wang, M. Williams, D.D. Baldocchi, and R.M. Cushman. 2004. Oak forest carbon and water simulations: Model intercomparisons and evaluations against independent data. Ecological Monographs 74: 443-489

Harrison, S. P., and C. I. Prentice. 2003. Climate and CO_2 controls on global vegetation distribution at the last glacial maximum: analysis based on palaeovegetation data, biome modelling and palaeoclimate simulations. Global Change Biology 9: 983-1004.

Harte, J., M. S. Torn, F. R. Chang, B. Feifarek, A. P. Kinzig, R. Shaw, and K. Shen. 1995. Global warming and soil microclimate: results from a meadow-warming experiment, Ecological Applications 5: 132-150.

Hastings, W. K. 1970. Monte Carlo sampling methods using Markov chain and their applications, Biometrika 57: 97 - 109.

Hendrey, G. R., D. S. Ellsworth, K. F. Lewin, and J. Nagy, 1999. A free-air enrichment system for exposing tall forest vegetation to elevated atmospheric CO2. Global Change Biology 5: 293 - 309.

Holland E. A. et al., 2000. Uncertainties in the temperature sensitivity of decomposition in tropical and subtropical ecosystems: Implications for models. Global Biogeochemical Cycles 14: 1137-1151.

Hughes, R. F., Kauffman, J. B. and Jaramillo, V. J. 1999. Biomass, carbon, and nutrient dynamics of secondary forests in a humid tropical region of Mexico. Ecology 80: 1892-1907.

Huxman, T.E., B.P. Wilcox, R.L. Scott, K. Snyder, K. Hultine, E. Small, D. Breshears, W. Pockman, R.B. Jackson. 2005. Ecohydrological implications of woody plant encroachment. Ecology 86: 308-319.

IPCC, 2007: Summary for Policymakers. In: Climate Change 2007: The Physical Science Basis. Contribution of Working Group I to the Fourth Assessment Report of the Intergovernmental Panel on Climate Change [Solomon, S., D. Qin, M. Manning, Z. Chen, M. Marquis, K.B. Averyt, M.Tignor and H.L. Miller (eds.)]. Cambridge University Press, Cambridge, United Kingdom and New York, NY, USA.

Jackson, R. B., C. W. Cook, J. S. Pippen, and S. M. Palmer, 2009. Increased belowground biomass and soil CO2 fluxes after a decade of carbon dioxide enrichment in a warm-temperate forest. Ecology 90: 3352 - 3366.

Jackson, R.B, J. Canadell, J.R. Ehleringer, H.A. Mooney, O.E. Sala, and E.D. Schulze. 1996. A global analysis of root distributions for terrestrial biomes, Oecologia 108: 389-411.

Jastrow, J. D., R. M. Miller, R. Matamala, R. J. Norby, T. W. Boutton, C. W. Rice, and C. E. Owensby. 2005. Elevated atmospheric carbon dioxide increases soil carbon, Global Change Biology 11: 2057–2064.

Jaynes, E. T. 1957. Information theory and statistical mechanics. Physical Review 106: 620 - 630.

Johnstone, J. F., Hollingsworth, T. N., Chapin, F. S., Mack, M. C., 2010. Changes in fire regime break the legacy lock on successional trajectories in Alaskan boreal forest. Global Change Biology 16: 1281-1295.

Jones, C.D., P. M. Cox, and C. Huntingford. 2006. Climate-carbon cycle feedbacks under stabilization: uncertainty and observational constraints. Tellus 58B: 603 - 613.

Kashian, D. M., M. G. Turner, and W. H. Romme. 2005. Changes in leaf area and stemwood increment with stand development in Yellowstone National Park: relationships between forest stand structure and function. Ecosystems 8: 48-61.

Kashian, D. M., W. H. Romme, D. B. Tinker, M. G. Turner, and M. G. Ryan. 2006. Carbon storage on landscapes with stand-replacing fires. BioScience 56: 598-606.

Kätterer T et al. 1998. Temperature dependence of organic matter decomposition: a critical review using literature data analyzed with different models. Biology and Fertility of Soils 27: 258~262.

Katul, G., A. Porporato, and R. Oren. 2007. Stochastic dynamics of plant-water interactions. Annual Review of Ecology, Evolution, and Systematics 38: 767-791.

Katz, R. W., G. S. Brush, and M. B. Parlange. 2005. Statistics of extremes: modeling ecological disturbances. Ecology 86: 1124-1134.

Knapp, A. K., C. Beier, D. D. Briske, A. T. Classen, Y. Q. Luo, M. Reichstein, M. D. Smith, S. D. Smith, J. E. Bell, P. A. Fay, J. L. Heisler, S. W. Leavitt, R. A. Sherry, B. Smith and E. Weng. 2008. Consequences of more extreme precipitation regimes for terrestrial ecosystems. BioSciences 58, 811-821.

Knapp, A. K., E. P. Hamerlynck, and C. E. Owensby. 1993. Photosynthetic and water relations responses to elevated CO_2 in the C_4 grass Andropogon gerardii, International Journal of Plant Sciences 154: 459–466.

Knapp, A. K., P. A Fay, J. M. Blair, S. L. Collins, M. D. Smith, J. D. Carlisle, C. W. Harper, B. T. Danner, M. S. Lett, and J. K. McCarron. 2002. Rainfall variability, carbon cycling, and plant species diversity in a mesic grassland, Science 298: 2202-2205.

Knorr, W., and J. Kattge. 2005. Inversion of terrestrial ecosystem model parameter values against eddy covariance measurements by Monte Carlo sampling. Global Change Biology 11: 1333 - 1351.

Knorr, W., and M. Heimann. 2001. Uncertainties in global terrestrial biosphere modeling. Part I: A comprehensive sensitivity analysis with a new photosynthesis and energy balance scheme. Global Biogeochemical Cycles 15: 207 - 225.

Knorr, W., I. C. Prentice, J. I. House, and E. A. Holland. 2005. Long-term sensitivity of soil carbon turnover to warming. Nature 433: 298-301.

Kolmogorov, A. N. 1968. Three approaches to the quantitative definition of information. International Journal of Computer Mathematics, 2: 157 - 168.

Körner, C., M. Diemer, B. Schäppi, P. Niklaus, and J. Arnone. 1997. The responses of alpine grassland to four seasons of CO2 enrichment: a synthesis, Acta Oecologia 18: 165-175.

Kucharik, C. J., J. A. Foley, C. Delire, V. A. Fisher, M. T. Coe, J. Lenters, C. Young-Molling, N. Ramankutty, J. M. Norman, and S. T. Gower. 2000. Testing the performance of a dynamic global ecosystem model: Water balance, carbon balance and vegetation structure. Global Biogeochemical Cycles 14: 795 - 825.

Kullback, S., and R. A. Leibler. 1951. On information and sufficiency. The Annals of Mathematical Statistics 22: 79 - 86.

Kurz, W. A. and M. J. Apps. 1999. A 70-year retrospective analysis of carbon fluxes in the Canadian forest sector. Ecological Applications 9: 526-547.

Kurz, W. A., C. C. Dymond, G. Stinson, G. J. Rampley, E. T. Neilson, A. L. Carroll, T. Ebata, and L. Safranyik. 2008. Mountain pine beetle and forest carbon feedback to climate change. Nature 452: 987-990.

Kurz, W. A., G. Stinson, and G. Rampley. 2008. Could increased boreal forest ecosystem productivity offset carbon losses from increased disturbances? Philosophical Transactions of the Royal Society B 363: 2259-2268.

Lane, D. R., D. P. Coffin, and W. K. Lauenroth. 1998. Effects of soil texture and precipitation on above-ground net primary productivity and vegetation structure across the central grassland region of the United States, Journal of Vegetation Science 9: 239-250.

Lauenroth, W. K., and J. B. Bradford, 2006. Ecohydrology and the partitioning AET between transpiration and evaporation in a semiarid steppe, Ecosystems 9: 756–767.

Law, B. E., O. J. Sun, J. Campbell, S. V. Tuyl, and P. E. Thornton. 2003. Changes in carbon storage and fluxes in a chronosequence of ponderosa pine. Global Change Biology 9: 510-524

Leuning, R., Kelliher, F.M., de Pury, D.G.G., and Schulze, E.-D., 1995. Plant, Cell and Environment, 18, 1183-1200.

Lewis, S. L., et al. 2009. Increasing carbon storage in intact African tropical forests. Nature 457: 1003-1006.

Lichter, J., S. A. Billings, S. E. Ziegler, D. Gaindh, R. Ryals, A. C. Finzi, R. B. Jackson, E. A. Stemmler, and W. H. Schlesinger. 2008. Soil carbon sequestration in a pine forest after 9 years of atmospheric CO2 enrichment. Global Change Biology 14: 2910 - 2922.

Lichter, J., S. Barron, A. Finzi, K. Irving, M. Roberts, E. Stemmler, and W. Schlesinger. 2005. Soil carbon sequestration and turnover in a pine forest after six years of atmospheric CO_2 enrichment. Ecology 86: 1835 - 1847.

Lloyd, J., and J. A. Taylor. 1994. On the temperature dependence of soil respiration, Functional Ecology 8: 315-323.

Luo, Y. 2007. Terrestrial carbon cycle feedback to climate warming, Annual Review of Ecology, Evolution, and Systematics. 38: 683–712.

Luo, Y. Q., and E. S. Weng. 2011. Dynamic disequilibrium of the terrestrial carbon cycle under global change. Trends in Ecology and Evolution. 26: 96-104.

Luo, Y., and J. F. Reynolds. 1999. Validity of extrapolating field CO_2 experiments to predict carbon sequestration in natural ecosystems, Ecology 80: 1568-1583.

Luo, Y., C. B. Field, and H. A. Mooney. 1994. Predicting responses of photosynthesis and root fraction to elevated CO2: Interaction among carbon, nitrogen and growth. Plant, Cell and Environment 17: 1195-1204

Luo, Y., C. B. Field, and H. A. Mooney. 1994. Predicting responses of photosynthesis and root fraction to elevated CO2: Interaction among carbon, nitrogen and growth. Plant, Cell and Environment 17: 1195-1204

Luo, Y., D. Gerten, G. le Maire, W.J. Parton, E. Weng, X. Zhou, C. Keough, C. Beier, P. Ciais, et al. 2008. Modelled Interactive Effects of Precipitation, Temperature, and CO2 on Ecosystem Carbon and Water Dynamics in Different Climatic Zones. Global Change Biology 14: 1986-1999.

Luo, Y., D. Hui, and D. Zhang. 2006. Elevated CO_2 stimulates net accumulations of carbon and nitrogen in land ecosystems: a meta-analysis. Ecology 87: 53–63.

Luo, Y., K. Ogle, C. Tucker, S. Fei, C. Gao, S. LaDeau, J. Clark, and D. Schimel. 2011. Data assimilation and ecological forecasting in a data-rich era. Ecological Applications, in press

Luo, Y., L. H. Wu, J. A. Andrews, L. White, R. Matamala, K. V. R. Schafer, and W. H. Schelesinger. 2001a. Elevated CO2 differentiates ecosystem carbon processes: deconvolution analysis of Duke Forest FACE data. Ecological Monographs 71: 357 - 376.

Luo, Y., L.W. White, J.G. Canadell, E. H. DeLucia, D. S. Ellsworth, A. Finzi, J. Lichter, and W. H. Schlesinger. 2003. Sustainability of terrestrial carbon sequestration: A case study in Duke Forest with inversion approach. Global Biogeochemical Cycles 17: doi: 10.1029/2002GB001923.

Luo, Y., P.A. Meyerhoff, and R. S. Loomis. 1995. Seasonal patterns and vertical distributions of fine roots of alfalfa (Medicago sativa L.), Field Crops Research 40: 119–127.

Luo, Y., S. Wan, D. Hui, L. Wallace. 2001b. Acclimatization of soil respiration to warming in a tall grass prairie. Nature 413: 622-625.

Luyssaert, S. et al. 2008. Old-growth forests as global carbon sinks. Nature 455: 213-215.

McAuliffe, J. R. 2003. The atmosphere-biosphere interface: the importance of soils in arid and semi-arid environments, in Changing precipitation regimes and terrestrial ecosystems: A north America perspective, edited by J. F. Weltzin, and G. R. McPherson, pp. 9–27, Univ. Arizona Press, Tucson

McCarthy, H. R., R. Oren, A. C. Finzi, and K. H. Johnsen. 2006. Canopy leaf area constrains [CO_2]-induced enhancement of productivity and partitioning among aboveground carbon pools. Proceedings of the National Academy of Sciences (USA) 103: 19356-19361.

McGuire, A. D., J. M. Melillo, L. A. Joyce, D. W. Kicklighter, A. L. Grace, B. Moore III, C. J. Vorosmarty. 1992. Interactions between carbon and nitrogen dynamics in estimating net primary productivity for potential vegetation in North America. Global Biogeochemical Cycles 6: 101-124.

McGuire, A. D., S. Sitch, J.S. Clei, R. Dargaville, G. Esser, J. Foley, M. Heimann, F. Joos, J. Kaplan, D.W. Kicklighter, R.A. Meier, et al. 2001. Carbon balance of the terrestrial biosphere in the twentieth century: Analyses of CO2, climate, and land use effects with four process-based ecosystem models. Global Biogeochemical Cycles 15: 183 - 206.

McGuire, A.D., D.J. Hayes, D.W. Kicklighter, M. Manizza, Q. Zhuang, M. Chen, M.J. Follows, K.R. Gurney, J.W. McClelland, J.M. Melillo, B.J. Peterson, and R. Prinn. 2010. An analysis of the carbon balance of the Arctic Basin from 1997 to 2006. Tellus 62B: 455-474

Metropolis, N., A.W. Rosenbluth, M. N. Rosenbluth, A. H. Teller, and E. Teller. 1953. Equation of state calculation by fast computer machines. Journal of Chemical Physics 21: 1087 - 1092.

Miao, S., C. B. Zou, and D. D. Breshears. 2009. Vegetation responses to extreme hydrological events: sequence matters. American Naturalist 173: 113-118.

Miller, D. A., and R. A. White. 1998. A Conterminous United States multi-layer soil characteristics data set for regional climate and hydrology modeling, Earth Interactions 2: 1–26.

Moore, L. A., and C. B. Field, 2006. The effects of elevated atmospheric CO_2 on the amount and depth distribution of plant water uptake in a California annual grassland, Global Change Biology 12: 578–587.

Morgan, J.A., D. E. Pataki, C. Korner, H. Clark, S. J. Del Grosso, J. M. Grunzweig, A. K. Knapp, A. R. Mosier, P .C. D. Newton, P. A. Niklaus, J. B. Nippert, R. S. Nowak, W. J. Parton, H. W. Polley, and M. R. Shaw. 2004. Water relations in grassland and desert ecosystems exposed to elevated atmospheric CO_2. Oecologia 140: 11–25.

Niklaus, P. A., D. Spinnler, and C. Körner. 1998. Soil moisture dynamics of calcareous grassland under elevated CO_2. Oecologia 117: 201–208.

Nippert, J. B, and A. K Knapp. 2007. Linking water uptake with rooting patterns in grassland species. Oecologia 153: 261–272.

Nowak, R. S., S. F. Zitzer, D. Babcock, V. Smith-Longozo, T. N. Charlet, J. S. Coleman, J. R. Seemann, and S. D. Smith. 2004. Elevated atmosphericCO_2 does not conserve soil water in the Mojave Desert. Ecology 85: 93–99.

Noy-Meir, I. 1973. Desert ecosystems: Environment and producers, Annual Review of Ecology, Evolution, and Systematics 4: 25–51.

Owensby, C. E., Ham, J. M., Knapp, A. K., and Auen, L. M. 1999. Biomass production and species composition change in a tallgrass prairie ecosystem after long-term exposure to elevated atmospheric CO_2. Global Change Biology 5: 497–506.

Palmroth, S., R. Oren, H. R. McCarthy, K. H. Johnsen, A. C. Finzi, J. R. Butnor, M. G. Ryan, and W. H. Schlesinger. 2006. Aboveground sink strength in forests controls the allocation of carbon below ground and its [CO_2]-induced enhancement. Proceedings of the National Academy of Sciences (USA) 103: 19362-19367.

Parmesan, C. 2006. Ecological and evolutionary responses to recent climate change. Annual Review of Ecology, Evolution, and Systematics 37: 637-669.

Parton, W. J., J. A. Morgan, G. Wang, and S. D. Grosso. 2007. Projected ecosystem impact of the Prairie Heating and CO_2 Enrichment experiment, New Phytologist 174: 823-834.

Parton, W. J., J.M.O. Scurlock, D. S. Ojima, D. S. Schimel, D. O. Hall, and SCOPEGRAM members. 1995. Impact of climate change on grassland production and soil carbon worldwide. Global Change Biology 1: 13–22.

Perry, G. L.W. 2002. Landscapes, space and equilibrium: shifting viewpoints. Progress in Physical Geography 26: 339-359.

Peterson, D.W. and P. B. Reich. 2001. Prescribed fire in Oak Savanna: fire frequency effects on stand structure and dynamics. Ecology Applications 11: 941-927.

Prentice, I. C., W. Cramer, S. P. Harrison, R. Leemans, R. A. Monserud, and A. M. Solomon. 1992. A global biome model based on plant physiology and dominance, soil properties and climate. Journal of Biogeography 19: 117 - 134.

Pretzsch, H., R. Grote, B. Reineking, T.H. Rötzer, and S.T. Seifert. 2008. Models for forest ecosystem management: a European perspective. Annals of Botany 101: 1065 - 1087.

Pritchard, S. G., A. E. Strand, M. L. McCormack, M. A. Davis, A. C. Finzi, R. B. Jackson, R. Matamala, H. H. Rogers, and R. Oren. 2008. Fine root dynamics in a loblolly pine forest are influenced by free-air-CO_2-enrichment: a six-year-minirhizotron study. Global Change Biology 14: 588 - 602.

Randerson, J. T., F. M. Hoffman, P. E. Thornton, N. M. Mahowald, K. Lindsay, Y. H. Lee, C. D. Nevison, S. C. Doney, G. Bonan, R. Stockli, C. Covey, S. W. Running, and I. Y. Fung. 2009. Systematic assessment of terrestrial biogeochemistry in coupled climate-carbon models. Global Change Biology 15: 2462 - 2484.

Rastetter, E. B. 1996. Validating models of ecosystem response to global change: How can we best assess models of long-term global change? BioScience 46: 190 - 198.

Raupach, M. R., P. J. Rayner, D. J. Barrett, R. S. Defries, M. Heimann, D. S. Ojima, S. Quegan, and C. C. Schmullius. 2005. Model-data synthesis in terrestrial carbon

observation: methods, data requirements and data uncertainty specifications. Global Change Biology 11: 378 - 397.

Reichstein, M. F. Bednorz, G. Broll, and T. Kátterer 2000. Temperature dependence of carbon mineralization: conclusions from a long-term incubation of subalpine soil samples. Soil Biology and Biochemistry 32: 947-958.

Rényi, A. 1960. On measures of entropy and information. Proceeding of the 4th Berkeley Symposium on Mathematics, Statistics, and Probability 1960: 547 - 561.

Reynolds, J. F., P. R. Kemp, and J. D. Tenhunen. 2000. Effects of long-term rainfall variability on evapotranspiration and soil water distribution in the Chihuahuan Desert: A modeling analysis. Plant Ecology 150: 145-159

Rodriguez-Iturbe, I., and A. Porporato. 2004. Ecohydrology of water-controlled ecosystems: Soil moisture and plant dynamics, 442 pp., Cambridge Univ. Press, New York

Rosenbloom, N. A., S. C. Doney, and D. S. Schimel. 2001. Geomorphic evolution of soil texture and organic matter in eroding landscapes, Global Biogeochemical Cycles 15: 365–382.

Rotenberg, E. and D. Yakir. 2010. Contribution of semi-arid forests to the climate system. Science 327: 451-454.

Running, S. W. 2008. Ecosystem disturbance, carbon, and climate. Science 321: 652

Rustad, L. E., J. L. Campbell, G. M. Marion, R. J. Norby, M. J. Mitchell, A. E. Hartley, J. H. C. Cornelissen, J. Gurevitch, and GCTE-NEWS. 2001. A meta-analysis of the response of soil respiration, net nitrogen mineralization, and aboveground plant growth to experimental ecosystem warming. Oecologia 126: 543–562.

Ryan, C.M. and M. Williams. 2010. How does fire intensity and frequency affect miombo woodland tree populations and biomass? Ecology Applications in press.

Ryan, M. G. 1991, Effects of climate change on plant respiration, Ecological Applications 1: 157–167.

Ryan, M. G., D. Binkley, and J. H. Fownes. 1997. Age-related decline in forest productivity: pattern and process. Advances of Ecological Research 27: 213-262.

Ryan, M. G., Phillips, N., and Bond, B. J., 2006. The hydraulic limitation hypothesis revisited. Plant, Cell and Environment 29: 367-381.

Sala, O. E., W. J. Parton, L. A. Joyce, and W. K. Lauenroth. 1988. Primary production of the central grassland region of the United States, Ecology 69: 40–45.

Saleska, S., J. Harte, and M. Torn. 1999. The effect of experimental ecosystem warming on CO2 fluxes in a montane meadow, Global Change Biology 5: 125–141.

Schimel, D. S., et al. 1997. Continental scale variability in ecosystem processes: models, data, and the role of disturbance. Ecological Monographs 67: 251-271.

Schmid S., E. Thurg, E. Kaufmann, H. Lischke, H. Bugmann. 2006. Effects of forest management on future carbon pools and fluxes: A model comparison. Forest Ecology and Management 237: 65 - 82.

Schröter D., W. Cramer, R. Leemans, I.C. Prentice, M.B. Araújo, N.W. Arnell, A. Bondeau, H. Bugmann, T.R. Carter, C.A. Gracia, A.C. de la Vega-Leinert, M. Erhard, F. Ewert, M. Glendining, J.I. House, S. Kankaanpää, R.J.T. Klein, S. Lavorel, M. Lindner, M.J. Metzger, J. Meyer, T.D. Mitchell, I. Reginster, M. Rounsevell, S. Sabaté, S. Sitch, B. Smith, J. Smith, P. Smith, M.T. Sykes, K. Thonicke, W. Thuiller, G. Tuck, S. Zaehle, and B. Zierl. 2005. Ecosystem Service Supply and Vulnerability to Global Change in Europe. Science 310: 1333 - 1337.

Schulze, E. D., R. H. Robichaux, J. Grace, P. W. Rundel, and J. R. Ehleringer. 1987. Plant water balance. Bioscience 37: 30–37

Scott, R. L., T. E. Huxman, W. L. Cable, and W. E. Emmerich. 2006. Partitioning of evapotranspiration and its relation to carbon dioxide exchange in a Chihuahuan Desert shrubland, Hydrological Processes 20: 3227–3243.

Sellers, P. J., Berry, J. A., Collatz G. J., Field, C. B., and Hall, F. G., 1992. Canopy reflectance, photosynthesis, and transpiration. III. A reanalysis using improved leaf models and a new canopy integration scheme. Remote Sensing of Environment 42, 187-216.

Sellers, P. J., D. A. Randall, G. J. Collatz, J. A. Berry, C. B. Field, D. A. Dazlich, C. Zhang, G. D. Collelo, and L. Bounoua. 1996. A Revised Land Surface Parameterization (SiB2) for Atmospheric GCMs. Part I: Model Formulation, Journal of Climate 9: 676–705.

Shannon, C.E. 1948. A Mathematical Theory of Communication. Bell System Technical Journal, 27: 379 - 423 & 623 - 656.

Shaver G. R., J. Canadell, F. S. III Chapin, J. Gurevitch, J. Harte, G. Henry, I. Ineson, S. Jonasson, J. Melillo, L. Pitelka, and L. Rustad. 2000. Global warming and terrestrial ecosystems: a conceptual framework for analysis. BioScience 50: 871–882.

Sherry, R. A., E. S. Weng, J. A. Arnone III, D. Johnson, D. S. Schimel, P. S. Verburg, L. L .Wallace and Y. Q. Luo. 2008. Lagged effects of experimental warming and doubled precipitation on annual and seasonal aboveground biomass production in a tallgrass prairie. Global Change Biology 14: 2923 - 2936.

Shinozaki, K. K. Yoda, K. Hozumi, T. Kira. 1964. A quantitative analysis of plant form – the pipe model theory I. basic analyses. Japanese Journal of Ecology 14: 97-105.

Singh, J.S., D.G. Milchunas, and W.K. Lauenroth. 1998. Soil water dynamics and vegetation patterns in a semiarid grassland, Plant Ecology 134: 77–89.

Sitch, S., B. Smith, I. C. Prentice, A. Arneth, A. Bondeau, W. Cramer, J. O. Kaplan, S. Levis, W. Lucht, M. T. Sykes, K. Thonicke, and S. Venevsky. 2003. Evaluation of ecosystem dynamics, plant geography and terrestrial carbon cycling in the LPJ Dynamic Vegetation Model. Global Change Biology 9: 161 - 185

Sitch, S., C. Huntingford, N.Gedney, P. E. Levy, M. Lomas, S. L. Piao, R. Betts, P. Ciais, P. Cox, P. Friedlingstein P, C. D. Jones, I. C. Prentice, and F. I. Woodward. 2008. Evaluation of the terrestrial carbon cycle, future palnt geography and climate-carbon cycle feedbacks using five Dynamic Global Vegetation Models (DGVMs). Global Change Biology 14: 2015 - 2039.

Smithwick, E. A. H., D. M. Kashian, M. G. Ryan, and M. G. Turner. 2009. Long-term ecosystem nitrogen storage and soil nitrogen availability in post-fire lodgepole pine ecosystems. Ecosystems 12: 792–806.

Stöckli, R., D. M. Lawrence, G.-Y. Niu, K. W. Oleson, P. E. Thornton, Z.-L. Yang, G. B. Bonan, A. S. Denning, and S. W. Running. 2008. Use of FLUXNET in the Community Land Model development, Journal of Geophysical Research 113: G01025, doi:10.1029/2007JG000562.

Stoy, P., G. G. Katul, M. B. S. Siqueira, J. Y. Juang, K.A. Novick, J. M. Uebelherr, and R. Oren. 2006. An evaluation of models for partitioning eddy covariance-measured

net ecosystem exchange into photosynthesis and respiration, Agricultural and Forest Meteorology 141: 2 - 18.

Thornton, P. E., and Zimmermann, N. E., 2007. An improved canopy integration scheme for a land surface model with prognostic canopy structure. Journal of Climate, 20, 3902-3921.

Thornton, P., B.E. Law, H. Gholz, K.L. Clark, E. Falge, D.H. Ellsworth, A.H. Goldstein, R.K. Monson, D. Hollinger, M. Falk, J. Chen, and J.P. Sparks. 2002. Modeling and measuring the effects of disturbance history and climate on carbon and water budgets in evergreen needleleaf forests. Agricultural and Forest Meteorology 113: 185-222.

Tilman, D., P. Reich, H. Phillips, M. Menton, A. Patel, E. Vos, D. Peterson, J. Knops. 2000. Fire suppression and ecosystem carbon storage. Ecology 81: 2680-2685.

Turetsky, M. R., Kane, E. S. Harden, J. W., Ottmar, R. D., Manies, K. L., Hoy, E, & Kasischke, E. S. 2010. Recent acceleration of biomass burning and carbon losses in Alaskan forests and peatlands. Nature-geoscience 4: 27-31.

Turner, M. G. 2010. Disturbance and landscape dynamics in a changing world. Ecology 91: 2833-2849.

Turner, M. G., W. H. Hargrove, R. H. Gardner, and W. H. Romme. 1994. Effects of fire on landscape heterogeneity in Yellowstone National Park, Wyoming. Journal of Vegetation Science 5:731–742.

Turner, M. G., W. H. Romme, R. H. Gardner, R. V. O'Neill, and T. K. Kratz. 1993. A revised concept of landscape equilibrium: Disturbance and stability on scaled landscapes. Landscape Ecology 8: 213-227.

Vargas, R., M. F. Allen, and E. B. Allen. 2008. Biomass and carbon accumulation in a fire chronosequence of a seasonally dry tropical forest. Global Change Biology 14: 109-124

VEMAP Members. 1995. Vegetation/Ecosystem Modeling and Analysis Project (VEMAP): Comparing biogeography and biogeochemistry models in a continental-scale study of terrestrial ecosystem responses to climate change and CO_2 doubling. Global Biogeochemical Cycles 9: 407 - 437.

Volk, M., A. Niklaus, and C. Körner. 2000. Soil moisture effects determine CO2 responses of grassland species, Oecologia, 125, 380–388.

Wan, S., D. Hui, L.L. Wallace, and Y. Luo. 2005. Direct and indirect effects of experimental warming on ecosystem carbon processes in a tallgrass prairie, Global Biogeochemical Cycyls 19: GB2014, doi:10.1029/2004GB002315.

Wan, S., Y. Luo, and L. L. Wallace. 2002. Changes in microclimate induced by experimental warming and clipping in tallgrass prairie, Global Change Biology 8: 754-768.

Wang, Y. P., and R. Leuning. 1998. A two-leaf model for canopy conductance, photosynthesis and partitioning of available energy I: Model description and comparison with a multi-layered model, Agricultural and Forest Meteorology 91: 89–111.

Wang, Y. P., D. Baldocchi, R. Leuning , E. Falge, and T. Vesala. 2007. Estimating parameters in a land surface model by applying nonlinear inversion to eddy covariance flux measurements from eight FLUXNET sites. Global Change Biology 13: 652 - 670.

Webster, P.J., G. J. Holland, J. A. Curry, and H.-R. Chang. 2005. Changes in tropical cyclone number, duration, and intensity in a warming environment. Science 309: 1844-1846.

Weng, E. S., and G. S. Zhou. 2006. Modeling distribution changes of vegetation in China under future climate change. Environmental Modeling and Assessment 11: 45 - 58.

White, L., and Y. Luo. 2008. Modeling and inversion of net ecological exchange data using an Ito stochastic differential equation approach. Applied Mathematics and Computation 196: 686 - 704.

White, L., F. White, Y. Luo, and T. Xu. 2006. Estimation of parameters in carbon sequestration models from net ecosystem exchange data. Applied Mathematics and Computation 181: 864 - 879.

White, P.S. and A. Jentsch, 2001. The search for generality in studies of disturbance and ecosystem dynamics. Progress in Botany 62: 399-450.

Williams, M., A. D. Richardson, M. Reichstein, P. C. Stoy, P. Peylin, H. Verbeeck, N. Carvalhais, M. Jung, D. Y. Hollinger, J. Kattge, R. Leuning, Y. Luo, E. Tomelleri,

C. Trudinger, and Y.-P. Wang. 2009. Improving land surface models with FLUXNET data. Biogeosciences 6: 1341-1359.

Williams, M., P. A. Schwarz, B. E. Law, J. Irvine, and M. R. Kurpius. 2005. An improved analysis of forest carbon dynamics using data assimilation. Global Change Biology 11: 89 - 105.

Williams, R. J., G. A. Duff, D. M. J. S. Bowman, and G. D. Cook. 1996. Variation in the Composition and Structure of Tropical Savannas as a Function of Rainfall and Soil Texture Along a Large-Scale Climatic Gradient in the Northern Territory, Australia, Journal of Biogeography 23: 747-756.

Wirth, C. in Old‐Growth Forests (eds Wirth, C., Gleixner, & G., Heimann, M.), Ecological Studies 207, pp. 465-491 (Springer-Verlag Berlin Heidelberg 2009).

Wu, X., Y. Luo, E. Weng, L. White, Y. Ma, and X. Zhou, 2009. Conditional inversion to estimate parameters from eddy-flux observations. Journal of Plant Ecology 2: 55 - 68.

Wullschleger, S. D., T. J. Tschaplinski, and R. J. Norby. 2002. Plant water relations at elevated CO2 - implications for water-limited environments, Plant Cell and Environment 25: 319–331.

Wutzler, T. and M. Reichstein. 2007. Soils apart from equilibrium – consequences for soil carbon balance modeling. Biogeosciences 4: 125 - 136.

Wythers, K. R., W. K. Lauenroth, and J. M. Paruelo. 1999. Bare-soil evaporation under semiarid field conditions, Soil Science Society of America Journal 63: 1341–1349.

Xu, T., L., D. White, D. Hui, and Y. Luo. 2006. Probabilistic inversion of a terrestrial ecosystem model: Analysis of uncertainty in parameter estimation and model prediction. Global Biogeochemical Cycles 20: doi: 10.1029/2005GB002468.

Zaehle, S., S. Sitch, B. Smith, and F. Hatterman. 2005. Effects of parameter uncertainties on the modeling of terrestrial biosphere dynamics. Global Biogeochemical Cycles 19: GB3020, doi:10.1029/2004GB002395.

Zavaleta, E. S., B. D. Thomas, N. R. Chiariello, G. P. Asner, M. R. Shaw, and C. B Field. 2003. Plants reverse warming effect on ecosystem water balance, Proceedings of National Academy of Sciences USA. 100: 9892~9893.

Zavaleta, E. S., M. R. Shaw, N. R. Chiariello, B. D. Thomas, E. E. Cleland, C. B. Field, and H. A. Mooney. 2003. Grassland responses to three years of elevated temperature, CO_2, precipitation, and N deposition, Ecological Monographs 73: 585–604.

Zeide, B. 1993. Primary unit of the tree crown. Ecology 74: 1598-1602.

Zeng, H. et al. 2009. Impacts of tropical cyclones on U.S. forests tree mortality and carbon flux from 1851 to 2000. Proceedings of National Academy of Sciences U.S.A. 106: 7888-7892.

Zhou, T., and Y. Q. Luo. 2008. Spatial Patterns of Ecosystem Carbon Residence Time and NPP-Driven Carbon Uptake in the Conterminous USA. Global Biogeochemical Cycles 22: GB3032, doi:10.1029/2007GB002939.

Zhou, X., X. Liu, L. L. Wallace, and Y. Luo. 2007. Photosynthetic and respiratory acclimation to experimental warming for four species in a tallgrass prairie ecosystem. Journal of Integrated Plant Biolology 49: 270–281.